NAVAL POSTGRADUATE SCHOOL

MONTEREY, CALIFORNIA

THESIS

MULTI-SENSOR IMAGE FUSION FOR TARGET RECOGNITION IN THE ENVIRONMENT OF NETWORK DECISION SUPPORT SYSTEMS

by

Michail Pothitos

December 2015

Thesis Co-Advisors: Alex Bordetsky
Gamani Karunasiri
Murali Tummala

Approved for public release; distribution is unlimited

THIS PAGE INTENTIONALLY LEFT BLANK

REPORT DOCUMENTATION PAGE			Form Approved OMB No. 0704–0188

Public reporting burden for this collection of information is estimated to average 1 hour per response, including the time for reviewing instruction, searching existing data sources, gathering and maintaining the data needed, and completing and reviewing the collection of information. Send comments regarding this burden estimate or any other aspect of this collection of information, including suggestions for reducing this burden, to Washington headquarters Services, Directorate for Information Operations and Reports, 1215 Jefferson Davis Highway, Suite 1204, Arlington, VA 22202-4302, and to the Office of Management and Budget, Paperwork Reduction Project (0704-0188) Washington, DC 20503.

1. AGENCY USE ONLY *(Leave blank)*	2. REPORT DATE December 2015	3. REPORT TYPE AND DATES COVERED Master's thesis

4. TITLE AND SUBTITLE MULTI-SENSOR IMAGE FUSION FOR TARGET RECOGNITION IN THE ENVIRONMENT OF NETWORK DECISION SUPPORT SYSTEMS	5. FUNDING NUMBERS
6. AUTHOR(S) Michail Pothitos	
7. PERFORMING ORGANIZATION NAME(S) AND ADDRESS(ES) Naval Postgraduate School Monterey, CA 93943-5000	8. PERFORMING ORGANIZATION REPORT NUMBER
9. SPONSORING /MONITORING AGENCY NAME(S) AND ADDRESS(ES) N/A	10. SPONSORING / MONITORING AGENCY REPORT NUMBER

11. SUPPLEMENTARY NOTES The views expressed in this thesis are those of the author and do not reflect the official policy or position of the Department of Defense or the U.S. Government. IRB Protocol number ____N/A____.

12a. DISTRIBUTION / AVAILABILITY STATEMENT Approved for public release; distribution is unlimited	12b. DISTRIBUTION CODE A

13. ABSTRACT (maximum 200 words)

This thesis proposed a concept of distributed management of littoral operations at the tactical level, in which timeliness of information and reduced decision cycles are of critical importance. The use of mesh tactical networks augmented by sensor management, operational databases, and an appropriate level of automation of target recognition can turn the obstacles of land masses in littoral environments into a tactical advantage. Ultimately, this thesis concept aimed to enhance situational awareness by enabling the timely exploitation and dissemination of imagery data from small satellites and unmanned systems at the tactical level.

Analyses of simulation and field experimentation results that focused on mobile ad-hoc networks (MANETs)—which connected dissimilar imaging sensors and enabled fusion of captured images—supported this concept. Mesh tactical radios provided an adequate range and quality of service (QoS) to enable networking of kinetic and non-kinetic assets equipped with imaging or data relaying capabilities and to support dissemination of imagery data. Additionally, multi-spectral image fusion of thermal and visual images for target recognition yielded the best classification performance after the use of speeded-up robust features (SURF) and artificial neural networks (ANNs).

14. SUBJECT TERMS artificial neural networks, automatic target recognition, mobile ad-hoc networks, network decision support systems, speeded-up robust features, wireless mesh networks, image fusion	15. NUMBER OF PAGES 145
	16. PRICE CODE

17. SECURITY CLASSIFICATION OF REPORT	18. SECURITY CLASSIFICATION OF THIS PAGE	19. SECURITY CLASSIFICATION OF ABSTRACT	20. LIMITATION OF ABSTRACT
Unclassified	Unclassified	Unclassified	UU

NSN 7540–01-280-5500 Standard Form 298 (Rev. 2–89) Prescribed by ANSI Std. 239–18

THIS PAGE INTENTIONALLY LEFT BLANK

Approved for public release; distribution is unlimited

MULTI-SENSOR IMAGE FUSION FOR TARGET RECOGNITION IN THE ENVIRONMENT OF NETWORK DECISION SUPPORT SYSTEMS

Michail Pothitos
Lieutenant Commander, Hellenic Navy
B.S., Hellenic Naval Academy, 1999

Submitted in partial fulfillment of the
requirements for the degrees of

MASTER OF SCIENCE IN COMBAT SYSTEMS TECHNOLOGY

and

MASTER OF SCIENCE IN SYSTEMS TECHNOLOGY
(COMMAND, CONTROL & COMMUNICATIONS)

from the

NAVAL POSTGRADUATE SCHOOL
December 2015

Approved by: Alex Bordetsky
Thesis Co-Advisor

Gamani Karunasiri
Thesis Co-Advisor

Murali Tummala
Thesis Co-Advisor

Kevin Smith
Chair, Department of Physics

Dan Boger
Chair, Department of Information Sciences

THIS PAGE INTENTIONALLY LEFT BLANK

ABSTRACT

This thesis proposed a concept of distributed management of littoral operations at the tactical level, in which timeliness of information and reduced decision cycles are of critical importance. The use of mesh tactical networks augmented by sensor management, operational databases, and an appropriate level of automation of target recognition can turn the obstacles of land masses in littoral environments into a tactical advantage. Ultimately, this thesis concept aimed to enhance situational awareness by enabling the timely exploitation and dissemination of imagery data from small satellites and unmanned systems at the tactical level.

Analyses of simulation and field experimentation results that focused on mobile ad-hoc networks (MANETs)—which connected dissimilar imaging sensors and enabled fusion of captured images—supported this concept. Mesh tactical radios provided an adequate range and quality of service (QoS) to enable networking of kinetic and non-kinetic assets equipped with imaging or data relaying capabilities and to support dissemination of imagery data. Additionally, multi-spectral image fusion of thermal and visual images for target recognition yielded the best classification performance after the use of speeded-up robust features (SURF) and artificial neural networks (ANNs).

THIS PAGE INTENTIONALLY LEFT BLANK

TABLE OF CONTENTS

I. INTRODUCTION 1
- **A. MOTIVATION 1**
- **B. RESEARCH QUESTIONS 3**
- **C. HYPOTHESIS AND EXPLANATION 4**
- **D. SCOPE AND LIMITATIONS 5**
- **E. RELATED WORK 6**
- **F. SIMULATION AND EXPERIMENTATION STEPS AND TOOLS 10**
  - **1. Systems Tool Kit 10**
  - **2. QualNet 12**
  - **3. MATLAB 14**
- **G. ORGANIZATION OF THE THESIS 15**

II. THEORETICAL AND TECHNICAL BACKGROUND 17
- **A. SIMULATING MANET AND MESH NETWORKS IN MARITIME LITTORAL ENVIRONMENT 17**
  - **1. Wireless Networks 17**
    - ***a. MANETs 18***
    - ***b. Wireless Mesh Networks 20***
    - ***c. Operational Advantages of Wireless Mesh Tactical Radios 22***
  - **2. Wave Relay MANET Nodes 23**
    - ***a. Wave Relay 24***
  - **3. Types of Nodes 27**
    - ***a. Small Satellites 27***
    - ***b. Unmanned Systems 30***
    - ***c. Other Nodes 30***
  - **4. Network Operations Centers 31**
    - ***a. Network Decision Support Systems 31***
- **B. IMAGING SENSORS 32**
  - **1. The Electromagnetic Spectrum 33**
  - **2. EM Radiation 34**
  - **3. Terms and Theory 35**
  - **4. Imaging Sensors 36**
    - ***a. Photodetectors 37***
    - ***b. Thermal Sensors 37***
    - ***c. Focal Plane Arrays 38***

5. Sensors Used 40
6. Digital Image Representation and Data Visualization 41
C. CLASSIFICATION PROCESS 42
1. Image Processing 43
2. Feature Detection and Description 43
a. Speeded-Up Robust Features (SURF) 43
3. Multi-Sensor Data Fusion 46
4. Machine Learning 47
a. Artificial Neural Networks 48
b. Training the Neural Network 51
c. Classification 52
D. USING CENETIX TNT TESTBED FOR EXPERIMENTATION WITH SENSORS 55

III. SIMULATION MODELING OF ATR THROUGH A MESH NETWORK OF IMAGING SENSORS 57
A. SIMULATION AND EVALUATION OF A WIRELESS MESH NETWORK 58
1. STK Simulation 59
2. Simulation in QualNet 66
B. IMAGE FUSION AND CLASSIFICATION SCHEME 67
1. Image Capture and Collection 68
2. Low Level Image Fusion Implementation 71
3. Image Processing 72
4. SURF Features: Detection and Description 73
5. Medium Level Image Fusion Implementation 76
6. Image Classification Using an Artificial Neural Network 76
a. Training the Artificial Neural Network 77
b. Classification 79
C. CENETIX EXPERIMENTATION MODELING 80
1. Mesh Networking Implementations for Imagery Data Dissemination 80
2. CodeMettle's Network Monitoring and Management Tool 81

IV. SIMULATION AND EXPERIMENTATION RESULTS 83
A. STK AND QUALNET SIMULATION 83
1. STK 83
2. QualNet 87
B. CENETIX FIELD EXPERIMENTS 87

1. Wave Relay Performance 88
2. CodeMettle 89
3. Wireless Communication with Divers and UGV 91
C. IMAGE FUSION AND CLASSIFICATION 93
1. Feature Extraction and Training Results 94
2. Testing Classification Results 97
3. Summary of Image Classification Results 101

V. CONCLUSIONS 103
A. MESH TACTICAL NETWORKING 104
B. IMAGE FUSION AND CLASSIFICATION 105
C. RECOMMENDATIONS FOR FUTURE WORK 106
1. Multi-Sensor Data Fusion and Classification 106
2. Mesh Tactical Networking 107

APPENDIX. IMAGE TO IMAGE REGISTRATION WITH ENVI 109

LIST OF REFERENCES 115

INITIAL DISTRIBUTION LIST 121

THIS PAGE INTENTIONALLY LEFT BLANK

LIST OF FIGURES

Figure 1. Structure of a Hierarchical Mesh Network Model in the Battlefield.....7
Figure 2. Network Operations Ecosystem and Dashboard from CodeMettle.....8
Figure 3. Systems Tool Kit.....11
Figure 4. STK Objects.....12
Figure 5. QualNet/STK Interaction Flow.....13
Figure 6. QualNet/STK Interaction Flow.....14
Figure 7. MATLAB Logo 14
Figure 8. Basic Mesh Topology 18
Figure 9. Assets and Agents 19
Figure 10. Network Topologies.....21
Figure 11. Samsung's Global Internet Access Satellite Network 22
Figure 12. Wave Relay MANET Radio Solutions.....23
Figure 13. The ISO/OSI Model.....24
Figure 14. Cloud Relay Groups.....25
Figure 15. Cubesats 28
Figure 16. PRISM Nanosatellite 29
Figure 17. PRISM's Boom.....29
Figure 18. NWDSS Decision-making Loop.....32
Figure 19. The EM Spectrum Showing Visible and IR Bands 33
Figure 20. EM Radiation Interaction with Materials 34
Figure 21. Atmospheric Transmission 35
Figure 22. Blackbody Spectra for a Set of Temperatures 36
Figure 23. Materials Used in Photodetectors 37
Figure 24. Bolometer Pixel 38
Figure 25. Bayern Pattern Filtration.....39
Figure 26. Image Sensing Steps 39
Figure 27. The CIE Chromaticity Diagram.....41
Figure 28. Digital Image Data Visualization.....42
Figure 29. SURF Detector.....45
Figure 30. SURF Descriptor.....46

Figure 31. Neuron Schematic 48
Figure 32. Artificial Neuron 49
Figure 33. Connections and Layers of ANNs 50
Figure 34. Transfer Functions of ANNs 51
Figure 35. Expected ROC Curves 54
Figure 36. CENETIX Tactical and Reachback Infrastructure 56
Figure 37. Subnets under TNT-MIO experimentation 56
Figure 38. Proposed Scheme 58
Figure 39. Terrestrial and Satellite Network 59
Figure 40. AOI in STK 60
Figure 41. Assets Used in the Simulation 61
Figure 42. Instance of the Object Browser 62
Figure 43. Satellites in Simulation 63
Figure 44. Orbit Parameters for Imaging Satellites 63
Figure 45. FOR and FOV for the Imaging Satellites 64
Figure 46. Basic UAV Parameters 65
Figure 47. Wave Relay Transmission and Antenna Parameters 66
Figure 48. Qualnet Nodes Configuration Browser 67
Figure 49. Image Classification Scheme 68
Figure 50. Categories of Captured Images 69
Figure 51. Sample Images with Different Background 70
Figure 52. Original and Zoomed Images 70
Figure 53. Fusion Result Comparison from MATLAB and ENVI 71
Figure 54. Image Processing 72
Figure 55. Image before and after Histogram Equalization 73
Figure 56. Steps for SURF Features Extraction 74
Figure 57. Total and Ten Strongest SURF Features in an Image 75
Figure 58. SURF Features after Histogram Equalization 75
Figure 59. Medium Level Fusion of SURF Features 76
Figure 60. Steps for Image Classification with ANNs 77
Figure 61. ANN Topology during Trials 78
Figure 62. Early Stopping 79

Figure 63. Networked Swimmers....81
Figure 64. CodeMettle Management Tool Graphics....82
Figure 65. Wireless Mesh Links of the Participating Nodes....84
Figure 66. Image of Cube-Satellites in STK Scenario....85
Figure 67. Image of Cub-Satellite Links....86
Figure 68. Communications Relay and Imaging Cube Satellite Constellations....87
Figure 69. Wave-Relay Node Tracks Replayed in Google Earth....89
Figure 70. CENETIX Backbone Network Details via CodeMettle Dashboard....90
Figure 71. CENETIX Wave-Relay Mesh Network Details via CodeMettle Dashboard....91
Figure 72. Enabling Communications with Divers....92
Figure 73. Enabling Communications with a UGV....93
Figure 74. Image Classification Steps....95
Figure 75. Ten Strongest SURF Features for the Different Image Sets....96
Figure 76. Confusion Matrix and ROC Curves for Training and Validation....97
Figure 77. Confusion Matrix and ROC Curve for One Trial....98
Figure 78. Average Correct Classification Performance for the 10 NNs....99
Figure 79. Correct Classification Performance for Each of the 1000 Trials of the 10 NNs....99
Figure 80. MSE over 1000 trials....100
Figure 81. Cross-entropy over 1000 Trials....100
Figure 82. ENVI Classic Menu Bar....109
Figure 83. Images Shown in Different Displays....109
Figure 84. Define Displays....110
Figure 85. Ground Control Point Selection Window....110
Figure 86. Corresponding Points Selection....111
Figure 87. Saving GCPs....111
Figure 88. Select Warp and Base Image....112
Figure 89. Save the File....112
Figure 90. Registration in ENVI....113

THIS PAGE INTENTIONALLY LEFT BLANK

LIST OF TABLES

Table 1. Wave Relay Specifications 26
Table 2. Satellites Categories Based on Size 27
Table 3. PRISM Optics 30
Table 4. Technical Characteristics of FLIR C2 Camera 40
Table 5. Technical Characteristics of FLIR SC640 Camera.....41
Table 6. Confusion Matrix for Binary Classification Problem.....53
Table 7. Performance Measures for Binary Classification Problem.....53
Table 8. Description of Tests and Number of Inputs 78
Table 9. Datasets for Testing 94
Table 10. Overall Classification Results.....101

THIS PAGE INTENTIONALLY LEFT BLANK

LIST OF ACRONYMS AND ABBREVIATIONS

AI	Artificial intelligence
ANN	Artificial neural network
AP	Access point
AGI	Analytical Graphics, Inc.
AOI	Area of interest
ATR	Automatic target recognition
AUC	Area under the curve
BER	Bit error rate
BLOS	Beyond-line-of-sight
CCD	Charge-coupled devices
CDF	Cumulative distribution function
CENETIX	Center for Network, Innovation and Experimentation
CIE	Commission Internationale d' Eclairage
CMOS	Complementary metal oxide semiconductors
COI	Contact of interest
CSMA/CA	Carrier sense multi-access with collision avoidance
DEM	Data elevation model
DHCP	Dynamic host configuration protocol
EM	Electromagnetic
EMCON	Emission control
FP	False positive
FPR	False positive rate
FIR	Far-infrared
FLIR	Forward looking infrared
FOR	Field of regard
FOV	Field of view
GEO	Geosynchronous, or geostationary, earth orbit
HEO	Highly elliptical earth orbit
HTTP	Hypertext transfer protocol
HTTPS	Hypertext transfer protocol over SSL or secure

IFOV	Instantaneous field of view
IGW	Internet gateways
IR	Infrared
ISP	Internet service provider
ISO	International Standardization Organization
IR	Infrared
LEO	Low earth orbit
LWIR	Long-wavelength infrared
LOS	Line-of-sight
MANET	Mobile ad-hoc network
MEO	Medium earth orbit
MIO	Maritime interdiction operation
MIMO	Multiple-input multiple-output
MSE	Mean squared error
MSX	Multi-spectral
MWIR	Mid-wavelength infrared
NETD	Noise equivalent temperature difference
NIR	Near-infrared
NN	Neural network
NWDSS	Network decision support systems
NOC	Network operations center
OFDM	Orthogonal frequency division multiplexing
PDF	Probability density function
PRISM	Pico-satellite for remote-sensing and innovative space missions
QoS	Quality of service
RMA	Revolution in military affairs
RMS	Root mean squared
ROC	Receiver operating characteristic
SA	Situational awareness
SCG	Scale conjugate gradient
SIFT	Scale invariant feature transform
SWIR	Short-wave IR

STK	Systems tool kit
SURF	Speeded-up robust features
TNT	Tactical network topology
TP	True positive
TPR	True positive rate
UAS	Unmanned airborne system
UMS	Unmanned system
VLWIR	Very long-wavelength infrared
WMN	Wireless mesh network

THIS PAGE INTENTIONALLY LEFT BLANK

ACKNOWLEDGMENTS

First of all, I would like to express my sincere gratitude to my beloved wife, Anna, for her continuous support and care. She was always there for me and our family during the endless hours I had to spend at school, not to mention that she gave birth to my lovely third daughter, Maria-Adamantia, here in Monterey. Of course, I am also thankful to my other two daughters, Elissavet-Alexia and Spyridoula, for bearing my absence and making me proud of their efforts at school. I cannot forget my parents, Aristidis and Elissavet, for supporting me throughout my life.

I also have to express my appreciation to the Hellenic Navy and the Greek people for giving me the opportunity to study in this amazing academic environment at the Naval Postgraduate School. I hope they feel I did my best.

I would also like to express my profound gratitude to my advisors, Dr. Alex Bordetsky and Dr. Gamani Karunashiri, as well as Dr. Murali Tummala, for giving me the knowledge, insight, means, and freedom to accomplish this thesis. A special thanks goes out to Professor Charlie Racoosin. Furthermore, I could not forget to thank Steve Mullins, Eugene Bourakov, and Lieutenant Matthew Maupin for their help and support during my research. Sharing the CENETIX lab and having the opportunity to work with them was a great experience.

Of course, this journey started long before I arrived at the Naval Postgraduate School, and I owe my sincere gratitude to Dr. John Koukos and Dr. Georgios Kolostoumpis for believing in me and my ideas.

Last but not least, I would like to thank my writing coach, Noel Yucuis, for teaching me how to write a thesis and for making sure that the final result would meet the proper standards.

THIS PAGE INTENTIONALLY LEFT BLANK

I. INTRODUCTION

A. MOTIVATION

Homeland security and military operations depend heavily on timely, accurate recognition of friendly and hostile assets, or contacts of interest (COIs), to increase the level of situational awareness (SA) and facilitate decision-making. Generally, surveillance, battlefield monitoring, and target recognition are non-stop processes that involve several resources. These processes are a major concern throughout all kinds of operations and require the engagement of various types of sensors, such as radar, infrared (IR), and thermal. The combined use of these sensors is the key for accomplishing this highly important process. The platforms participating in such operations often have limited capabilities to perform stand-alone recognition of targets under any given circumstances. Therefore, collaboration between platforms is necessary. Fusion of various data collected from different platforms and a variety of dissimilar sensors enables the real or near real-time recognition of COIs.

Furthermore, the ubiquitous mobility of these platforms raises the challenge of uninterrupted and robust communications to facilitate data exchange. The need for continuous monitoring of available assets and exploitation of their capabilities in real time is more than obvious. Allowing the data value to expire could prove fatal. Consequently, we need combinations of flexible communication schemes as part of the system of systems. Such a system should exploit data gathered from networked assets in a timely manner and allow for the extraction of vital information in real or near real-time. Automating specific procedures within short processing times can increase effectiveness, especially for cases in which human operators' performance is not equivalent. Artificial intelligence (AI), machine-learning, and data-mining can support this idea, at least starting with well-defined procedures concerning structured decisions [1] and database exploitation. The more sensors we are able to operate and integrate into automated processes, the closer we will be to real-time information that covers any spots that would otherwise be blind due to lack of data exchange and exploitation.

Databases serve as assisting mechanisms for human decision-making processes. Although there are cases in which improper use of data, based on lack of integrity, might lead to wrong assumptions, in general, databases facilitate decision-makers. In our case, and for the scope of this research, it is impossible for a human operator to remember thousands of images of different types of vessels. Previous work from ship companies has shown that creating databases from such kinds of data accompanied by the appropriate metadata has proven crucial for recognizing COIs. The use of such data during operations has demonstrated significant results in the efforts of crews for target recognition by type or even by identity. Especially in the case of recognizing targets by type, the effective distance of personnel after a six-month period of training was doubled by the use of such data [2]. The downside of this process is that it requires significant time, resources, and personnel.

The implementation of an automated process that is specifically focused on the recognition of ship types or identities could prove crucial in the effort to increase SA. A similar concept that was implemented in the areas of face and fingertip classification and matching has proven beneficial. Feineigle, Morris, and Snyder [3] described the need for automatic target recognition (ATR) systems using imaging sensors and databases as well as the benefits of these systems for maritime domain awareness (MDA) in harbors. Our research further expands these ideas and presents the challenges of recognition in larger areas of interest (AOIs) through networking kinetic and non-kinetic platforms. In addition, we consider the need for extending these capabilities during night operations.

Another very important aspect of this research is that it considers implementing an appropriate level of automation in certain tasks and procedures to increase SA and improve the decision-making process. Some crucial features of this process include flexible networking solutions and automated asset monitoring to capture and disseminate data; these considerations are especially challenging in the littoral environment. Emphasis is also given to the automatic exploitation of this data to enable filtering and to focus only on targets that demonstrate characteristics of potential COIs. Technological advancements in sensor-imaging, processing speed, computer-vision, and machine-learning seem to support this idea.

Based on these concepts, this research—through simulation and experimentation in the focus areas of wireless mesh networks (WMNs), computer-vision, and machine-learning—emphasizes the apparent need for adopting new tactics, techniques, procedures, and doctrines in littoral water operations. Proliferation and imaging capabilities of unmanned systems (UMSes) and small satellites are factors we need to consider through this process. Networking and exploiting data from unmanned assets and dispersed sensors as well as adopting ATR procedures with certain levels of automation can increase SA and effectiveness in combat. Then, we can support decisions by providing the decision-maker timely access to the appropriate information.

B. RESEARCH QUESTIONS

The overall concept is a vision of a system that through distributed database centers aboard main units and wireless mesh technologies enhances SA and reduces decision-making cycles. Distributed management of littoral operations at the tactical level should provide flexibility and alternatives in this type of operation, in which timeliness of information and reduced decision cycles are of critical importance. In cases where geography permits, such as in Greece and the Aegean Sea, this concept could prove beneficial in a form of a system-of-systems for innovative tactical solutions in all kinds of military and homeland security missions. All the participating assets, from humans to unmanned systems, could become part of an ad-hoc network that contributes in multiple ways to current operations. Some of these solutions could include agile communication relays and planning, extension of coverage ranges for sensors, distributed lethality, as well as video and image streaming from multiple dissimilar sensors.

Since the scale of such a concept is beyond the scope of a single thesis, we are focusing the research in two main categories of questions that contribute to proving its feasibility. The first category of question is related to the capabilities of wireless mesh-networking and its potential use by maritime units with the additional functionality of distributed data centers and network operations centers (NOCs). The following questions fall under this category:

- Can we achieve flexible and robust wireless network schemes to extend sensor networks connecting human or machine agents on terrestrial or satellite networks in littoral waters?
- Is it possible by using mesh radio technology to develop and manage a robust, ad-hoc, and seamless network to facilitate near real or real-time data dissemination from networked imaging sensors?

The second category of question involves an automated process that takes advantage of distributed imagery databases. Solutions that could provide for ATR and the potential benefits of applying multi-sensor image fusion are explored. The following questions are relevant to this category:

- Does image fusion from dissimilar sensors provide better classification performance of potential targets than single sensors?
- What is an appropriate scheme to facilitate ATR through image fusion of networked sensors?

C. HYPOTHESIS AND EXPLANATION

We attempted to find answers for these questions by performing simulations and experiments as well as by capturing data in the field from multiple dissimilar sensors. First, wireless mesh networks were simulated. Then, quality of service (QoS) in terms of provided throughput, bit error rate (BER), and packet losses was investigated. Next, field experiments were analyzed to support our simulation results. These experiments tested Wave Relay performance, network-management feasibility, and innovative wireless-networking solutions for imagery data dissemination. Furthermore, two different cameras—both with color-visual and thermal recording capabilities—were used to capture images from the field. Although FLIR C2 and FLIR SC640 cameras had similar capabilities, the different analysis techniques for the images posed additional challenges, similar to those of real situations. Finally, fusion of the acquired images was evaluated in our ATR-implemented process. We sought to propose a simulation model that could work well, even if characteristics of the images were different.

Our hypotheses were that

- QoS provided by WMNs can accommodate imagery data dissemination.

- Fusion of images from dissimilar sensors will provide richer features to distinguish between different classes of ships in a highly cluttered and challenging littoral environment.

In the case that our hypotheses were proven correct, there would be a high value in finding ways to extend sensor networks that could contribute to, among other things, the ATR process of COIs in the operational environment of littoral waters. This means that we had to prove that this network would be resilient and capable of transferring in a timely manner the acquired data from heterogeneous platforms. We attempted to prove this concept by simulating the conditions and parameters of equipment that have already been tested through field experimentation. We also considered the overall benefits that the whole concept could bring to the operational doctrine of littoral waters since the proliferation of unmanned systems and small satellites with imaging and networking capabilities.

D. SCOPE AND LIMITATIONS

This thesis sought to explore the feasibility and advantages of combining the data from similar or dissimilar sensors aboard platforms in and out of mobile ad-hoc networks in a littoral environment. In such a challenging environment, the speed and accuracy of information obtained plays a vital role in the decision-making process of the various missions assigned to military and homeland security forces. Inevitably, we sought for real or near real-time data transfer and exploitation by classifying the obtained data from the available sensors. Our intention was that the methods and processes should not limit the use of certain sensors but help find ways for exploiting the available data for fusion, no matter the source.

Fusion methods can be applied in several ways and in different stages of such processes while the sources can be either passive or active sensors. In this thesis, only passive means for obtaining images were exploited, specifically for fusion of color-visual and thermal sensors in early or late stages of the proposed classification process. Additionally, we limited our research to a binary classification problem of distinguishing between sailing and power boats by type from the images captured in the field. This limitation did not guarantee that the techniques used would be directly applicable for

classifying other categories of objects or for using different combinations of sensors. However, special care was taken, so the collection of images could address the challenges of classifying ships in a littoral environment.

Although the sensors used for the research were not of the type that will be used in a tactical environment, the transferring capability of the images was used to derive results for the relative research questions. The simulations of the mesh network were conducted with inputs as close as possible to equipment already in use while the Center for Network, Innovation and Experimentation (CENETIX) provided the opportunity for evaluating and assessing the obtained results.

E. RELATED WORK

Recent advancements in technology show that Cebrowski's vision for network-centric warfare, which connects not only platforms but also individual fighters, has become a reality. This revolution in military affairs (RMA)—combined with the proliferation and advancement of UMSes that are replacing human agents in the battlefield—has slowly changed not only how but more importantly who fights, as argued by Singer [4].

This evolution has no meaning if we are unable to support the decision-making process in the highly mobile and fluid environment of networks formed by human and machine agents. Iapichino et al. proposed a hybrid use of satellites and WMNs to support broadband communications in areas with no infrastructure [5]. The proposed scheme offered a viable solution for establishing reliable communications between various mobile nodes in emergency situations and was based on the IEEE 802.11s standard [6], [7], [8]. Additionally, Bordetsky and Dolk introduced the concept of a network decision support system (NWDSS) [9], which connected available nodes through wireless ad-hoc networks to aid the decision-making process. Gerla, Lau, and Oh [10] built upon the same concept by proposing the use of content-centric networking (CCN) when emergency wireless ad-hoc networks are needed on the battlefield. A hierarchical network structure model in the battlefield is depicted in Figure 1. In this way, efficient network resource management—among other crucial characteristics such as security and

scalability—was achieved for mobile ad-hoc networks (MANETs). Especially in the complex and challenging environment of littoral waters, the aforementioned evolutions are providing new insight into updating current doctrine, as mentioned by Bordetsky, Benson, and Hughes [11].

Figure 1. Structure of a Hierarchical Mesh Network Model in the Battlefield

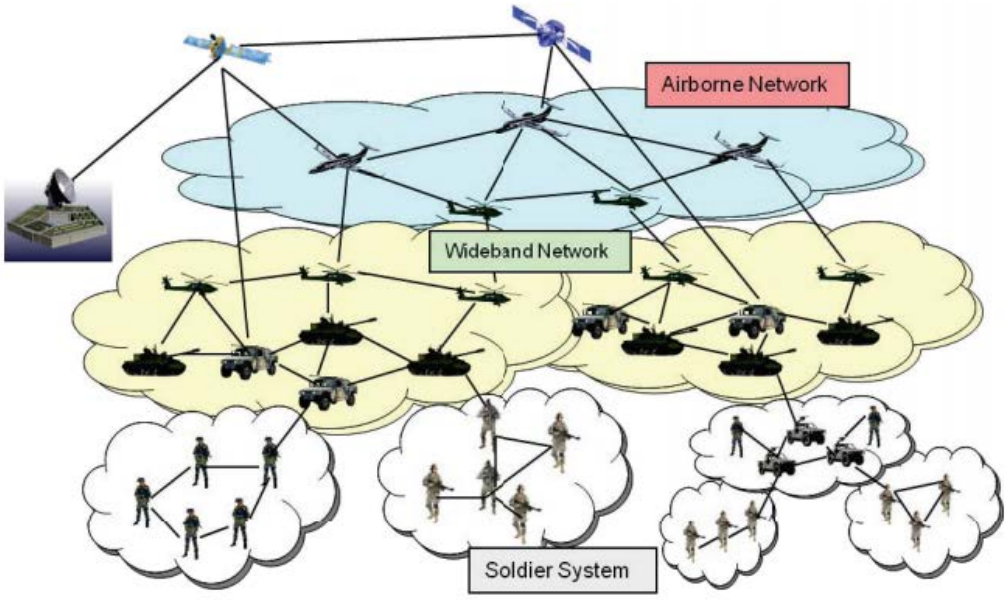

This structure model shows how group-based mobility can facilitate tactical and emergency operations. Source: Oh, Lau, and Gerla, "Content Centric Networking in tactical and emergency MANETs," 2010.

Distributed network operations centers (NOCs) aboard major units or ground stations are considered crucial to efficiently managing these highly kinetic nodes and the data acquired in the field. Experience on the battlefield as well as research and experiments by CENETIX have proven that using such applications could greatly enhance SA. Effort in this direction, including the CodeMettle ecosystem and dashboard for network management and monitoring (see Figure 2), has demonstrated very promising results [12], [13].

Figure 2. Network Operations Ecosystem and Dashboard from CodeMettle

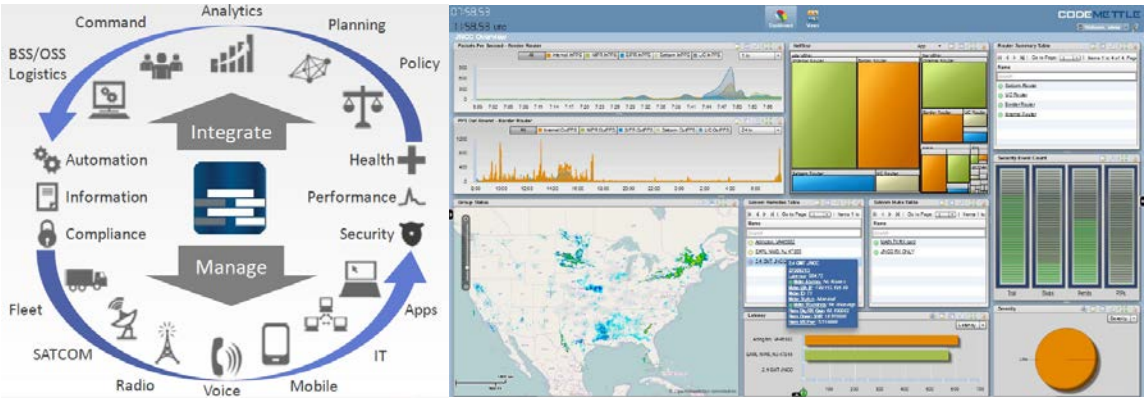

The ecosystem and dashboard from CodeMettle demonstrates how network management can contribute to decision making by converging vital information in a dashboard and applying the necessary level of automation. Source: CodeMettle, LLC, "The CodeMettle Ecosystem for Network Management in support of the DOD's NMS convergence efforts," 2015.

Given the fluid nature of these formed networks and the need to support traditional decision-making models, such as Boyd's observe-orient-decide-act (OODA) loop [14], [15], new challenges have emerged in monitoring systems since the proliferation of unmanned airborne systems (UASes) and small satellites. Spitzer, Kappes, and Boker [16] recognized this need for interoperability, automatic dissemination, and exploitation of data derived from systems deployed in the operational theatres. Their proposed model for tasking, collecting, processing, exploiting, and disseminating data provides insight into the effective fusion of data obtained from intelligence, surveillance, and reconnaissance (ISR) missions and networked assets. Mesh networks can be one of the means to achieve this goal as they provide low probability of detection, high throughput, the flexibility to override challenges posed in littoral environments, distributed lethality [17], and agile emission control (EMCON) [18].

In such a complex environment as the modern battlefield, automating procedures in which computers perform better than humans is necessary. One of the procedures that contributes to SA and target allocation is ATR. Research in the field of ATR has produced only partial solutions—with certain limitations—because the concept is complex and requires application in greatly diversified environments and conditions.

Several attempts have been made to design and develop ATR procedures that could support classification of COIs. Menon, Boudreau, and Kolodzy [19] introduced such a process to classify naval targets from imagery captured by inverse synthetic aperture radar. Features were extracted from the images and classified using neural networks. Additionally, Alves, Herman, and Rowe [20] tried another approach to classify forward-looking infrared (FLIR) images of ships using neural networks that were trained with models of ship classes of various aspects and scale-invariant moments as features. In other attempts for all-aspect ship recognition using IR images, the importance of role, range, and aspect angle was described [21], [22],. Although these works demonstrated good results of more than seventy percent of correct classification, image processing methods used were not always automated [22], and the training and testing processes were time consuming .

Feineigle, Morris, and Snyder [3] seemed to overcome the aforementioned problems by introducing the classification features of scale invariant feature transformation (SIFT), local interest point detection, and descriptors of optical imagery. In this way, features that compared in the classification process were invariant to scale and rotation and partially invariant to illumination and aspect. Furthermore, introduction of speeded-up robust features (SURF) [23], which were mainly used in matching problems in computer vision, demonstrated better and faster results in the feature-detection process.

Our approach in the proposed ATR process tried to take advantage of the SURF characteristics for real-time classification of ships. Furthermore, we considered that any proposed scheme should be applicable to a system of multiple dissimilar or similar sensors. For this reason, different cameras were used for the collection of the images for this experiment. The use of fused multi-spectral infrared (IR) and visual images were also tested—as previous work has proven that fusion results in images that provide additional information even at night [24].

F. SIMULATION AND EXPERIMENTATION STEPS AND TOOLS

The method we used in this research was quantitative experimentation using computer simulations, experiments, and data collection in the field in an attempt to simulate the conditions and stages of a conceptual model for ATR through mesh tactical networking of participating nodes. Evaluation and analysis of results from field experiments conducted under CENETIX were used to support specific parts of the concept. The steps in this thesis included the following:

- Simulating a wireless hybrid mesh network in a littoral environment using the Systems Tool Kit (STK);
- Analyzing the communication links by studying the physical layer of the network in STK;
- Analyzing the network from the MAC layer and above with QualNet;
- Evaluating the QoS provided by the network to support video streaming and imagery data dissemination;
- Analyzing CENETIX field experiments;
- Capturing imagery data from multiple dissimilar sensors (visual and thermal) in the field; and
- Evaluating multi-sensor image fusion for ATR by using computer-vision and machine-learning techniques.

Various software tools were employed to meet the objectives and the standards of our experiments and simulations. Descriptions and characteristics of STK, QualNet, and MATLAB, some of the main tools utilized in this thesis, are described in the next subsections.

1. Systems Tool Kit

STK is physics-based software released by Analytical Graphics, Inc. (AGI). Its simulation capabilities span land, sea, air, and space environments where various assets and attached sensors can be modeled and displayed. The software automatically calculates spatial relationships, such as line-of-sight (LOS), among the various platforms and nodes. The final product after implementing desired properties can be simulated for

specified time intervals in both two and three dimensions (2D and 3D). Additionally, images and video can be recorded during the simulations with the available tools [25].

Figure 3. Systems Tool Kit

Adapted from "Systems Tool Kit version 10," http://blogs.agi.com/agi/2012/11/15/systems-tool-kit-version-10-is-here/, and "System Tool Kit – Because we model more than just satellites.," http://blogs.agi.com/agi/2012/07/25/systems-tool-kit-%E2%80%93-because-we-model-more-than-just-satellites/

The most important advantage of STK is the variety of missions and systems that it can simulate. STK can even help the user simulate and evaluate a system-of-systems and its desired or researched topology. Some modules that interoperate with STK to evaluate the simulations include MATLAB, QualNet, and ArcGIS. These additional modules contribute to a more thorough analysis and detailed simulation. After detailed parameters or snippets of code are imported into STK, data elevation models (DEMs) and maps can be imported, and the network's performance can be examined beyond link budgets.

Figure 4. STK Objects

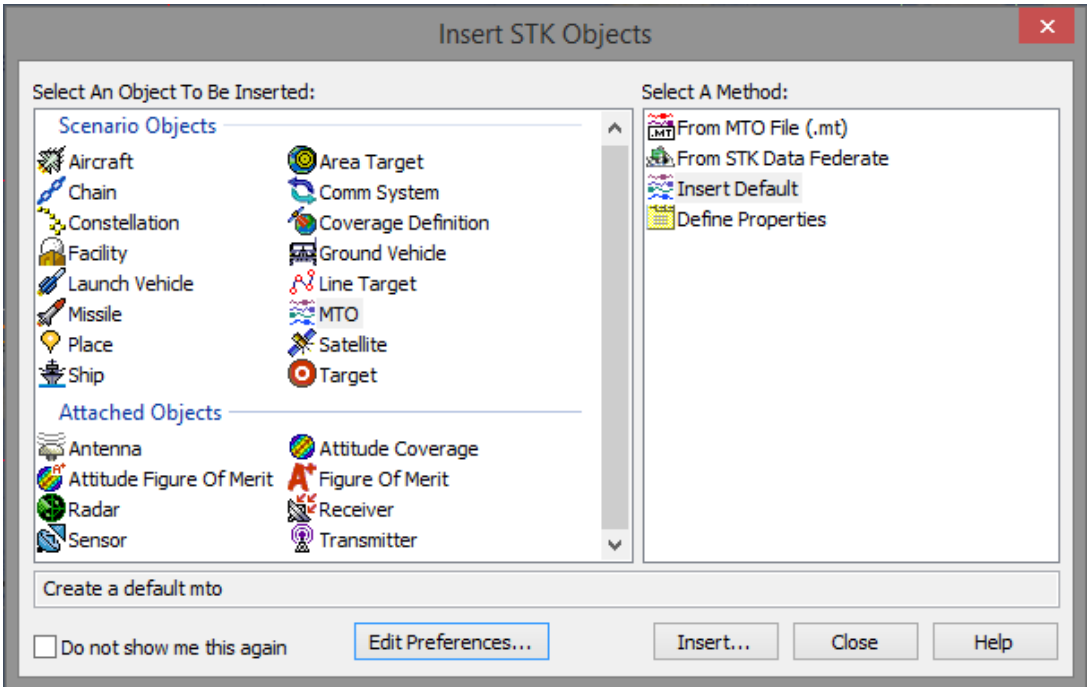

The STK objects available as they appear on the relevant pop-up window when insert of a new object is selected.

STK version 11, whose release is planned for January 2016, could contribute in a more thorough analysis for our simulation. Volumetric, EO/IR, and aviator capabilities, which will be part of the new version, could provide extra, useful details in our analysis above mesh network one.

2. QualNet

The QualNet interface is one of the off-the-self products that can interoperate with STK as an add-in module. It offers a network-modeling platform to plan and test a communication network's performance while taking advantage of the various kinetic and non-kinetic models, linking budget calculations, and augmenting visualization of STK. Hence, its use offers a more complete illustration of how network performance affects overall mission planning and execution [26], [27]. This interface allows the incorporation of all STK constraints, antennas, propagation loss, atmospheric absorption, as well as terrestrial and custom models for the purposes of network analysis. The exchange of data

between the QualNet and the STK model and objects results in a more thorough analysis by combining the advantages of both tools. During the QualNet analysis and whenever a communications link is established between the wireless nodes, the combined interactions and inputs/outputs are dynamically generated (see Figure 5).

Figure 5. QualNet/STK Interaction Flow

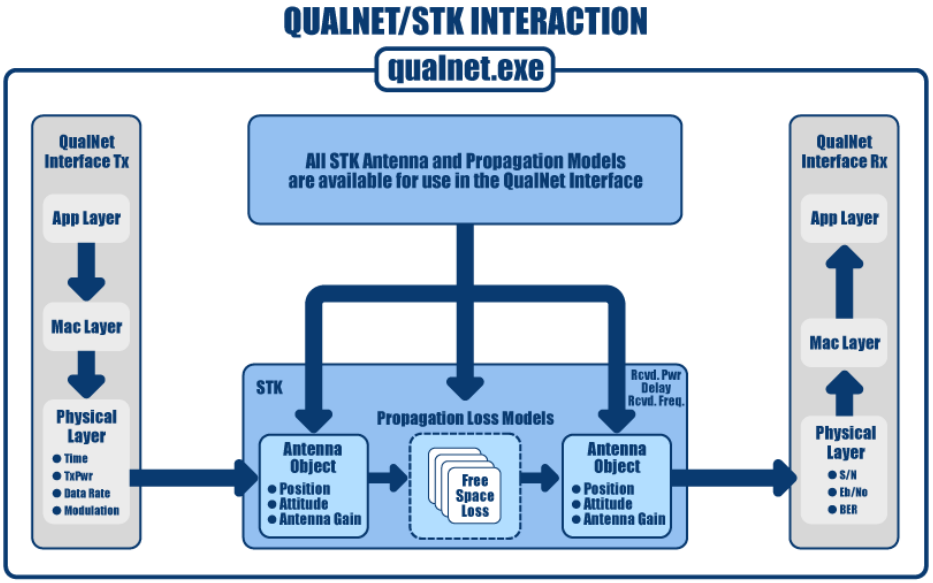

Source: "STK 10 Help," http://www.agi.com/resources/help/online/stk/10.1/

The procedure to install and integrate the Qualnet add-in in STK proved rather tedious but was finally achieved after following the steps described in QualNet and STK communication troubleshooting and installation and in a suggestion by Schlatow and Lefherz [28]. The steps to run QualNet and obtain its results after successful integration are shown in Figure 6.

Figure 6. QualNet/STK Interaction Flow

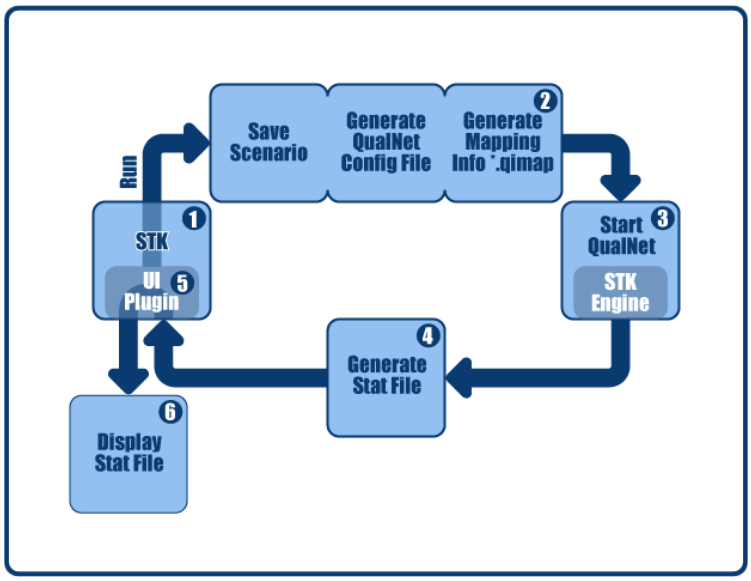

Source: "STK 10 Help," http://www.agi.com/resources/help/online/stk/10.1/

3. MATLAB

MATLAB is a high-level language that offers a variety of toolboxes and an environment for programming, numerical computation, and visualization of processed data. MATLAB's built-in functions and tools provide support for a wide range of domains, from signal processing to aerospace. In this research, image processing, computer-vision, as well as the neural network (NN) toolbox were used to build an algorithm for the ATR of boat images captured by color-visual and thermal sensors.

Figure 7. MATLAB Logo

Source: "Image Analysis with MATLAB," http://videreanalytics.ca/events/image-analysis-with-matlab-may-20-2015/

G. ORGANIZATION OF THE THESIS

This thesis is organized in five chapters in an effort to present and tie together different experiments and simulations for using mesh tactical networks of sensors efficiently for ATR. In Chapter II we present a brief theoretical background on mesh networks and relevant technologies, imaging sensors, and digital image representation, as well as the techniques and algorithms used in the image classification process. A proposed simulation model for the ATR through a hybrid mesh network is proposed in Chapter III along with a thorough explanation of the steps that were followed for the experiments and the simulations. The results derived from this research and their analysis are presented in Chapter IV. In Chapter V, conclusions from the results and potential benefits in the modern battlefield are discussed as well as recommendations for future work in the area of our research.

THIS PAGE INTENTIONALLY LEFT BLANK

II. THEORETICAL AND TECHNICAL BACKGROUND

This chapter provides a brief background of the equipment, concepts, techniques, and procedures used in the simulations and experiments for accomplishing this research.

A. SIMULATING MANET AND MESH NETWORKS IN MARITIME LITTORAL ENVIRONMENT

Simulation has been proven highly beneficial as it can support and assist in the thorough and detailed planning of an exercise or experiment with a profound cost benefit. Additionally, while resources are often limited, simulations can provide insight, results, and evaluation for large-scale scenarios. In the case of mobile ad-hoc networks (MANETs) and wireless mesh networks (WMNs), simulations can be used to predict performance. Furthermore, they can calculate or provide insight into the necessary link margins or antenna gains needed to improve the performance of certain links. Finally, when simulation results are compared with those from actual field experiments or real operations, they can provide patterns and insight for further research and development of new ideas and techniques.

1. Wireless Networks

Wireless networks are based on various technologies regulated by IEEE standards. Although they can provide short-distance communications with technologies like Bluetooth, wireless networks can also support long-range communications up to 30 miles or more depending on the antennas used. The most popular wireless technologies are Wi-Fi and WiMAX, under IEEE 802.11 and IEEE 802.16 standards, respectively. Via mobile WiMAX, kinetic nodes can connect with broadband communication channels using spread spectrum techniques, such as orthogonal frequency division multiplexing (OFDM), and can achieve data rates of up to one gigabit (Gbit) per second (s) [6]. The quality of service (QoS) provided can simultaneously support video streaming and voice traffic over the same channel [29]. Under the IEEE 802.11s standard, peer-to-peer nodal relationships for mesh networking allow for self-forming and self-healing characteristics [8]. In Figure 8, a basic mesh topology is depicted as well as the possible mesh paths.

Figure 8. Basic Mesh Topology

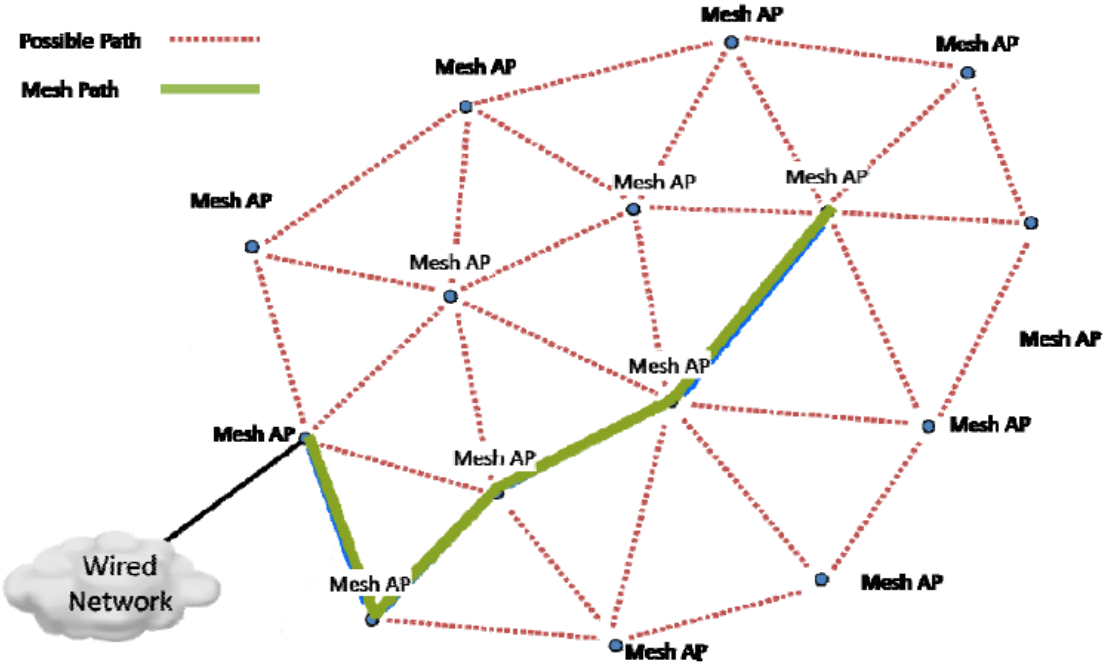

Source: [8] J. Henry and M. Burton, "802.11s Mesh Networking," CWNP Enterprise Wi-Fi Whitepaper, November 2011.

a. MANETs

MANETs are networks formed by devices that communicate with each other within link range and bandwidth constraints, without the underlying need of any infrastructure, base stations, or network configuration. Link range depends greatly on the frequency used and the rest of the characteristics that form the wireless transmissions, for example, RF modulations or power output. Each mobile node of these networks acts as both a terminal and a router that forwards any received data to the rest of the nodes within range. Obviously, determining which nodes are contributing to the network is a highly dynamic procedure as MANETs are decentralized networks. For this reason, all network activity, topology discovery, and message delivery are individually controlled by each node [7], [30], [6]. Types of nodes that can be networked in specific applications are shown in Figure 9.

Figure 9. Assets and Agents

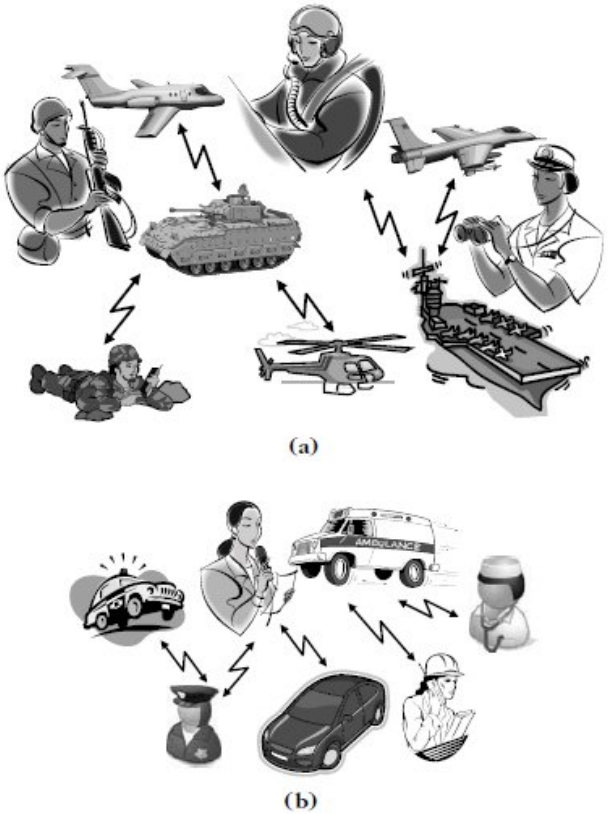

Examples of assets and agents that can be networked through ad-hoc networks in military (a) or Humanitarian assistance and disaster relief (HA/DR) applications (b). Source: [31] David Munoz, Frantz Bouchereau Lara, and Cesar Vargas, "Ad hoc and Sensor Network Scenarios," 2011, http://www.eetimes.com/document.asp?doc_id=1279149&.

Different techniques and protocols can be used for forwarding and relaying data and packets via MANETs. During routing, the messages propagate along an existing determined path, hopping from node to node until they reach the intended destination. In case a portion of the path breaks during the hopping process, the network finds a way around—illustrating its self-healing characteristic—via the remaining available links. Determining viable and robust paths in such networks is, therefore, a great challenge. In certain cases, packet losses inevitably occur [31]. A variety of factors influences these highly mobile and fluctuating networks, and routing protocols have to compensate for any of these issues. Continuous and unpredicted changes in network topology, power constraints, wireless link quality, path losses, and interference are some of these factors [30].

Three categories of routing are used by mobile routers in wireless, multi-hop networks such as MANETs and WMNs. These include table-driven, or proactive, routing; on-demand, or reactive, routing; and hybrid routing, a combination of the two former categories [32]. There is one primary difference between the two main categories of routing. In proactive routing, there is a requirement that routing information is stored by all routers, even for those that are inactive. Conversely, in reactive routing, only the routing information from active nodes requires storing [32], [33], [34]. Because each node in mobile ad-hoc networks acts simultaneously as a host and a router and due to the continually changing nature of nodes, hybrid protocols often provide better performance [35].

Despite the problems that these networks face, their use is rapidly proliferating, primarily because existing applications offer flexibility and reasonable ranges and capacities. Thus, MANETs and WMNs can be used in a variety of cases when the underlying infrastructure requires extension, it has been destroyed, or it does not exist at all. Humanitarian assistance and disaster relief (HA/DR) as well as military operations are such cases. These circumstances, especially military operations, require low probability of interception (LPI), high reliability, low latency, and resolution of security issues, all need to be achieved [30].

b. Wireless Mesh Networks

WMNs are a specific type of the aforementioned MANETs. Therefore, WMNs inherit the MANET attributes of self-discovery, self-organization, self-configuration, and self-healing [7]. The difference that appears in WMNs is that part of the nodes can remain stationary or carry advanced capabilities. Therefore, there is the potential to interconnect with existing networks through gateways that coexist with the mesh routers. The mesh in WMNs directly relates to the fully connected topology shown in Figure 10.

Figure 10. Network Topologies

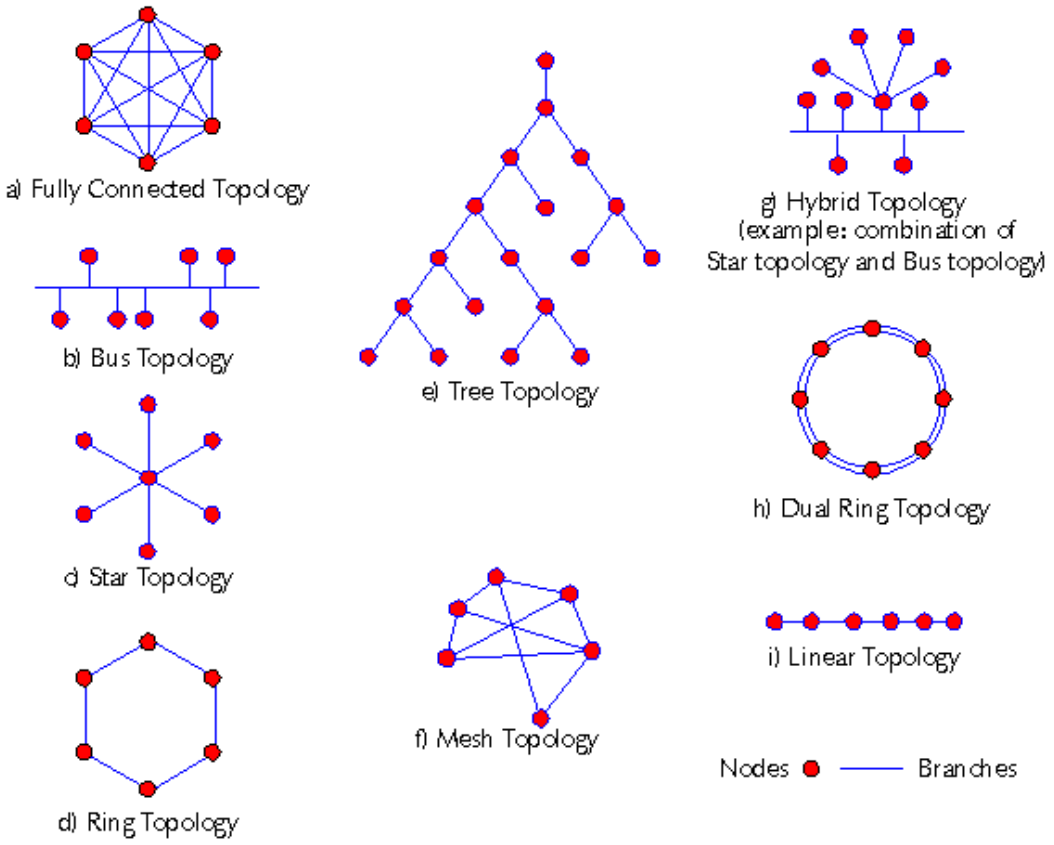

Source: "Network topology," http://homepages.uel.ac.uk/u0322392/top.html.

In actual implementation, though, a fully connected mesh is difficult to maintain as these networks are characterized by high mobility that involves nodes dynamically entering and exiting the network. Nevertheless, the participation of nodes as Internet gateways (IGWs) shows great potential for the formation of extendible and highly kinetic broadband Internet networks in locations where no infrastructure is present. IGWs can provide interconnection among such networks and existing terrestrial, satellite, or mobile Internet networks, such as 3G, 4G, or even 5G, and may extend connectivity in areas out of coverage (see Figure 11). Moreover, the use of low earth orbit (LEO) satellites in mesh networks can reduce latency in medium- and long-distance communications [36]. Additionally, connectivity without Internet access can be maintained between the networked assets, even when the infrastructure malfunctions or the IGWs are out of reach.

Figure 11. Samsung's Global Internet Access Satellite Network

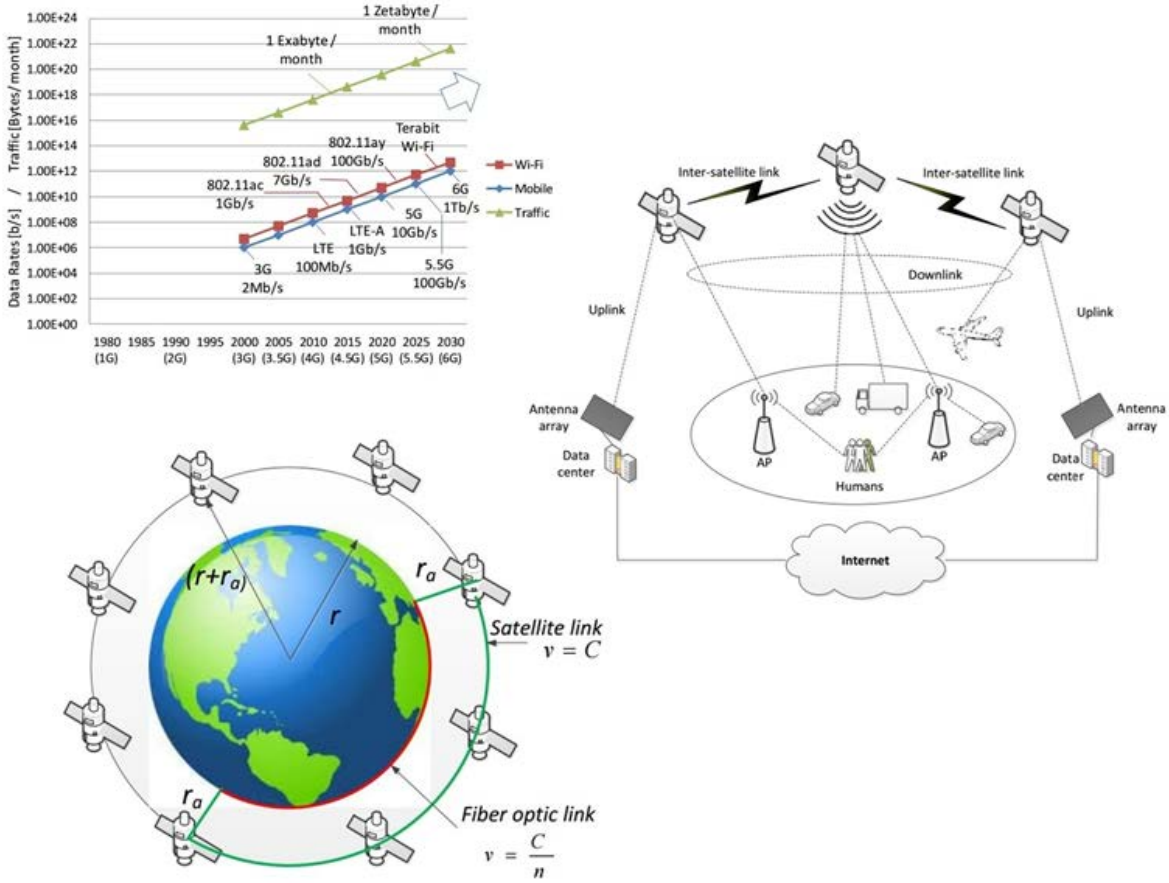

Samsung's proposal involving 4,600 low earth orbit (LEO) satellites for global Internet coverage. Adapted from D. Borghino, "Samsung's giant satellite network could enable high-speed Internet access across the globe," 2015, http://www.gizmag.com/samsung-satellite-network-Internet-access/38971/

c. Operational Advantages of Wireless Mesh Tactical Radios

The operational advantages gained from the use of mesh tactical radios, as proven in several CENETIX field experiments, are briefly described below:

- No infrastructure is needed.
- Immediate interoperability between platforms of different branches with no other equipment is common.
- High throughput exists to accommodate simultaneous video, data, and voice communications.
- They are easy to transfer in the field.

- Versions of man-portable devices allow for human agent nodes as part of the network.
- Security is embedded.
- They transmit low power and, thus, LPI.
- They allow for legacy-radio tethering.

From all the advantages that such systems demonstrate, we see that mesh tactical radios are appropriate for teaming up small ad-hoc groups of highly kinetic manned or unmanned systems and human agents in the battlefields. Communications of this type can facilitate agile EMCON plans and offer ad-hoc solutions when traditional means of communication are unavailable or deemed inappropriate for tactical use.

2. Wave Relay MANET Nodes

Nodes that are connected through the Wave Relay MANET become part of a secure mesh network. The patented wireless networking protocol by Persistent Systems, LLC supports the connectivity of kinetic and non-kinetic nodes as well as the exchange of real-time data, video, voice, and other applications [37]. The following paragraphs present the capabilities of these radios (see Figure 12) as the simulations center on their performance in a littoral environment.

Figure 12. Wave Relay MANET Radio Solutions

Quad radio router and man portable units Gen3 and Gen 4 Source: "Wave Relay MANET RadioSolutions,"http://www.oceanologyinternational.com/en/Exhibitors/191060/Steatite-Ltd/Products/666963/Wave-Relay-MANET-Radio-Solutions

a. Wave Relay

The Wave Relay system is a peer-to-peer wireless MANET network in which no server or master node exists. The nodes also serve as routers that establish and maintain the network even if one of them fails to communicate. The implemented techniques increase multicast reliability, maximize capacity over the RF spectrum under use, and minimize network control requirements. Unlimited devices can be part of the resulting highly scalable network as there is no hop limit. This rapid self-forming and self-healing network operates at the data-link layer, which is the second layer of the Open Systems Interconnection (OSI) seven-layer model, as shown in Figure 13 [6].

Figure 13. The ISO/OSI Model

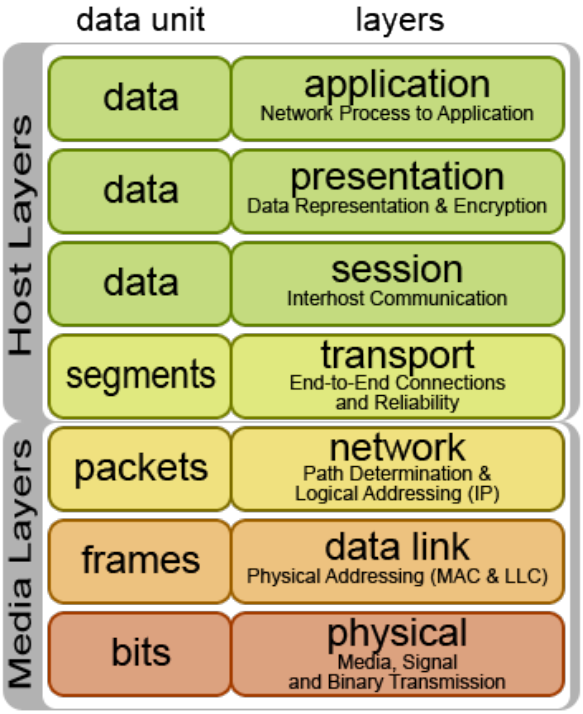

Source: "The Open Systems Interconnection (OSI) seven-layer model standardized by the International Standardization Organization ISO," https://commons.wikimedia.org/wiki/File:Osi-model.png.

Currently, the fifth generation of Wave Relay radios is ready for release and provides more advanced capabilities than the fourth generation that has already been used in CENETIX field experiments. For shared access coordination, the random access

protocol of carrier-sense multi-access with collision avoidance (CSMA/CA) is used as the basis for the wireless networks [6], [37]. Wave Relay uses a 3x3 multiple-input multiple-output (MIMO) technology and delivers high throughput of up to 150 megabytes per second (Mbps) in extended ranges. It is IPv4 and IPv6 compatible and includes a server with an integrated dynamic host configuration protocol (DHCP) [6]. The embedded cloud-relay technology makes it possible to bridge beyond-line-of-sight (BLOS) with line-of-sight (LOS) networks using the network layer, the third layer of the OSI seven-layer model, techniques, and protocols. In this way, distributed groups, as shown in Figure 14, smoothly participate in the network as if locally connected via Internet or private networks. Table 1 presents the basic specifications of Wave Relay along with some imported parameters from Systems Tool Kit (STK) to simulate objects.

Figure 14. Cloud Relay Groups

Source: "Cloud Relay," http://www.persistentsystems.com/persistent-systems-cloud-relay/.

Table 1. Wave Relay Specifications

3 x 3 MIMO TECHNOLOGY	Extended Range 150 Mbps of throughput Maximal Ratio Combining Spatial Multiplexing Antenna Detection
MODULAR RADIO	RF Modulations: OFDM (64-QAM, 16-QAM, QPSK, BPSK) 6W Transmit Power* Swappable Radio Modules/Radio Boards •RF-1000/RF-1100 - L-Band Frequency Range: 1350 - 1390 MHz* •RF-2000/RF-2100 - S-Band Frequency Range: 2200 - 2500 MHz† •RF-3000/RF-3100 - C-Band Radio in Development Software configurable bandwidths: 2.5 MHz, 5 MHz, 10 MHz, 20 MHz, 40 MHz TX/RX Operating Modes: All modes from SISO to 3x3 MIMO
RoIP	Legacy Radio Tethering Legacy Radio Detection USB Host / RS-232 Serial
VIDEO	HD-BNC Connection 3G-SDI & Composite Input Integrated HD H.264 Video Encoding/Decoding
GPS	3.3V Active Situational Awareness Cursor-on-Target Compliant 1 Second Updates
PTT / EUD	Dual Active PTT Channels End User Device (EUD) Data / Charging USB Host / RS-232 Serial HD Video Output
DATA	USB On-the-Go RS-232 Serial Ethernet HD Video Input
BATTERY	Low Battery Alert Standard Twist-Lock Connector
NETWORKING	Advanced multicast algorithms Seamless Layer 2 network connectivity Integrated serial-to-Ethernet capability Cloud Relay™ DLEP Certified IPv4 and IPv6 compatible Integrated DHCP server USB RNDIS Host and Device
SECURITY	Integrated Hardware Cryptographic Acceleration CTR-AES-256 Encryption HMAC-SHA-256 Authentication & Integrity Utilizes Suite-B Algorithms Cryptographically authenticated Over-the-Air Rekey and Key Zero FIPS 140-2 Level 1 Rechargeable 30 Day Hold-Up for Keys and Configuration Settings
PHYSICAL SPECIFICATIONS	1.5 x 2.6 x 4.7 inches / 38.1mm x 66mm x 119.4mm (NO BATTERY) 1.5 x 2.6 x 7.9 inches / 38.1mm x 66mm x 200.7mm (WITH BATTERY) 17.3 oz / 490.5 grams (NO BATTERY) 29.6 oz / 839.1 grams (WITH BATTERY)
MANUFACTURING & ENVIRONMENTAL	ISO 9001:2008 certified Manufactured to MIL-STD specifications IP68 Coated to meet MIL-C-64159 / MIL-C-53039A(2) standards Operating temperature: -40° to 85° C / -40° to 185° F

Source: "Wave Relay 5 Integration Unit," http://www.rugged-systems.com/products/radio-communications/manet-radio-solutions/wave-relay-5.html.

3. Types of Nodes

The types of nodes that can be part of a MANET or WMN are numerous and can extend from single human agents to unmanned systems and satellites. Some main characteristics and capabilities of the most important nodes are described in the following paragraphs. Satellites and unmanned systems can prove highly beneficial for these types of networks. They can assume multiple roles, acting as relays to extend the network and also as platforms for imaging or other types of sensors.

a. Small Satellites

In general, depending on their orbits, satellites fall under the categories of low earth orbit (LEO), medium earth orbit (MEO), geosynchronous or geostationary earth orbit (GEO), and highly elliptical earth orbit (HEO) [38]. Furthermore, if we consider the actual size of the spacecraft, satellites are also categorized as large, medium, or small, as shown in Table 2. During the last few years, there has been a focus on research and development of small satellites. Cube satellites, or Cubesats, usually with a mass of less than 100 kilograms (kg), are very promising because of their small size and low manufacturing cost. An advantage comes from their potential to be launched in groups from platforms other than the traditional rockets—and thus readily available.

Table 2. Satellites Categories Based on Size

Satellite Category	Net Weight	
Large	> 1000 kgr	
Medium	500 - 1000 kgr	
Mini	100 – 500 kgr	SMALL SATELLITES
Micro	10 -100 kgr	
Nano	1 – 10 kgr	
Pico	0.1 – 1 kgr	
Femto	< 100 gr	

Satellite categorization according to their net weight and size. Source: A. Bordetsky, "Micro and Pico Satellites in Maritime Interdiction Operations," 15th Int. Command Control Res. Technol. Symp. Track 2 Networks Netw, 2010.

Cubesats in particular have a volume equal to one liter, or ten cubic centimeters (cm^3) or 1U. They can also be combined to form bigger satellites by attaching multiple units together. In that way, 2U or multiple-U satellites can be constructed. Additionally, there are several kits available on the market that allow a do-it-yourself construction, as shown in Figure 15. Of course, their small size and, consequently, their payload limit their capabilities in terms of power, sensors, or antennas that can be mounted to them. Problems such as less precise orbital fidelity, limited orientation control, and imprecise pointing also limit their capabilities and make them prone to becoming debris. Since they are positioned in LEO, though, they need less power and demonstrate smaller latencies in communication. Other factors that should be considered are the revisit time, the coverage, the lifetime expectancy, the number and position of the ground stations, and the altitude within the range of LEO, which is roughly 200 to 2000 kilometers (km) [38].

Figure 15. Cubesats

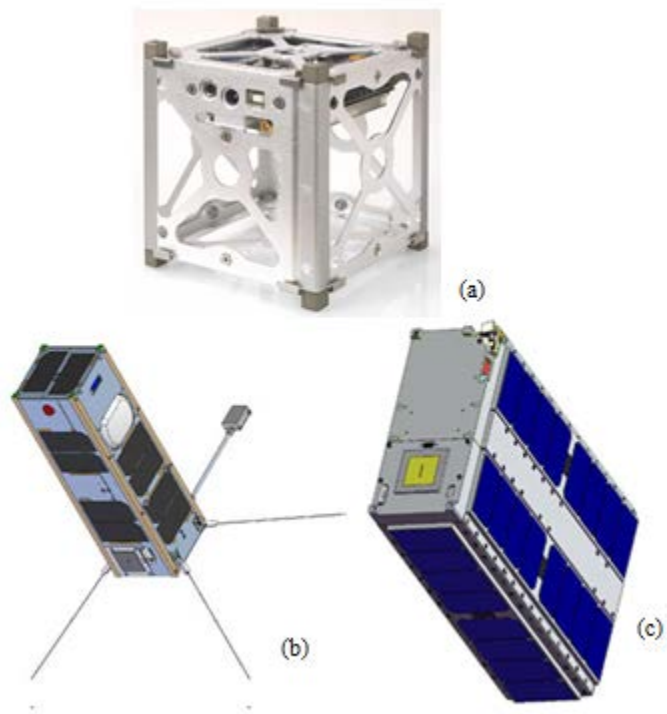

In (a) a home kit framework of a Cubesat is shown. Source: "Begin your CubeSat Mission with the CubeSat Kit," http://www.cubesatkit.com/. In (b) a 3U Cubesat and in (c) a 6U Cubesat are presented. Source: "CubeSat," http://space.skyrocket.de/doc_sat/cubesat.htm.

For the purpose of our STK scenario, we simulated the capabilities of an existing satellite. A Pico-satellite for Remote-sensing and Innovative Space Missions (PRISM), shown in Figure 16, was chosen. Its optical characteristics are presented in Table 3. The extensible boom, shown in Figure 17, allows for a ground resolution of 10 meters (m) per pixel from the 800 km altitude of its actual orbit. We altered our simulation parameters, such as orbit altitude and communication capabilities, to serve our simulation purpose of providing imagery data with an adequate ground resolution to detect small boats.

Figure 16. PRISM Nanosatellite

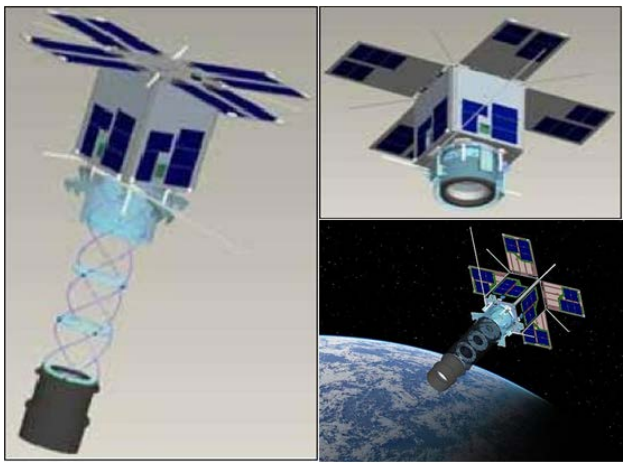

Theoretical illustration of the deployed PRISM nanosatellite in LEO and its extensible boom before and after it has been deployed Source: "PRISM," https://directory.eoportal.org/web/eoportal/satellite-missions/p/prism

Figure 17. PRISM's Boom

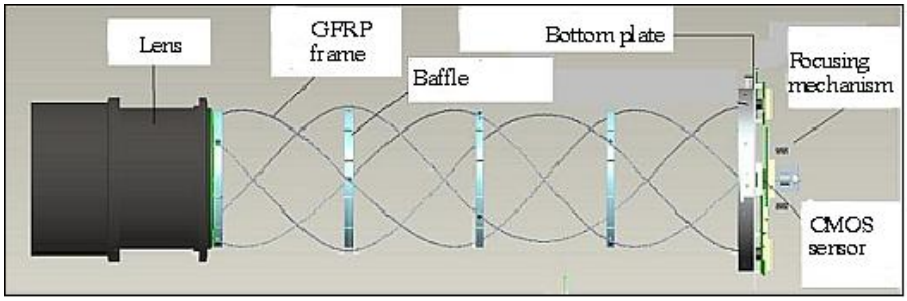

Components of the PRISM's extensible boom. Source: "PRISM," https://directory.eoportal.org/web/eoportal/satellite-missions/p/prism.

Table 3. PRISM Optics

Parameter	Value
Aperture of Lens	100mm
Focal Length	800mm
Wavelength (Min.)	380nm
Wavelength (Max.)	700nm
Rayleigh Limit	6.8μm
Pixel Size	4.7μm
Number of Pixels	1280×1024 (SXGA)
Size of Image Sensor	8.58×6.86mm
Ground Resolution	13.4m (theoretical)
Exposure Time	1.0msec

PRISM optics specifications. Source: "PRISM," https://directory.eoportal.org/web/eoportal/satellite-missions/p/prism.

b. Unmanned Systems

The use of unmanned systems is rapidly expanding in the commercial sector as well as in the armed forces. Various missions are assigned to such systems depending on their operational environments. Unmanned airborne systems (UASes), in particular, can potentially extend the capabilities of their mother platforms when deployed and controlled by them. Data that is fed back as well as network extension in the case of MANETs provide additional options and capabilities to enhance situational awareness (SA) on the battlefield. Furthermore, throwable and expendable nodes can also facilitate that purpose.

c. Other Nodes

As discussed previously, MANETs and WMNs can network various nodes and extend existing terrestrial or satellite networks. This concept can be used as an advantage especially in littoral environments to network manned or unmanned platforms, ground stations, and distributed link relays. Underwater systems or human agents could also become part of the network using floating platforms and wireless technologies as recently demonstrated by CENETIX experiments in the San Francisco Bay area in October 2015.

In this way, special and boarding operations can take advantage of MANETs to exchange images and messages, even with divers.

4. Network Operations Centers

Network operations centers (NOCs) or network management centers are specific locations from which management, control, supervision, and monitoring of networks can be performed [39]. The goal of this function is to support uninterrupted and robust accessibility in networked resources and applications to all subscribed assets by efficiently managing the available resources and security issues. Internet service providers (ISPs) operate such centers to enable visualization of the controlled and monitored networks as well as their statuses.

a. Network Decision Support Systems

The concept of a network decision support system (NWDSS) was introduced by Bordetsky and Dolk [9] to support agile and collaborative management of decision making when heterogeneous nodes are connected through wireless technologies. This concept offered a solution for enhanced decision making and SA in the modern battlefield. Since the proliferation of unmanned systems over the last fifteen years, this idea needs revision to address the challenges of highly kinetic platforms, especially in littoral waters. Timeliness in such environments is crucial, and the proposed sense-analyze-adapt-memory decision-making loop, shown in Figure 18, offers a team-centric solution.

Figure 18. NWDSS Decision-making Loop

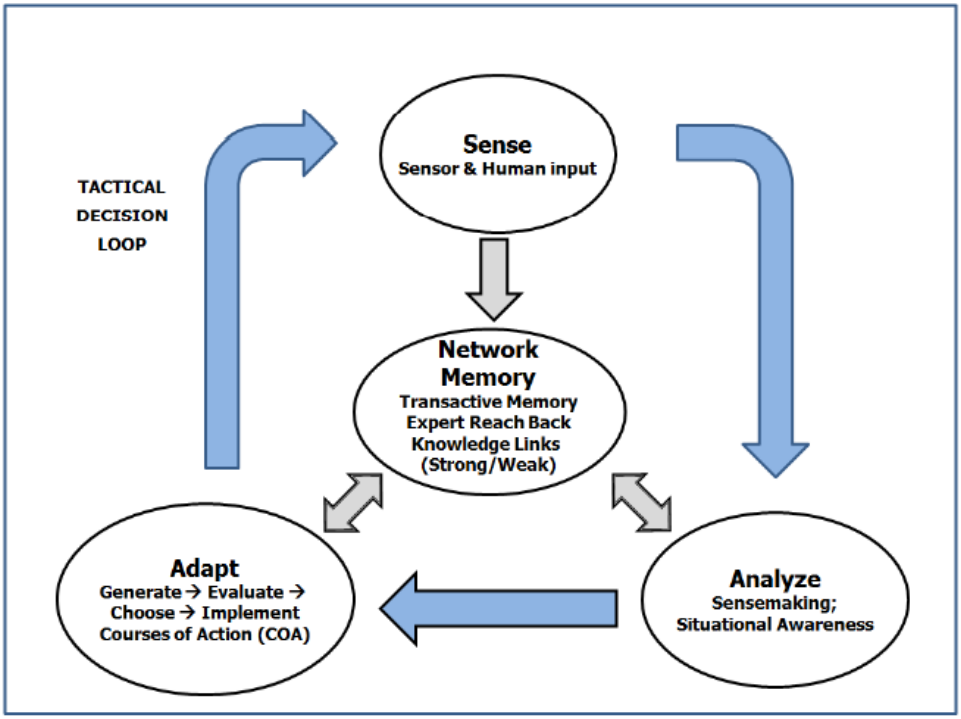

The Sense – Analyze – Adapt – Memory decision making loop. Source: Bordetsky and D. Dolk, "A Conceptual Model for Network Decision Support Systems," *Syst. Sci. (HICSS), 2013 46th Hawaii Int. Conf.*, pp. 1212–1221, 2013.

B. IMAGING SENSORS

Imaging sensors are widely used by armed forces in many applications. Various platforms as well as individual soldiers have been equipped with sensors covering a wide range of the visible and infrared (IR) spectrums. What led to this proliferation was the realization that these sensors were beneficial for SA enhancement and target recognition. During the day, they extend the capabilities of human eyes as well as support the ability of extracting additional information about the state of targets. For example, during daylight hours, IR sensors can provide information about operating equipment or incoming missiles as they capture thermal signatures otherwise undetectable by sensors operating in the visible range of the electromagnetic (EM) spectrum. Furthermore, during nighttime hours, IR sensors reveal thermal signatures when color-visual sensors become unusable. In the following subsections, we will briefly present the basic concepts and technologies used to capture and support the exploitation of that information.

1. The Electromagnetic Spectrum

To provide a better understanding of the differences between visible and IR imagery, we begin by investigating the EM spectrum. As Figure 19 shows, the visible region is only a small part of it the entire spectrum. Photoreceptors, or cones, of the human eye are sensitive only to colors in the visible spectrum [40] covering wavelengths 380–780 nanometers (nm) [41] .

While humans can only feel IR radiation in the form of heat, animals such as rattlesnakes can actually see that part of the spectrum. Using two different sensor types, one operating in the visible and the other in the IR region, it is possible to gather more information, depending on the prevailing conditions.

Figure 19. The EM Spectrum Showing Visible and IR Bands

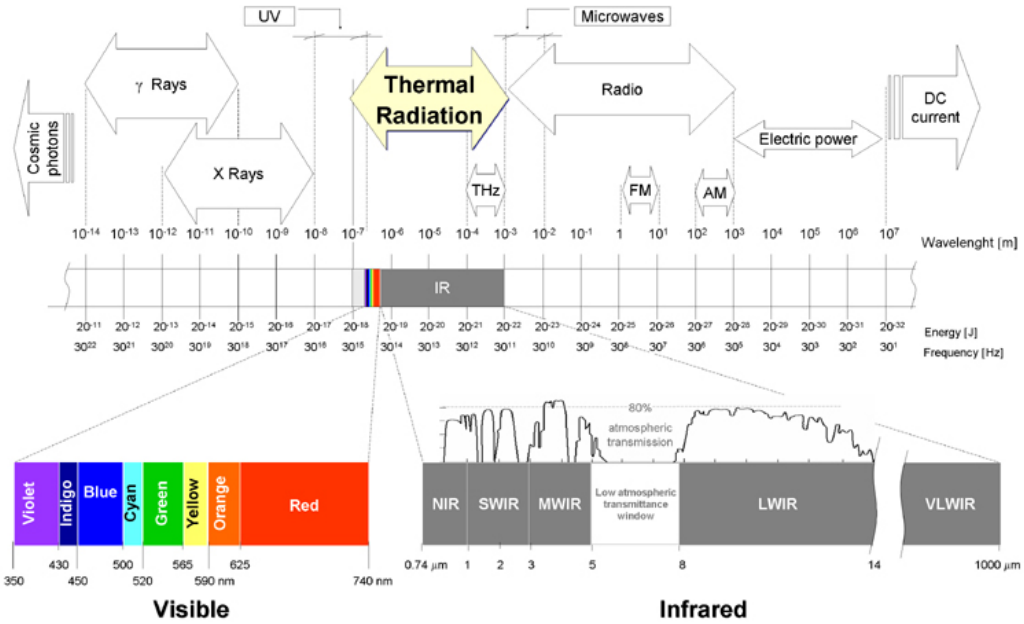

Source: "Fundamentals of IR Radiation," http://theses.ulaval.ca/archimede/fichiers/23016/apb.html

Based on atmospheric transmittance windows, discussed in the following subsection, the IR spectrum is further divided into near (NIR), short-wavelength (SWIR),

mid-wavelength (MWIR), long-wavelength (LWIR), and very long-wavelength (VLWIR), or far (FIR), infrared.

2. EM Radiation

Incident radiation can be transmitted, reflected, scattered, or absorbed, depending on the properties of the material it encounters, the frequency of the radiation, and the incident angle [42], as illustrated in Figure 20.

Figure 20. EM Radiation Interaction with Materials

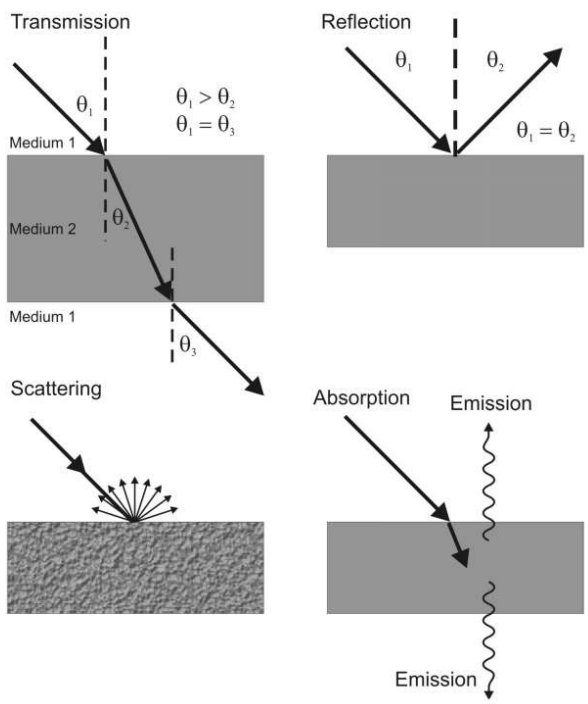

Source: "Electromagnetic Radiation (EMR)-Matter Interactions (Remote Sensing)." http://what-when-how.com/remote-sensing-from-air-and-space/electromagnetic-radiation-emr-matter-interactions-remote-sensing/ .

The distance that EM radiation can penetrate the atmosphere is determined by the wavelength. The study of incident radiation absorption is of special interest as it indicates the wavelength windows of radiation that can be detected by the appropriate sensors. The atmospheric windows from the MWIR of 3 to 5 micrometers (μm) to the LWIR of 8 to 12 μm, where transmissivity is higher, are the ones exploited by most of the IR sensors

(see Figure 21). Different sensors, which operate at distinct regions of the EM spectrum, generate signals based on the sensing mechanisms employed.

Figure 21. Atmospheric Transmission

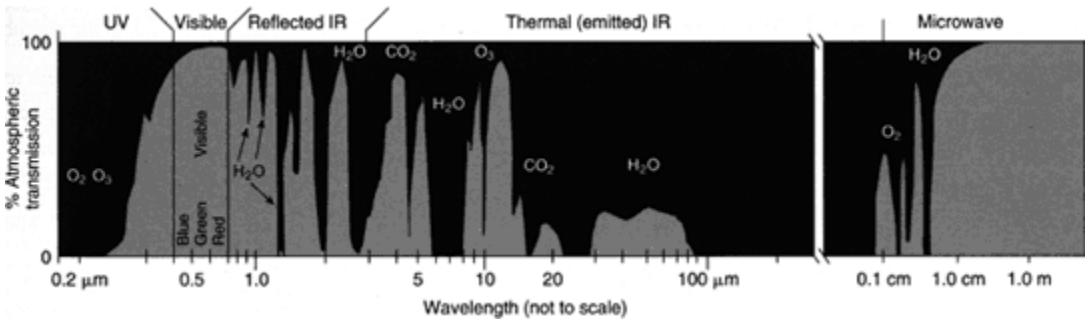

Diagram of atmospheric transmission as a function of the wavelength Source: "Remote Sensing," http://earthobservatory.nasa.gov/Features/RemoteSensing/remote_04.php.

3. Terms and Theory

In this section, some basic definitions and figures-of-merit are described to offer insight into the expected performance of the sensors used in this thesis research.

- The field-of-view (FOV) is the angle that can be viewed through an aperture.
- The instantaneous field-of-view (IFOV) is the angle that corresponds to each pixel of an array and measures the angular resolution of the detector.
- The noise-equivalent temperature difference (NETD) is a measure of the image noise level of an IR camera and represents the temperature change that results in a signal equal to the total root-mean-squared (RMS) noise.
- A blackbody is a totally non-reflective object that does not transmit incident radiation. Instead, it absorbs any incident radiation that strikes it at any wavelength. It turns out that good absorbers are also good emitters. According to Wien's displacement law [43], the maximum energy is observed at a wavelength that is inversely proportional to the temperature of the source blackbody. This statement can also be observed in the following equation and Figure 22:

$$\lambda_{\max} = \frac{2.898 \times 10^{-3} \left[m \cdot K \right]}{T}.$$

- Emissivity is defined as the fraction ε of the amount of radiation emitted from an object compared to that emitted from a blackbody at a given

temperature. It is given by a number between 0 and 1, in which 1 is the emissivity of a blackbody. The various values of ε for different bodies are given in tables, and sensors have to be adjusted accordingly before any measurements are recorded.

- Emittance is defined as the amount of energy emitted from an object per unit of time and per unit of area (W/m^2).

Figure 22. Blackbody Spectra for a Set of Temperatures

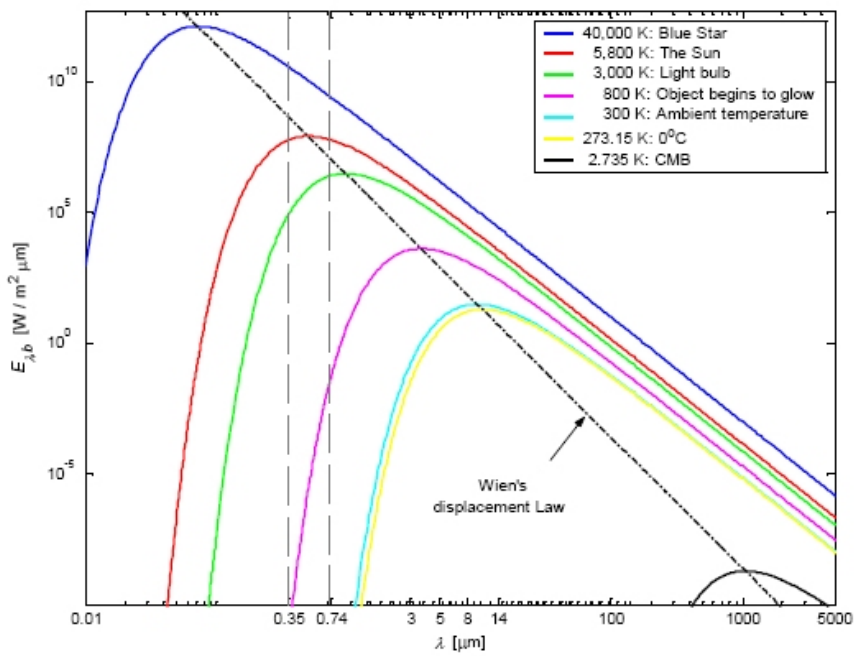

This graph illustrates blackbody's spectral radiant emittance according to Wien's displacement law as a function of wavelength λ plotted for different characteristic absolute temperatures. The relevant curves for non-blackbodies (gray bodies) would be of the same shape but of a different value according to ε. From this graph it becomes obvious that missiles will be most evident in 3–5 µm window, while humans in 8–12µm. Source: http://how-it-looks.blogspot.com/2010/01/infrared-radiation-black-bodies-and.html.

4. Imaging Sensors

The imaging sensors fall under two main categories: thermal sensors and photon sensors, or photodetectors. All the detectors under these categories respond to absorbed radiation.

a. Photodetectors

Photodetectors are further classified into photoconductors and photodiodes. Photoconductors, used in IR sensors, are semiconductor devices designed to detect radiated photons, the fundamental unit of EM waves. When semiconductors absorb photons, electrons in the valence band get excited and move to the conduction band [44], [45]. A signature is formed when an object reflects solar radiance or the object itself emits radiance. Figure 23 shows how different materials respond to wavelengths in the IR and visible spectra. These materials, based on their spectral characteristics, are used in the manufacturing of focal plane arrays

Figure 23. Materials Used in Photodetectors

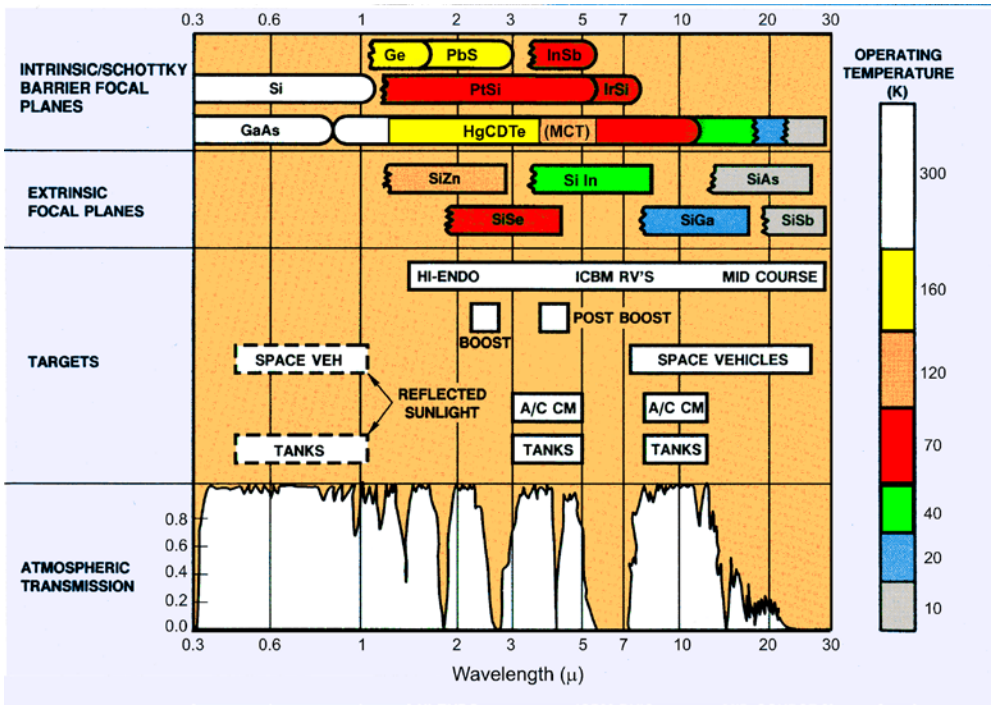

Source: R. Olsen C., "Remote sensing from air and space," SPIE, 2007.

b. Thermal Sensors

Thermal sensors operate based on temperature changes as IR radiation is absorbed. The temperature changes are subsequently converted into electric signals. Thermal sensors are further classified into thermoelectric, pyroelectric, and bolometric

sensors. In bolometers, which are thermally isolated resistors, a change in the temperature of the sensor will affect its resistance. The temperature coefficient-of-resistance (TCR) is used to quantify the resistance changes [41]. TCR is given in the following equation:

$$\alpha = \frac{1}{R}\frac{\Delta R}{\Delta T},$$

in which ΔR represents the change of the bolometer resistance triggered by the temperature variation ΔT, and R is the bolometer's resistance.

c. Focal Plane Arrays

In focal plane arrays (FPAs), the flux that enters the lens is focused on the plane where the array of the sensors is located. For the uncooled infrared imaging sensors, a 2D array of microbolometer pixels with defined spacing, referred to as the pitch, forms the thermal detector (see Figure 24). The changes in the resistance of these pixels provide the necessary information to produce an image from this thermal camera.

Figure 24. Bolometer Pixel

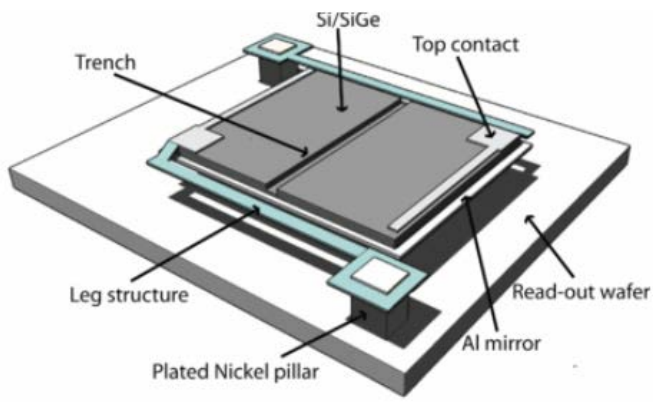

In the schematic drawing of the bolometer pixel, some key materials and parts are indicated. Source: F. Forsberg, A. C. Fischer, N. Roxhed, B. Samel, P. Ericsson, G. Stemme, and F. Niklaus, "Heterogeneous 3D integration of 17 μm pitch Si/SiGe quantum well bolometer arrays for infrared imaging systems," J. Micromechanics Microengineering, vol. 23, no. 4, p. 045017, 2013.

In visible image sensors, the two main categories for array composition include charge-coupled devices (CCDs) and complementary metal-oxide-semiconductors

(CMOSes). One of the patterns for generating color images is shown in Figure 25. In a CCD, photons accumulate on the sensors while in a CMOS, a photocurrent attracts additional electrons to the sensor [46], [44]. The steps involved for the final image by sensor type are shown in Figure 26.

Figure 25. Bayern Pattern Filtration

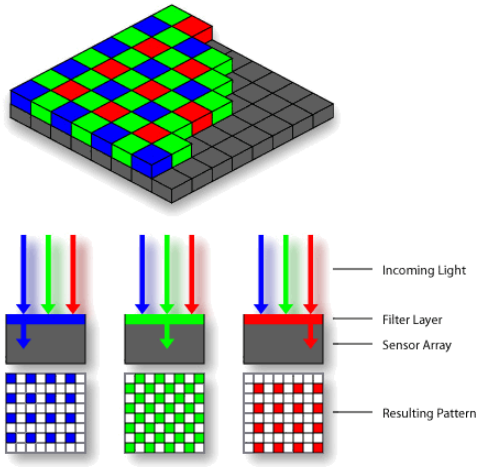

Traditional CCD / CMOS sensor. Source: "BayerPatternFiltration," https://commons.wikimedia.org/wiki/File:BayerPatternFiltration.png.

Figure 26. Image Sensing Steps

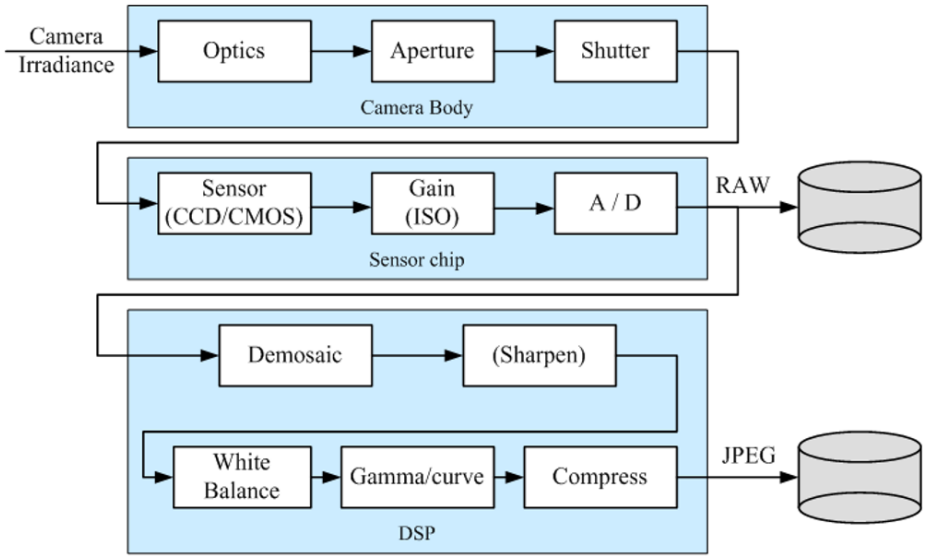

Source: R. Szeliski, Computer Vision : Algorithms and Applications, vol. 5. Springer, 2010.

5. Sensors Used

Two different cameras, a FLIR C2 and a FLIR SC640, were used for collecting images, both hosting dual sensors in the IR and visible spectra. Some of their main characteristics are presented in Tables 4 and 5, respectively. The IR sensors in both cameras comprise uncooled microbolometers in the LWIR region of the IR spectrum. The big difference comes from the IFOV of the cameras, in which we see a significant difference from 0.33 mrad to 11 mrads and, thus, a big difference in the spatial resolution. Additionally, in the thermal sensitivity of the cameras, there was a big difference, from 30 to 100 milli-Kelvins (mK). In spatial resolution and in thermal sensitivity, FLIR SC 640 demonstrated better characteristics.

Table 4. Technical Characteristics of FLIR C2 Camera

Imaging and optical data	
IR resolution	80 × 60 pixels
NETD	100 mK
Field of view	45° × 34°
Minimum focus distance	• Thermal: 0.15 m (0.49 ft.) • MSX: 0.3 m (1 ft.)
Focal length	1.54 mm (0.061 in.)
Spatial resolution (IFOV)	11 mrad
F-number	1.1
Image frequency	9 Hz
Focus	Focus free
Detector data	
Focal Plane Array	Uncooled microbolometer
Spectral range	8–14 µm
Detector pitch	17 µm
IR sensor size	80 × 60
Digital camera	
Digital camera	640 × 480 pixels
Digital camera, focus	Fixed focus
Digital camera, FOV	55° × 42° ±2°

Source: "User's manual – FLIR Cx series," http://www.farnell.com/datasheets/1903471.pdf.

Table 5. Technical Characteristics of FLIR SC640 Camera

Imaging and optical data	
IR resolution	640 × 480 pixels
Thermal sensitivity/NETD	<30 mK @ +30°C (+86°F)
Field of view (FOV) / Minimum focus distance	12° × 9° / 1.2 m (3.9 ft.)
Spatial resolution (IFOV)	0.33 mrad
Image frequency	30 Hz (60/120 Hz with windowing)
Focus	Automatic or manual (electric or on the lens)
Zoom	1–8x continuous, digital zoom, including panning
Focal Plane Array (FPA) / Spectral range	Uncooled microbolometer / 7.5–13 µm
Digital camera	
Built-in digital camera	3.2 Mpixel, auto focus, and video lamp

Source: "Technical Data – FLIR SC640," http://support.flir.com/DsDownload/Assets/40402-3601_en_40.pdf.

6. Digital Image Representation and Data Visualization

Commission Internationale d' Eclairage (CIE) has standardized RGB image representation using red, green, and blue primary colors, as shown in Figure 27. Under this standardization, colors are characterized by a point described by the *x* and *y* coordinates and luminance Y, which is a measure of intensity [47].

Figure 27. The CIE Chromaticity Diagram

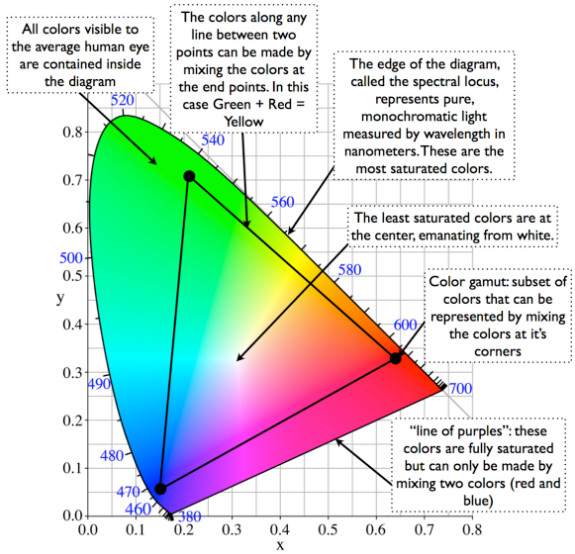

Source: "Anatomy of a CIE Chromaticity Diagram," http://dot-color.com/category/terminology/.

The data visualization coming from an image is a grid of numbers that represents intensities ranging from 0 to 255. In true color images, each of the pixels will have a set of three values that directly associates with the red, green, and blue channels. As a result, each true color image will be represented by a three-dimensional array with the size of each being the same as the size of the image's pixels. In grayscale images, only one matrix, which represents only brightness information, will be formed out of the 3D array [48]. In both cases, 0 represents black and 255 white, as shown in Figure 28. This grid is the computer's view of an image. These are the values that various image-processing operators use as inputs to produce desired patterns or as outputs for further analysis and modeling [46].

Figure 28. Digital Image Data Visualization

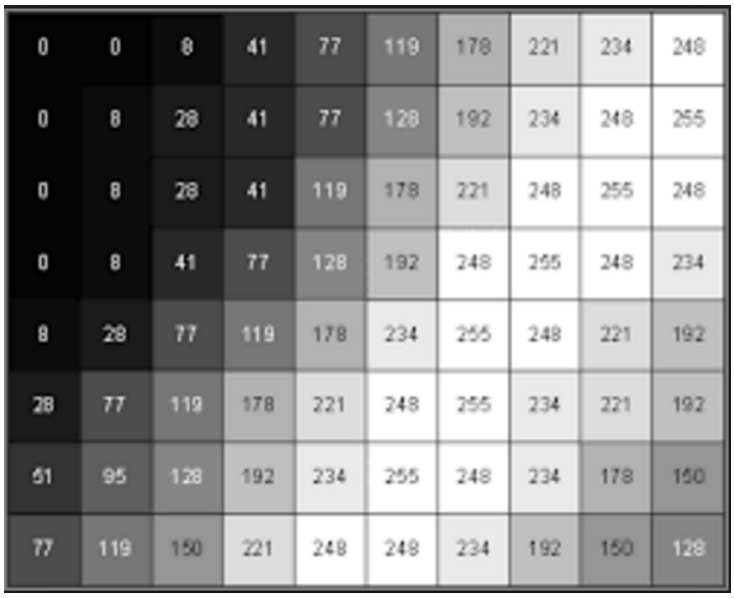

Digital image is composed of a rectangular pixel array in (x, y) coordinate with corresponding intensity values.

C. CLASSIFICATION PROCESS

The classification problem belongs to the category of supervised learning problems, in which we attempt to map inputs for specific outputs that represent our classes. In general, classification can be roughly described as the process by which models created with past data can be used to predict a class of new data with similar

attributes. In this way, discriminants are formed as classification rules that can distinguish between the examples in the different classes [49]. The following steps were carried out during the procedure to form these discriminants in our binary classification problem.

1. Image Processing

Image processing is the process through which captured images can be improved by enhancing characteristics, such as brightness and contrast, or by removing the noise [46], [50]. This step brings the images to a state that is more suitable and assists the specific feature-extraction process.

2. Feature Detection and Description

Feature detection or extraction is the process by which images are scanned in order to extract characteristic locations, or subsets of the image space. Consequently, the regions surrounding these locations will be exploited to generate invariant descriptors for our feature-description process. These descriptors characterize each image and the set of images for each class. The method for extracting these descriptors, and specifically, speeded-up robust features (SURF), is analyzed in the following paragraphs. This is a very important step as these features will become the inputs to form the discriminants for training the neural network.

a. Speeded-Up Robust Features (SURF)

Since the targets and platforms in battlefields are kinetic in unpredictable ways, we are also interested in the timeliness of the information. SURF features were finally selected to provide us the necessary descriptors. These features operate only in grayscale images, are rotation and scale invariant, and mainly used for matching applications. Other applications in which these features can be used include image registration, 3D reconstruction, and object recognition, as indicated by inventors [23]. Additionally, these features are rapidly computed, extracted, and compared. In several cases, SURF features were used to solve classification problems for facial expression [51], objects and their localization [52], automatic image annotation [53], and image-matching problems using supervised learning [54].

The implementation of the original method involves three steps mainly for matching applications, that is correspondence between images [23]. As a first step, appropriate interest points should be detected followed by the description of the area around these points in the form of a vector. Candidates for the interest points are those that represent objects in the image such as blobs, corners, and T-junctions. The metric for this step is a Hessian matrix-based detector, called the "Fast-Hessian" detector, that relies on integral images [55] for image convolutions. The descriptors have 64 dimensions and describe Haar-wavelet responses in the area surrounding the interest points.

(1) Fast-Hessian Detector

The detector of the interest points, based on the Hessian matrix, is characterized by stability and repeatability. Instead of a Gaussian or a Laplacian of Gaussian filter, an approximation of them with a box filter is used, as shown in Figure 29 (a). In this way, a scale-space is created, as shown in Figure 29 (d). Because we use integral images, there is no need to down-scale the images; instead, the increased dimensions of filters are applied to the integral images, as shown in Figure 29 (b). The result is faster performance by roughly a factor of three, without a negative effect on the detection of the interest points. The points are finally localized after a non-maximal suppression in a three by three by three neighborhood [23], [56], [57], as shown in Figure 29 (c). As a result, the detector is based on the determinant of the Hessian matrix for both the scale and the location of the interest points. Therefore, the Hessian matrix for a specific point $p_i = (x,y)$ on image I_{xy} is $H(p_i, \sigma)$ at p_i at a scale of σ, defined as follows:

$$H(p_i,\sigma) = \begin{bmatrix} L_{xx}(p_i,\sigma) & L_{xy}(p_i,\sigma) \\ L_{xy}(p_i,\sigma) & L_{yy}(p_i,\sigma) \end{bmatrix},$$

in which $L_{xx}(p_i,\sigma)$ is the convolution of the second order Gaussian derivative of the image I_{xy} at point p_i [56].

Figure 29. SURF Detector

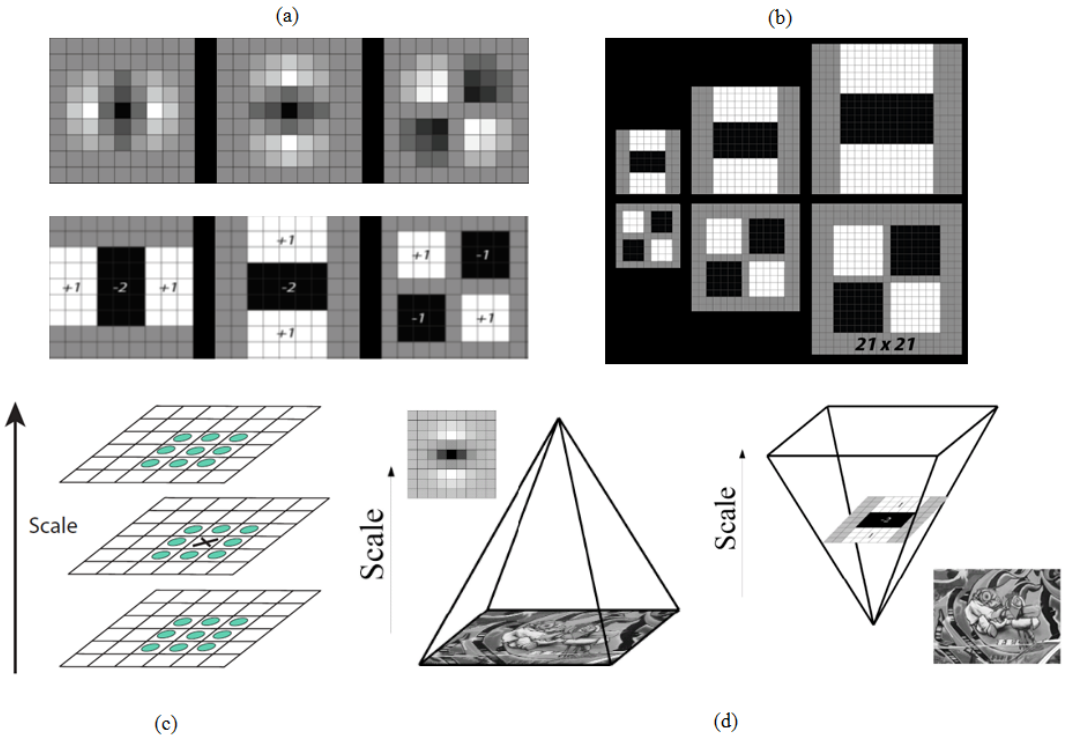

In (a): LoG and box filter approximations. In (b): the way the box filters grow while being kept to scale. In (c): the non-maximal suppression that results in the detection of the interest point. In (d): the scale-space pyramids for LoG (left) and box filters (right) Adapted from H. Bay, A. Ess, T. Tuytelaars, and L. Van Gool, "Speeded-Up Robust Features (SURF)," no. September, 2008 and S. Ili, "Feature Descriptors," Track. Detect. Comput. Vis., 2010.

(2) Descriptors

The method to extract the descriptors from the surrounding area of the interest points includes two more distinct steps. First, the Haar wavelet [50] responses will have to be calculated both in *x* and *y* directions within a certain area defined by scale parameters to detect the feature direction. In the second step, a square region needs to be defined around the interest point and subsequently rotated to match the feature direction, as shown in Figure 30 (a). Sub-regions of four by four are further defined, wherein simple features are computed in five by five grids inside these sub-regions, as shown in Figure 30 (b). The final 64 elements of the descriptor compose a four-element vector (Σdx, $\Sigma|dx|$, Σdy, $\Sigma|dy|$) multiplied by the sixteen sub-regions.

Figure 30. SURF Descriptor

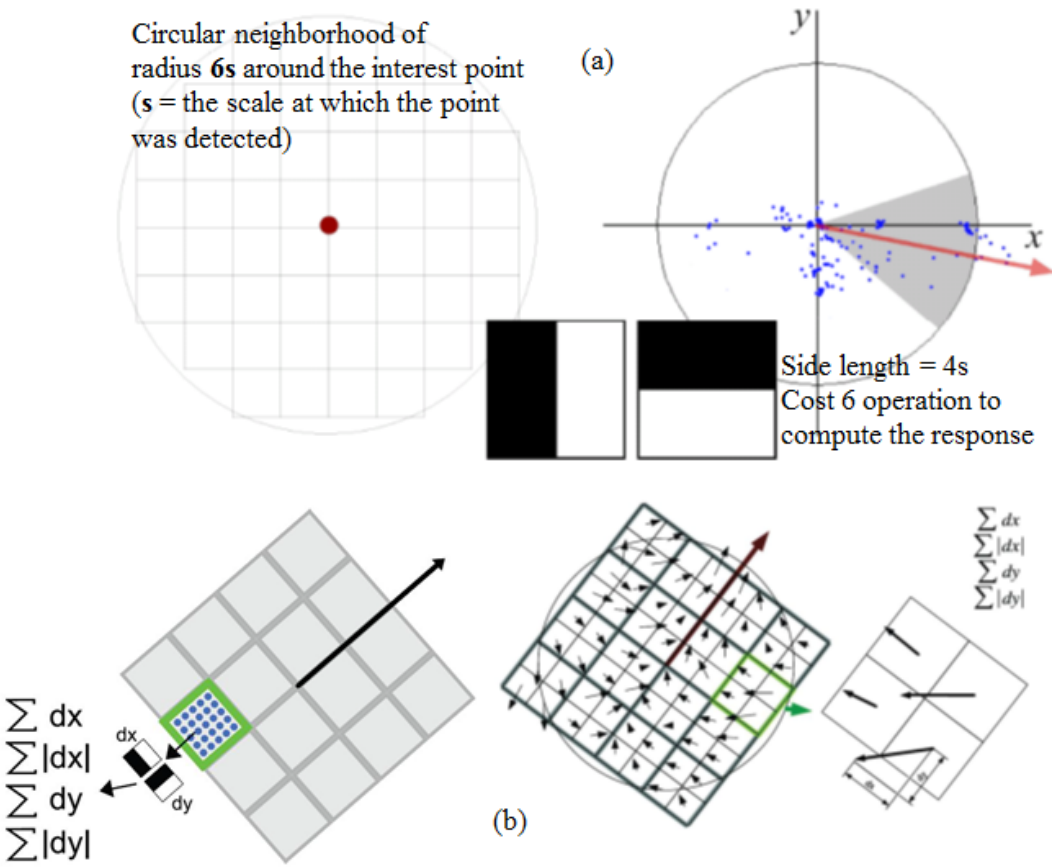

In (a): the scale-based parameters to detect the feature direction. In (b): the sub-regions, wherein descriptor elements are calculated. Adapted from D. Schmitt and N. McCoy, "Object Classification and Localization Using SURF Descriptors," *Object Classif. Localization Using SURF Descriptors*, pp. 1–5, 2011, and H. M. Sergieh, E. Egyed-Zsigmond, M. Doller, D. Coquil, J.-M. Pinon, and H. Kosch, "Improving SURF Image Matching Using Supervised Learning," 2012 Eighth Int. Conf. Signal Image Technol. Internet Based Syst., pp. 230–237, 2012

3. Multi-Sensor Data Fusion

If we consider the most accurate definitions that exist concerning data fusion, we can define multi-sensor data fusion as the collection and combined use of data originating from various sources to acquire enhanced information [58], [59]. Data fusion techniques and practices have been increasingly used in cases where a variety of sensors and sources are available. When such techniques are implemented, the expectation is that the results will become more accurate and reliable than data acquired from one source. Furthermore,

information fusion, which refers to the fusion of already processed data, can be implemented at a later stage or in combination with data fusion.

Several classification schemes of data and information fusion have been proposed, mainly because it is a technique that numerous disciplines can implement. Castanedo in his review of the existing data fusion techniques [58] presents and categorizes them according to certain criteria. We will use the classification based on abstraction levels to better describe the different ways that data fusion techniques have been implemented in our experiment. According to Castanedo's classification criterion, we can describe the following categories:

(1) Low level fusion, in which raw data are fed as an input to the data fusion process;

(2) Medium level fusion, also known as feature or characteristic level, in which features or characteristics are used as inputs to the fusion process;

(3) High level fusion, which is also known as decision fusion; and

(4) Multiple level fusion, in which data fusion involves some or all of the previous mentioned categories [58].

4. Machine Learning

Although machine learning uses data paradigms to form or predict patterns of data, it is not limited in finding solutions for database challenges. The main focus of this science is to produce the appropriate models that will enable computers to demonstrate a self-learning performance based on experience built on past data without being explicitly programmed [49], [60]. Artificial intelligence (AI) is a big part of this field. Furthermore, artificial neural networks (ANNs) are an attempt to create machine intelligence that can mimic human brain performance in the areas that still need development, such as computer vision or pattern recognition. In this thesis, ANNs are used to build the classifier for a binary classification problem since they are proven excellent classifiers when dealing with non-linear problems.

a. Artificial Neural Networks

Neurons are the basic elements of the human brain. Their operation is to accumulate input signals and when a certain threshold is reached, they will trigger an output signal, as shown in Figure 31. The same concept is the basis of the ANNs, or more simply, neural networks (NNs). A network of artificial neurons can in most cases be modeled to simulate the structure of biological neurons [61].

Figure 31. Neuron Schematic

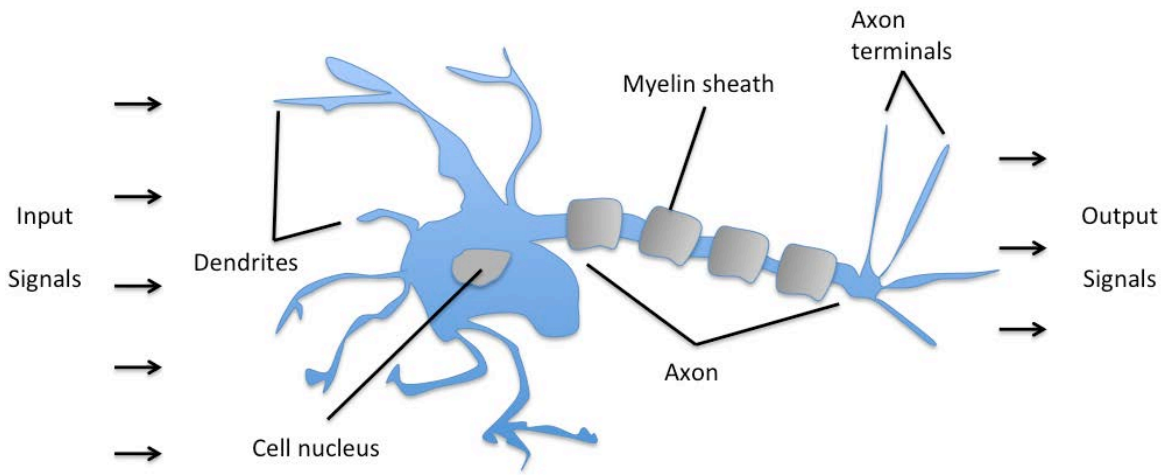

The input signals may be outputs from other neurons. When sufficient signals are accumulated, the neuron will trigger and fire an output signal. Source: S. Raschka, "Artificial Neurons and Single-Layer Neural Networks," 2015, http://sebastianraschka.com/Articles/2015_singlelayer_neurons.html.

The equivalent design of the artificial neuron, which is the basic processing element in NNs, is shown in Figure 32. A number of inputs x_i is assigned to coefficients or weights $w_{1j,}$ which control the impact of the specific connection, plus a bias w_0, to make the model more general. Each perceptron with the weighted sum of the inputs multiplied by the weights defines a hyper-plane.

Figure 32. Artificial Neuron

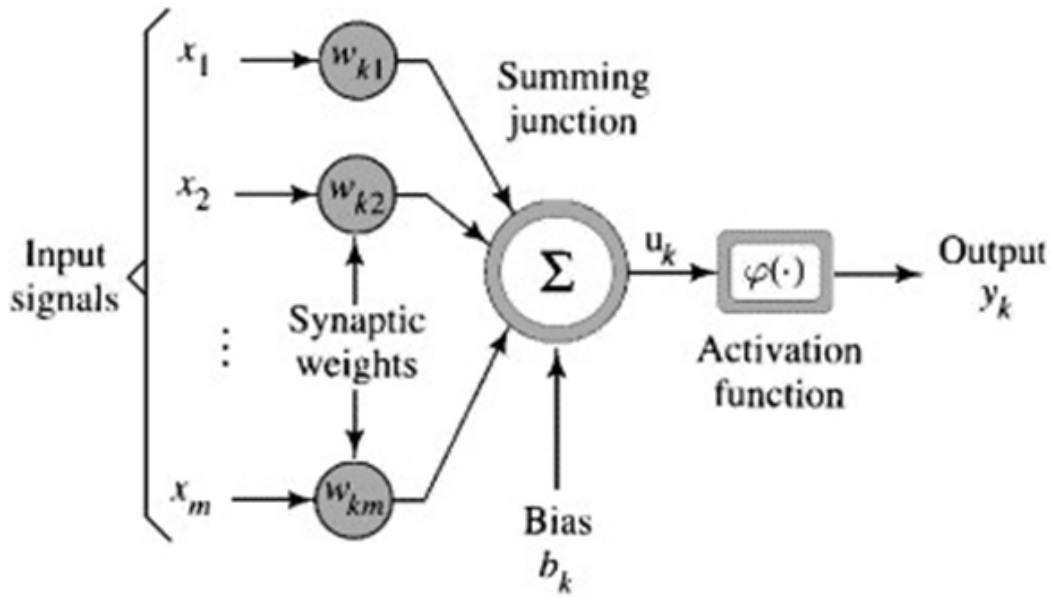

The weighted sum of the inputs multiplied by the weights plus the bias is fed into the activation function in which a threshold determines whether it will fire an output. Source: M. Triki, H. Chabchoub, and W. Hachicha, "A neural network-based simulation metamodel for a process parameters optimization: A case study," Logistiqua, 2011 4th Int. Conf., pp. 323–328, 2011.

Neurons are grouped in layers, which are fully connected through communication channels called connections. The first layer is the input layer in which the extracted outputs from the previous steps will be entered as inputs. Thus, the nodes on the input layer are limited by the number of the features that we define. Next, we find the hidden layers, which are the layers in between the input and the output layers. Although there are no rules to determine the number of hidden or total layers and their respective nodes, some empirical norms do exist based on experimentation and previous results from various categories of problems. One norm is that usually three layers are enough, but additional layers can be added if results are not satisfactory. The input layer is not taken into account when referring to the number of layers of a NN. The last layer is the output layer, which in our case is going to have two nodes corresponding to the two classes of our problem, as shown in Figure 33.

Figure 33. Connections and Layers of ANNs

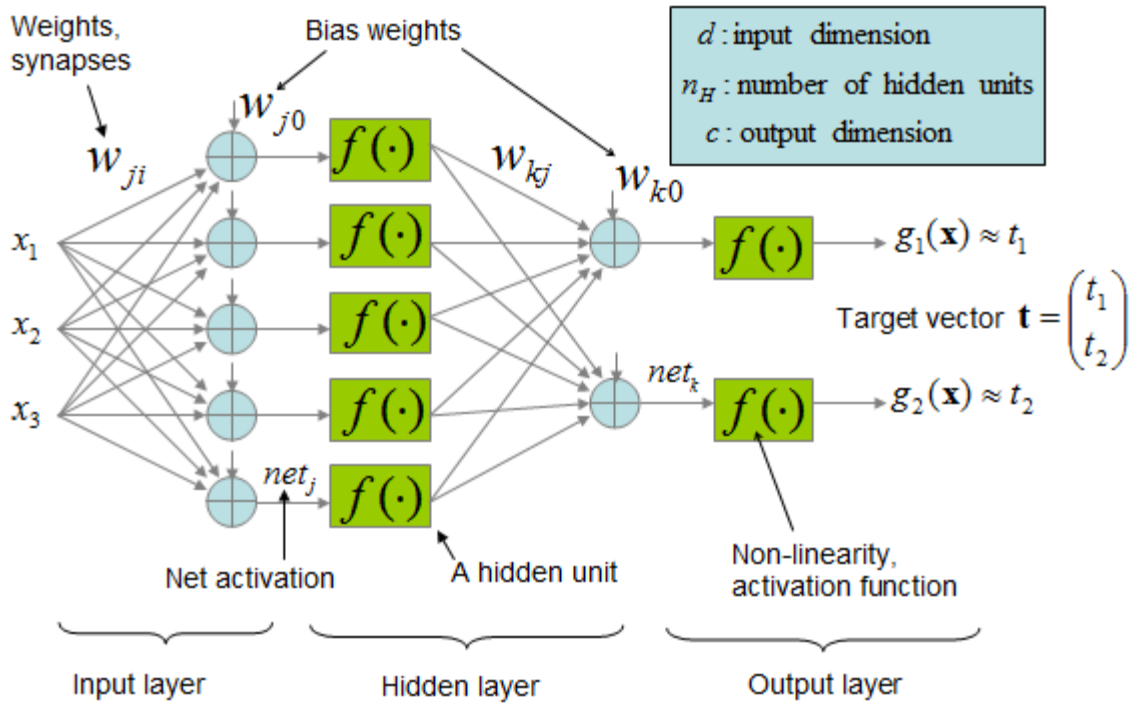

An example of an ANN topology. Source: "Neural Network Classifier," https://code.google.com/p/nll/wiki/ClassifierNeuralNetwork.

The two main network topologies are feedforward and feedback, or recurrent, neural networks. In the first category, neurons do not back propagate while in the latter, they do. One more difference that NNs have is determined by the kind of data that they can handle. The main data categories or variables that exist are the categorical and quantitative variables. Categorical data needs to be mapped into numbers before they are fed into the network [61]. ANNs can be characterized with a set of numbers that describes their topology. For example an X-100-2 ANN is a two-layer ANN with X inputs, 100 neurons in the hidden layer and two outputs, and it is the characteristic topology of the network used in this thesis.

ANNs usually have one or more hidden layers with neurons. The activation function applied on the weighted sums of the neurons can be either linear or non-linear. The main functions that can be met in NNs are presented in Figure 34. In classification

problems, as they are highly non-linear, the equivalent activation functions are used. In this classification problem, specifically the logsig(n) is used in the output layer since we want to constrain the output between 0 and 1 for the binary classification problem [62].

Figure 34. Transfer Functions of ANNs

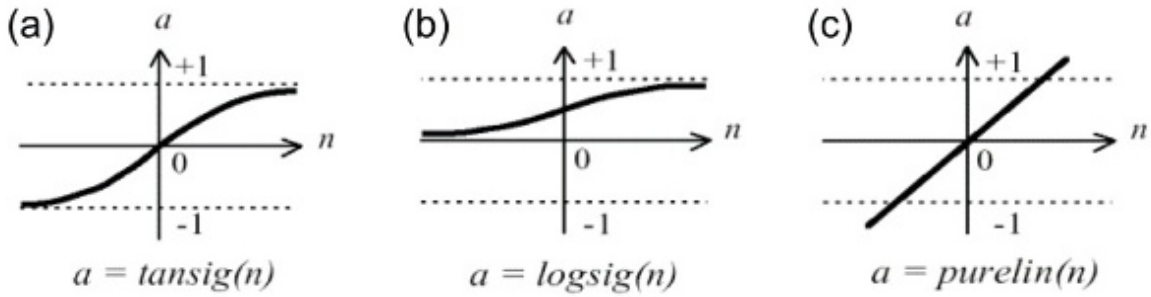

The main and most common activation or transfer functions that perform the decision in each neuron are depicted in this image: tan-sigmoid (a), log-sigmoid (b) and linear (c). Modified versions of them can be also used depending on the type of the ANN. Source: "Analysis of Pesticide Mixtures Using Intelligent Biosensors," http://www.intechopen.com/books/intelligent-and-biosensors/analysis-of-pesticide-mixtures-using-intelligent-biosensors

b. Training the Neural Network

For the training process of the ANN, an important parameter that we have to consider is the type of the ANN and the training algorithm that it uses. In MATLAB, several training algorithms can be implemented in the ANN, and the choice depends on factors such as the complexity of the problem or the amount of the available data. In classification problems, scale conjugate gradient (SCG), a backpropagation algorithm (trainscg), seems to outperform the rest of the available algorithms, especially when large number of weights exist [63], [64].

The typical work flow for the overall training process after selecting the training algorithm has the following steps [65]:

- Collect and prepare the data
- Create the network
- Configure the network parameters

- Initialize the weights and biases
- Train the network using the training data
- Validate the network
- Use the network to predict the testing data, which has to be separated from the training and validation steps.

c. Classification

The problem of classification, or in this case, category (class) recognition and image classification, can be seen as the task of creating general models or representations of attributes from a collection of data that characterizes a specific class then finding any existing correspondence between any set of testing data. Today, image classification continues to be one of the unresolved problems in the area of computer vision [46]. That is not to say solutions do not exist, but they are partial and applicable only to certain areas under constraints. The main comparison often used to support this statement is that current solutions cannot outperform the capability of a child to recognize and classify objects. Over the last fifteen years, it seems that new interest in NNs has made steps toward solving this problem [66]. In this thesis, the last step is to evaluate the performance of NNs in a binary classification problem of categorizing boats between the classes of sailing and power boats.

The performance measures used for this classification problem are the confusion matrix and the receiver operating characteristics (ROC) curves [49]. For a binary classification problem like the one investigated in this thesis, the confusion matrix will have the form of Table 6, wherein the corresponding definitions are presented. Further relevant definitions of performance measures are given in Table 7.

Table 6. Confusion Matrix for Binary Classification Problem

	Predicted class		
True class	Positive	Negative	Total
Positive (p) Negative (n)	TP: true positive FP: false positive	FN: false negative TN: true negative	p n
Total	p1	n1	N

Adapted from E. Alpaydin, "*Introduction to Machine Learning*," Thrird Edi. MIT Press, 2014.

Table 7. Performance Measures for Binary Classification Problem

Name	Formula
Error Accuracy	(FP+TP)/N (TP+TN)/N=1-Error
TP rate FP rate	TP/p FP/n
Precision Recall or TP rate	TP/p1 TP/p
Sensitivity or TP rate Specificity	TP/p TN/n=1-FP rate

Adapted from E. Alpaydin, "*Introduction to Machine Learning*," Thrird Edi. MIT Press, 2014.

ROC curves give us a graphical representation of the true positive rate (TPR) as a function of the false positive rate (FPR). An example of ROC curves with a rough representation based on the expected classifier performances is shown in Figure 35. As shown in the depicted curves, the more they shift to the upper left corner, the better the classifier is characterized. We can also measure the quality of the classifier with the area under the curve (AUC), in which 1 is the value corresponding to an ideal classifier [49].

Figure 35. Expected ROC Curves

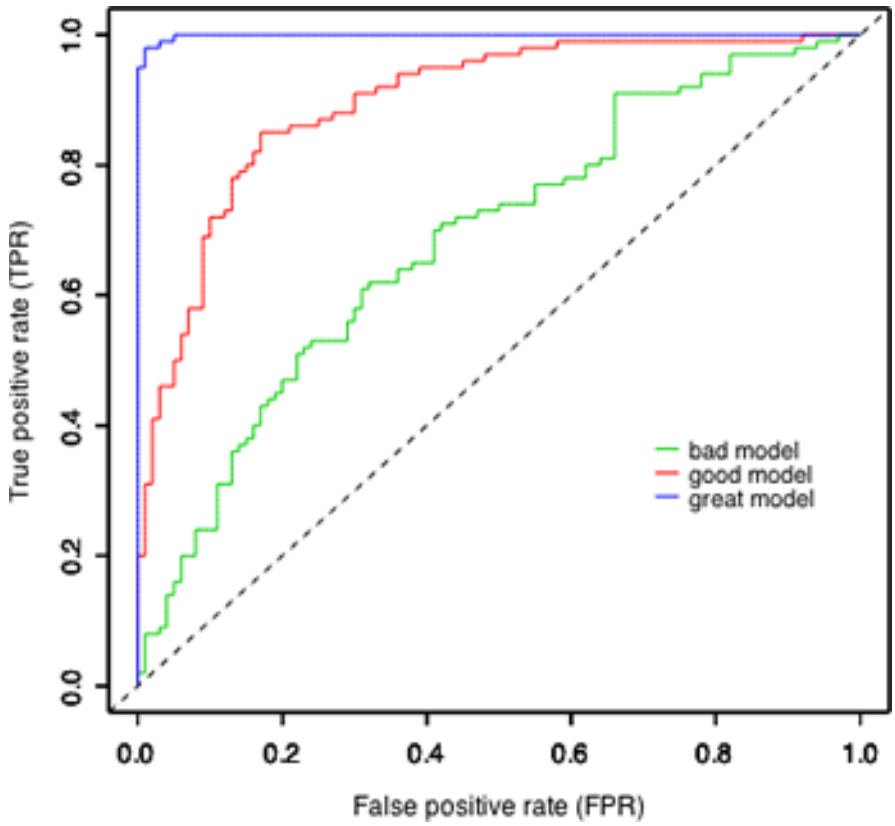

A rough representation of the expected ROC curves according to the performance of the used model is given for comparison later with the derived results from our binary classification. On the *x*-axis, FPR is the ratio of false positives over all negatives, and on the *y*-axis, TPR is the ratio of true positive over all positives. Source: "ROC curves," http://www.unc.edu/courses/2010fall/ecol/563/001/docs/lectures/lecture22a.htm.

Another way to evaluate the performance of an ANN is to use the mean squared error (MSE) and the cross-entropy or deviance as a measure of fit [67], [68], [69]. MSE is the output to be compared during the training or testing phase of the ANN implementation. The error is the difference between the target value representing an assigned class of the supervised process and the output value that was predicted from the ANN. The MSE and the cross-entropy are given in the following equations:

$$mse = \frac{1}{N}\sum_{i=1}^{N}(t_i - y_i)^2 ,$$

$$c = -\frac{1}{N}\sum_{i=1}^{N}(\mathrm{t_i} \times \log \mathrm{y_i} + (1-\mathrm{t_i}) \times \log(1-\mathrm{y_i})) ,$$

in which N represents the total number of samples, t_i the assigned target values, and y_i the predicted outputs.

D. USING CENETIX TNT TESTBED FOR EXPERIMENTATION WITH SENSORS

The Center for Network, Innovation and Experimentation (CENETIX) at the Naval Postgraduate School (NPS) is focused on extensive experimentation of self-organizing tactical networking and collaboration. Since it was founded in 2004, many experiments have been conducted with a focus on adaptive wireless and mesh networks to allow connectivity and collaboration of various manned and unmanned platforms, from UAVs to divers and satellites [70]. While the primary focus was on maritime interdiction operations (MIO) initially, numerous partners, whose cooperation supported several national as well as international-level field experiments, turned it into a leading innovative solution for the modern battlefields. Tactical Network Topology (TNT) and MIO test-beds allows for cooperation and experimentation with universities, military institutions and organizations such as MIT, NMIOTC, and LLNL. One of the latest innovative solutions proposed by CENETIX was for network divers; a real-time exchange of images and text was tested during the latest experiments in San Francisco Bay. Acquired results from this and other experiments will be subject for discussion in this thesis. In Figures 36 and 37, the tactical and reachback infrastructure as well as the available subnets under TNT-MIO experimentation are presented.

Figure 36. CENETIX Tactical and Reachback Infrastructure

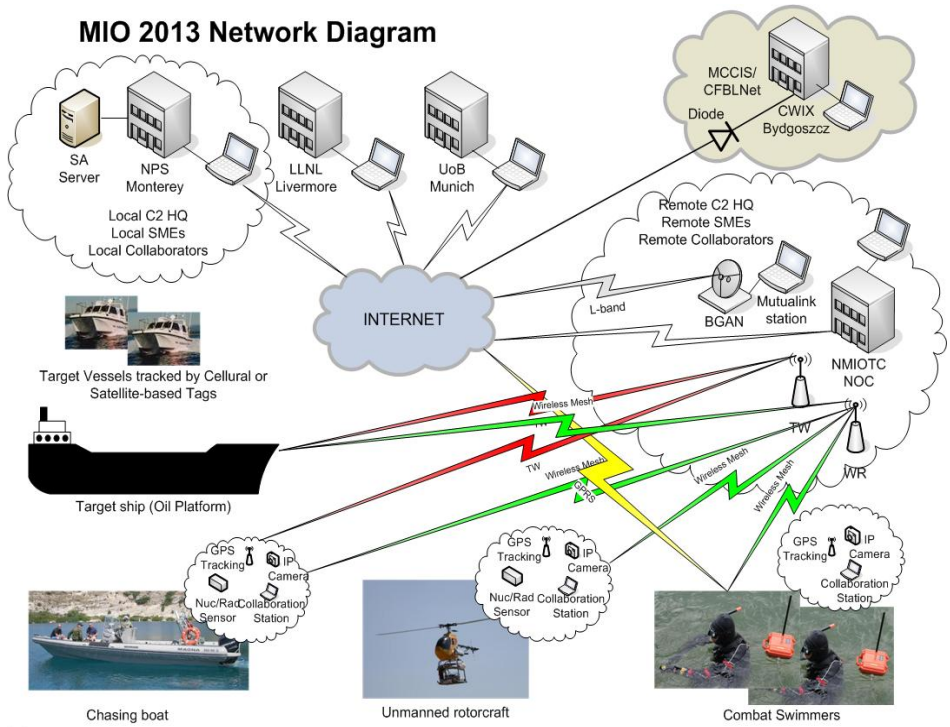

The CENETIX tactical and reachback infrastructure is extended through mesh networks to incorporate various heterogeneous nodes. Source: A. Bordetsky, "Maritime Threat Countering Networking and Collaboration Testbed." 2013.

Figure 37. Subnets under TNT-MIO experimentation

TNT-MIO Host IP configuration

CENTER FOR NETWORK CENETIX INNOVATION AND EXPERIMENTATION

The following subnets are currently configured to support TNT-MIO experimentation:

- 100 - OFDM backbone subnet 192.168.100.xx
- 112 - ITT Mesh 192.168.112.0/24
- 113 - WaveRelay Mesh 192.168.113.0/24
- 137 - Internet Connection Sharing (ICS)
- 72 - SF Bay Area MIO 192.168.72.xx
- 84 - Site300 subnet 192.168.84.0/24
- 85 - CNTX Reserved cluster 192.168.85.0/24
- 86 - SF Bay Area MIO cluster 192.168.86.0/24
- 96 - Portion of TNT subnet 192.168.96.0/22 (mask 255.255.252.0)
- 97 - Portion of TNT subnet 192.168.96.0/22 (mask 255.255.252.0)
- 98 - Portion of TNT subnet 192.168.96.0/22 (mask 255.255.252.0)
- 99 - Portion of TNT subnet 192.168.96.0/22 (mask 255.255.252.0)

Source: "TNT-MIO Host IP Configuration," http://cenetix.nps.edu/SA1/ipconfigmain.asp.

III. SIMULATION MODELING OF ATR THROUGH A MESH NETWORK OF IMAGING SENSORS

Assets operating in an area of interest (AOI) follow certain procedures to classify and, if possible, identify contacts of interest (COIs). This process becomes even more challenging when only passive sensors are used. Additionally, there are operational restrictions for how closely these assets can approach any of these potential COIs. These restrictions depend on the type and the capabilities of the assets as well as their overall mission. Oftentimes, the presence of other friendly assets in the area that could contribute to this effort remains unexploited. The proposed scheme of this thesis aims to detect and connect multiple assets through a mesh network and to facilitate the timely dissemination of critical information coming from their sensors, in a littoral environment. This scheme requires that available distributed database centers be part of the network. Additionally, automation should be applied in certain functions and processes. In this way, received data will be exploited for evaluation in the decision-making process before their value expires.

In this proposed scheme, we focus on a specific task of classifying image data of potential targets coming from the mesh nodes. Some of the challenges that this task poses are the need for high throughput as well as the ability to exploit imagery data coming from dissimilar sensors. The purpose of the simulations and experiments carried out to support the concept of this scheme is twofold. First, this thesis evaluates the feasibility, coverage, and quality of service (QoS) of the networked sensors in a maritime littoral environment. Second, this thesis evaluates data fusion and classification of images coming from dissimilar sensors. In this way, we allow assets that need to be undercover to safely operate in the area while other platforms that can take the risk of proximity to the target capture images from shorter distances.

In this chapter, certain steps of the overall conceptual scheme (see Figure 38) are explained in more detail. In the first part, the steps and parameters to simulate and evaluate a mesh network in a littoral environment are presented to show how existing terrestrial and satellite networks can be extended. Additionally, CENETIX's contribution

to the scope of this thesis is described. In the second part, image capture, fusion, training, and classification methods used in this thesis are further explained.

Figure 38. Proposed Scheme

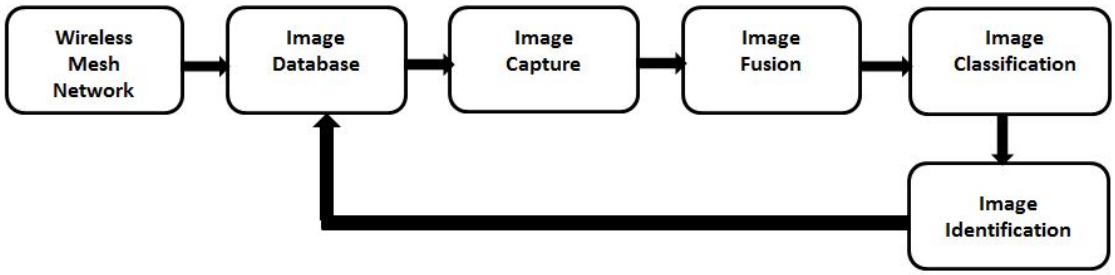

Proposed scheme for ATR through wireless mesh sensor networks. If and when the classified COIs are positively identified, they become part of the image database, and the system has to be retrained.

A. SIMULATION AND EVALUATION OF A WIRELESS MESH NETWORK

Initially and according to the STK and Qualnet simulation, a mesh network should be established with a quality of service (QoS) that could facilitate the timely dissemination of the captured images. At least one of the participating assets in the network should be a distributed data center with the functionality of a network operating center (NOC), capable of monitoring the status of the networked assets. These assets could be unmanned aerial vehicles (UAVs), unmanned ground vehicles (UGVs), ground stations, ships, air assets, satellites, or even human agents with or without imaging capabilities acting as relays to extend the network in the latter case. Figure 39 depicts this concept and displays the various assets in a littoral environment. In this challenging environment and through the use of the proposed technologies, the geographical obstacles are not a problem for the establishment of communications between the assets in the area. Instead, the land masses are used in a way that offers an advantage: hosting ground stations act as gateways and nodes for the interconnection of the existing subnets of the dynamic mesh network. The synthesis of these networks allows for dissemination of the images captured by the heterogeneous imaging sensors and their exploitation through the proposed scenario in STK.

Figure 39. Terrestrial and Satellite Network

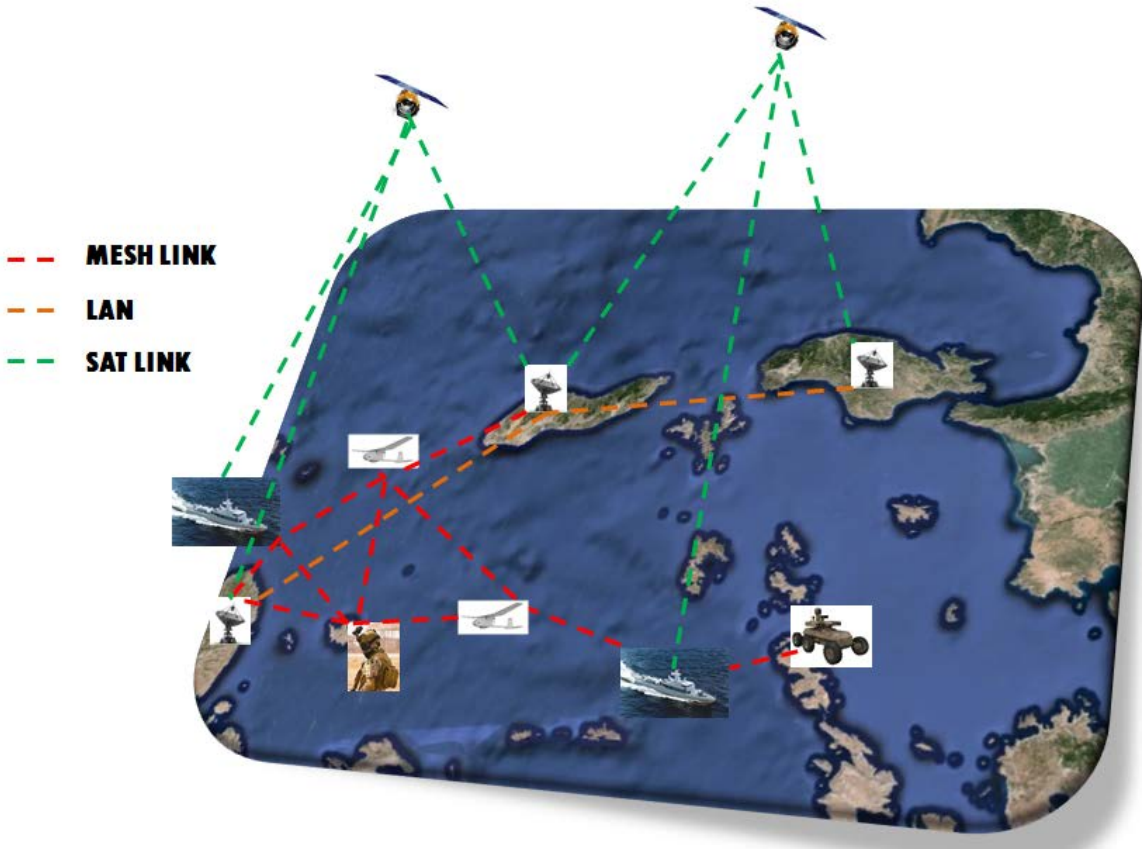

Extension of terrestrial and satellite network through a wireless mesh network (WMN) in a littoral environment to connect assets with imaging capabilities

1. STK Simulation

The STK simulation is focused in littoral waters and a limited area of interest (AOI) (see Figure 40), mainly because of the use of imagery satellites and the need to investigate the revisit time for a specific area. The objects inserted in the scenario include ships, UAVs, ground vehicles, ground stations, as well as imaging and communications relay satellites.

Figure 40. AOI in STK

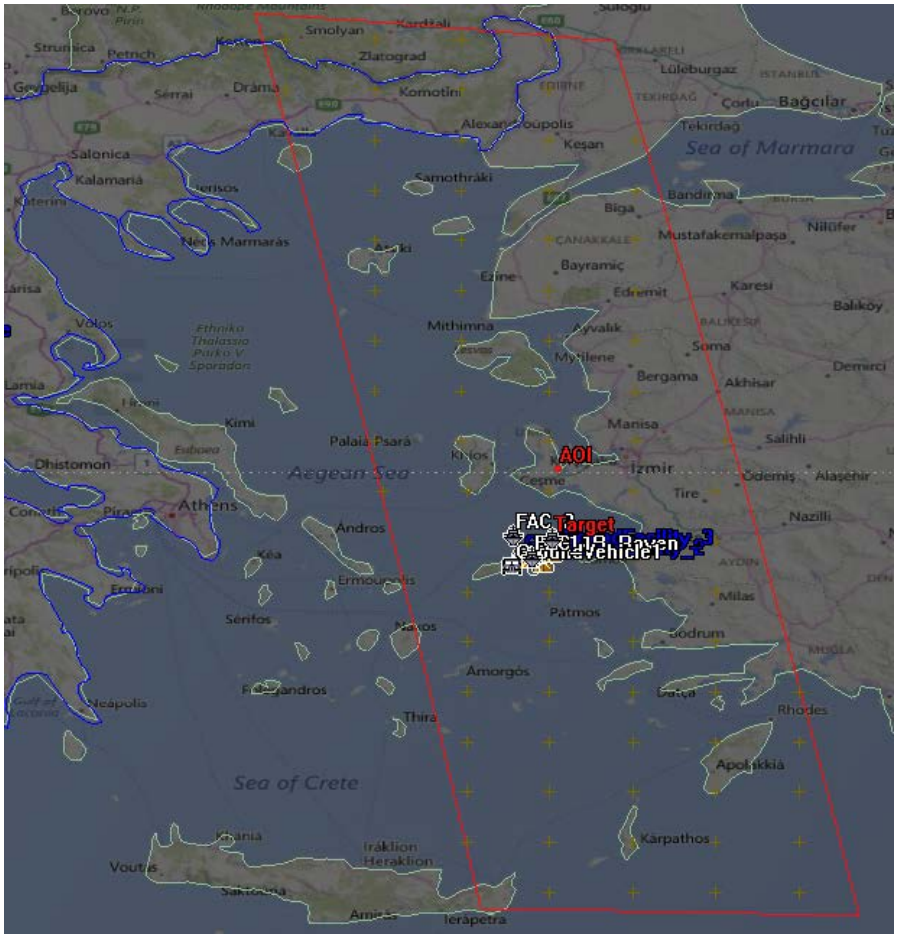

The AOI used for our simulation as extracted from STK 2D graphics.

The parameters and configurations of the simulated assets are presented in this section. Ground and sea tracks as well as flight orbits are designed for the several assets to demonstrate mesh-networking flexibility in the progress of time, as shown in Figure 41. The ability to replay the scenario offers insight into and rough measurements of the link ranges and communications success in the physical layer. The final scenario will be saved, along with images and videos from 2D and 3D graphics windows, for future evaluation of the fifth generation Wave Relay radios.

Figure 41. Assets Used in the Simulation

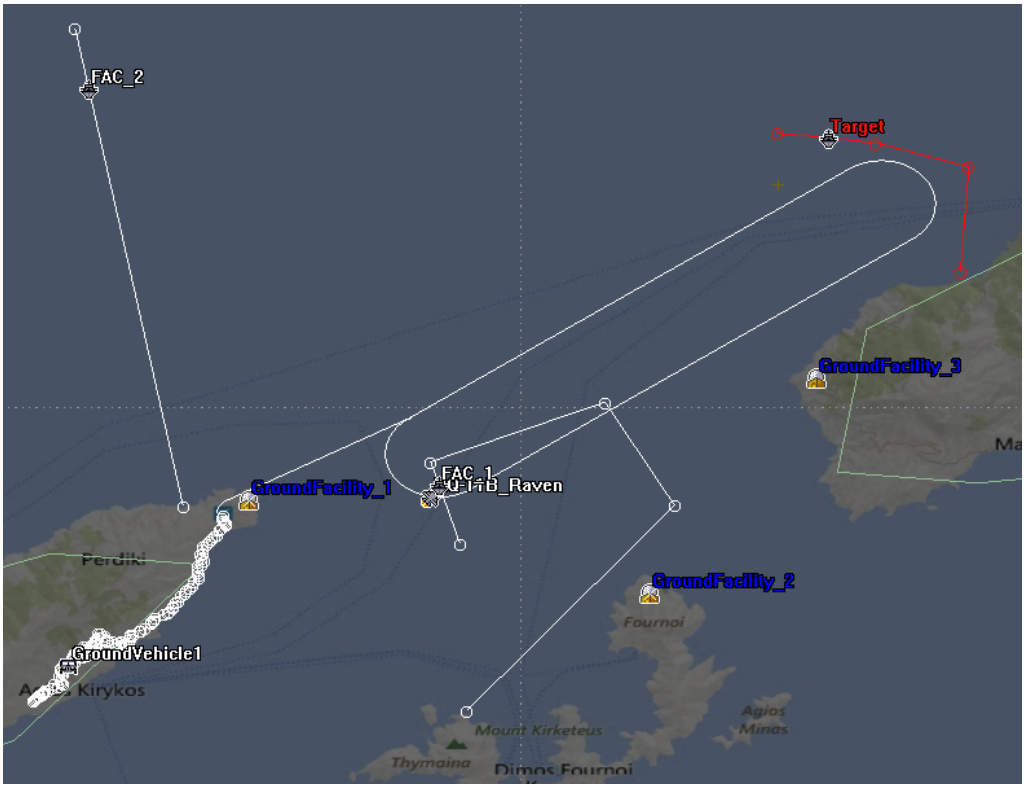

Assets used in the simulation and their designed tracks as extracted from STK 2D graphics.

The objects are imported in the simulation by inserting them into the scenario via the “Insert STK objects” window. In doing so, sensors, antennas, transmitters, and receivers are attached to them. Thereafter, they can be accessed for necessary configurations from the “Object Browser,” an instance of which is shown in Figure 42.

Figure 42. Instance of the Object Browser

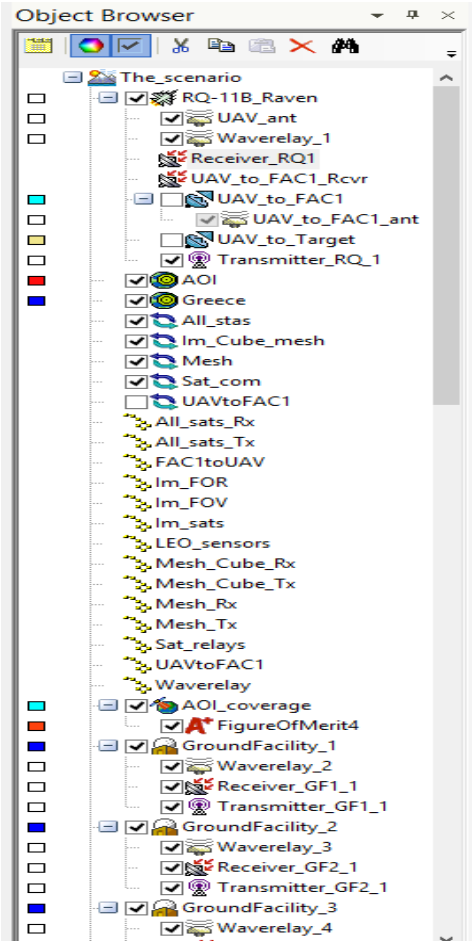

Instance of the Object Browser where all the objects are listed and can be accessed for configuration.

The imaging and communications relay satellites are shown in Figure 43. The integration of imaging cube-satellites into the mesh network is included in this scenario to demonstrate capabilities that already exist and to evaluate their potential contribution in intelligence, surveillance, and reconnaissance (ISR) missions in littoral waters. These satellites can provide imagery information during operations in areas where no assets are available or when other reasons prevent the presence of friendly assets. Since we are dealing with low earth orbits (LEOs), we expect the revisit times in the specified AOI to be small. However, if we can monitor the timeframes that these assets are available, the gain becomes obvious.

Figure 43. Satellites in Simulation

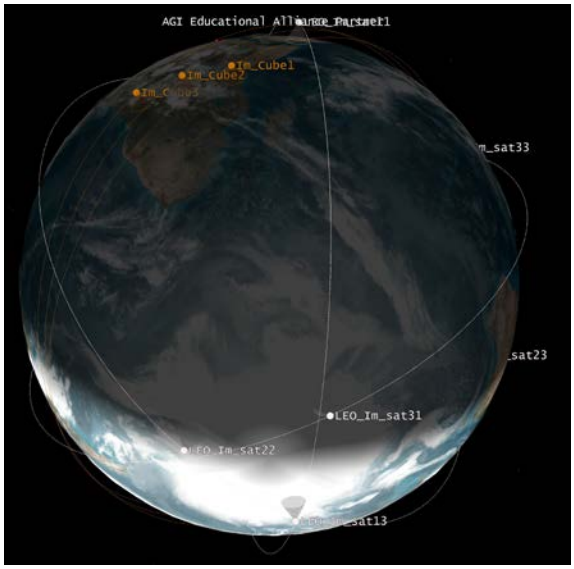

The satellites and their low earth orbits as extracted from the STK scenario 3D graphics.

The orbit parameters that were imported into STK for the imaging satellites are presented in Figure 44. The height was set at 300 km, and an inclination of 40 degrees was assigned.

Figure 44. Orbit Parameters for Imaging Satellites

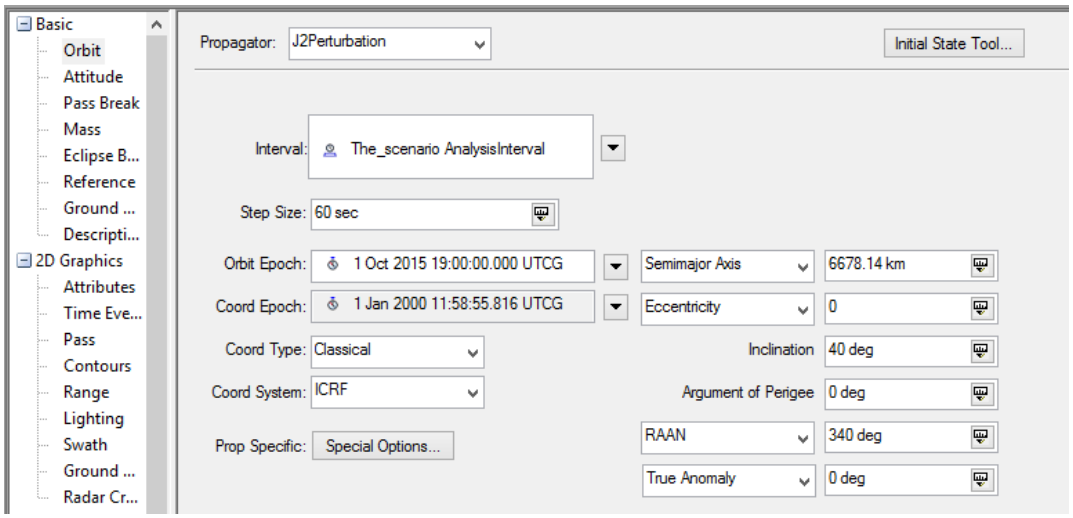

The basic orbit parameters that were assigned for the three imaging satellites were imported in the Orbit window of the Basic menu of the object.

The angle at which the sensor is pointing, or the look angle, , was set at nadir, and a field-of-regard (FOR) was assigned based on the capabilities of the sensor to alter its look angle. FOR sets the boundaries where the field of view (FOV)—the sensor's cone of visibility—can move. Figure 45 shows the FOR and FOV that were simulated. The concept of using these parameters is that the satellite will be tasked to change its look angle to acquire images from the desired area based on operational needs during the available time slots.

Figure 45. FOR and FOV for the Imaging Satellites

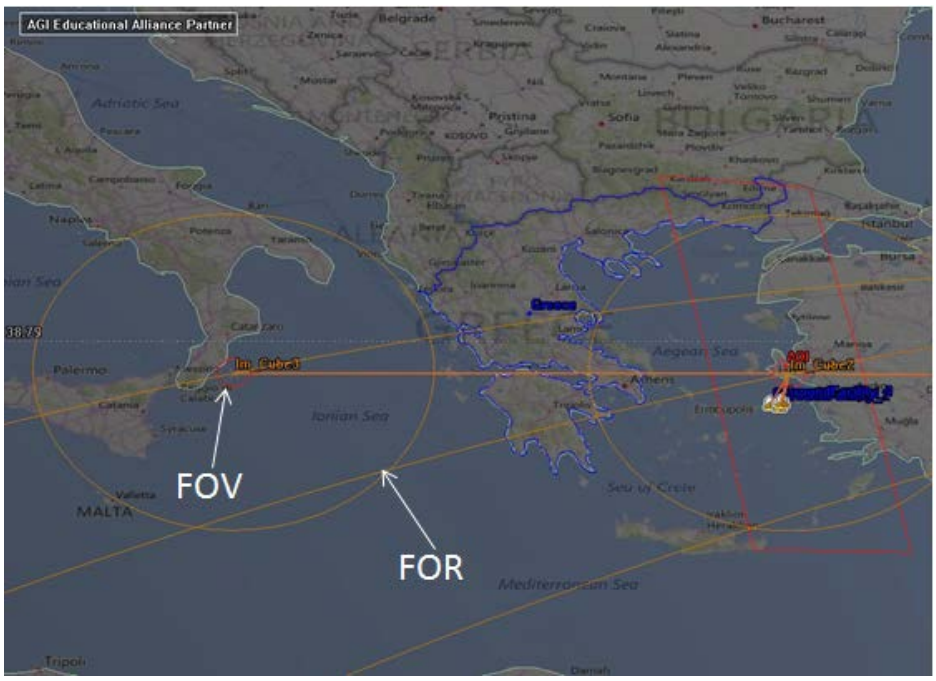

The FOR and FOV projected on the earth's surface are depicted in this figure. The FOV can be assigned a look angle inside the FOR boundaries as the satellite travels in its designated orbit.

Based on the following equation, the height of 300 km was selected to provide the desired ground sample distance (GSD) or resolution calculated for a nadir of 3.66 m:

$$GSD = \frac{2.44 \times \lambda \times h}{D},$$

in which λ is the wavelength, h the distance between the sensor and the object, and D the sensor's aperture diameter.

The UAV used for the simulation, an RQ-11B Raven, was extracted from the STK database. Its basic parameters are shown in Figure 46. A flight path was designed in the basic route menu and the height was set to 200 ft.

Figure 46. Basic UAV Parameters

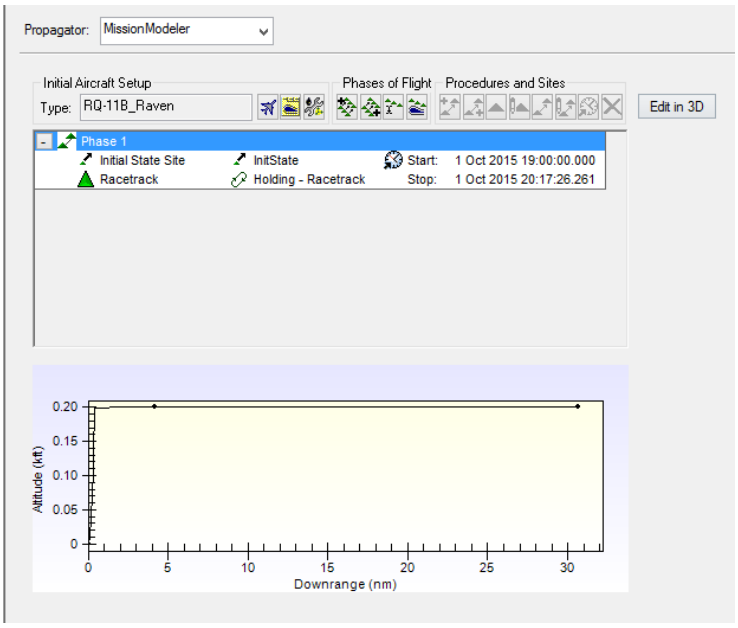

The rest of the imported nodes in the simulation were communications relay satellites, ships, ground facilities, and ground vehicles. Routes were assigned to all the kinetic nodes to demonstrate and study the expected fluid nature of the established links. Finally, the Wave Relay radios were simulated with the parameters that are presented in Figure 47. These parameters are not the precise parameters with which the actual radios may be configured. Since Wave Relay runs proprietary software, these settings were not open and, thus, impossible accurately simulate. Care was taken, though, for the theoretical performance of the selected settings to be comparable to those presented in Chapter II.

Figure 47. Wave Relay Transmission and Antenna Parameters

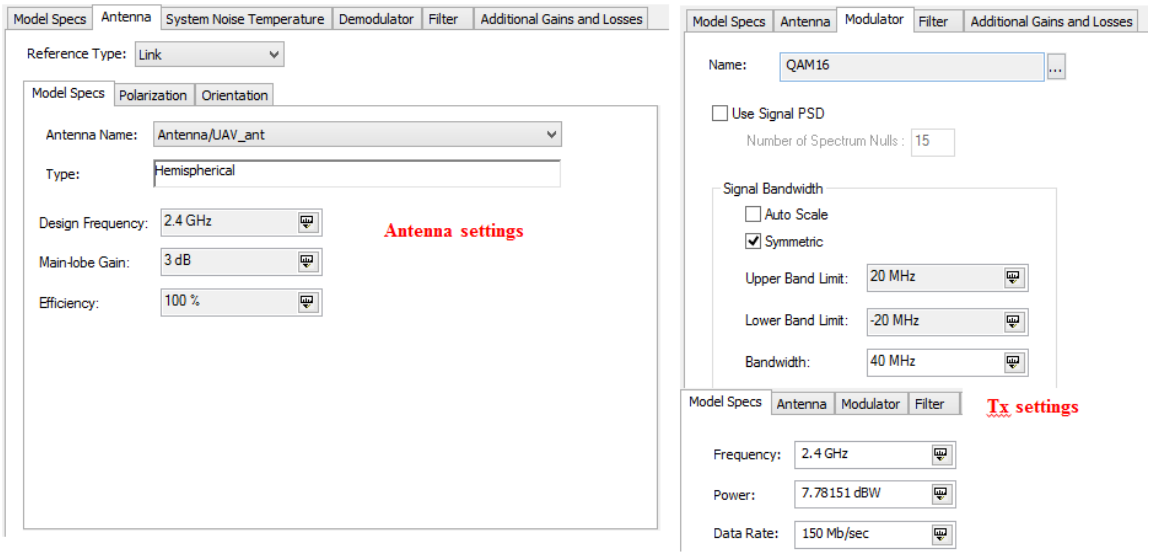

Some of the parameters that were inserted for the configuration of the Tx and antenna simulating the Wave Relay radios are shown in this figure.

2. Simulation in QualNet

For the QualNet simulation, the nodes participating in the network were configured according to the available Wave Relay radio parameters presented in Table 1. A second separate replay was possible through QualNet that gave us metrics to evaluate the network QoS from the MAC layer to the application layer of the OSI seven-layer model. An instance of the QualNet configuration browser and settings of the channel properties window are shown in Figure 48. As previously mentioned, the simulation could not be entirely accurate since the exact parameters of Wave Relay have not been released. Therefore, what we sought from this simulation was to set the basis that permits the comparison of simulation results with the ones obtained in future field experiments using fifth generation Wave Relay radios. Consequently, after a fine-tuning of the parameters in the simulation, the results will be comparable to the observed results in the field. Thus, it will be feasible for future scenarios and experiments to be simulated and adjusted accordingly to meet the desired requirements.

Figure 48. Qualnet Nodes Configuration Browser

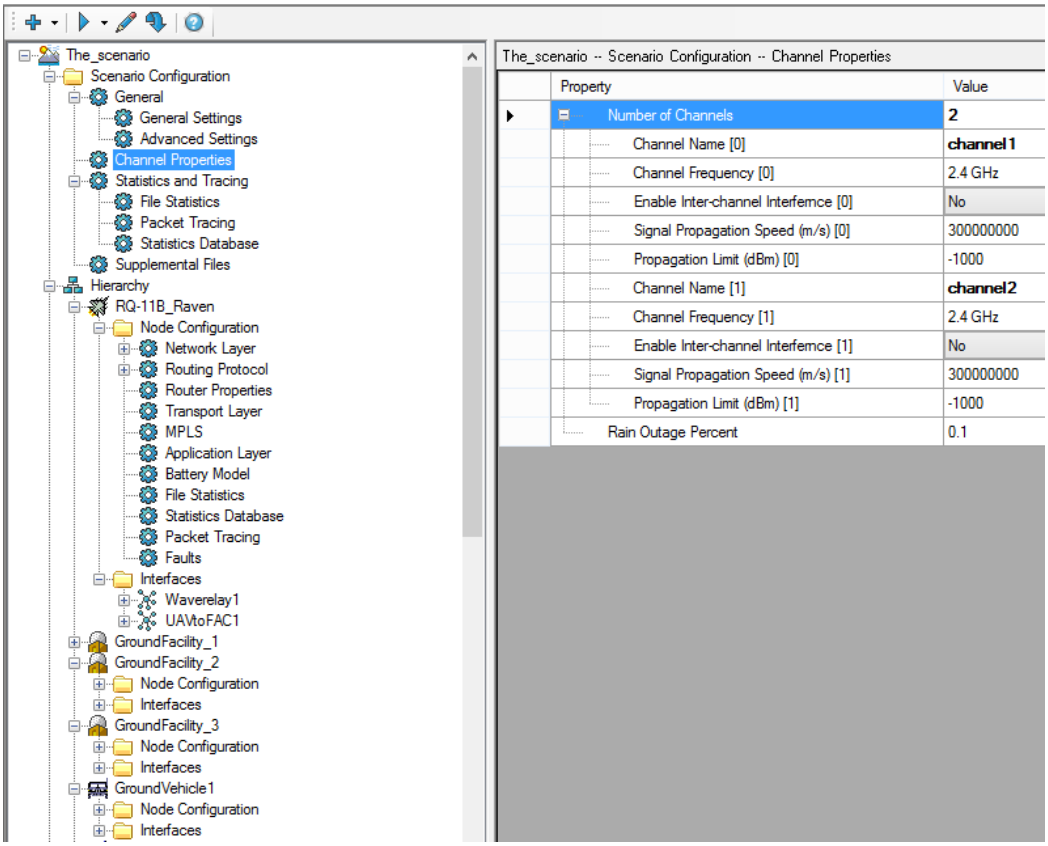

The participating nodes in the mesh network are listed in the configuration browser. Channel properties that were imported are also depicted.

B. IMAGE FUSION AND CLASSIFICATION SCHEME

The performed research in this thesis, even though limited due to lack of equipment and resources, proposed a scheme for classification of images from potential targets. Additionally, one of the main goals was to evaluate the gains from applying a fusion step for the images coming from dissimilar sensors in the field. This final proposal should also be applicable to littoral environments that pose additional challenges in terms of the wide variety of backgrounds that the acquired images usually have.

All the steps that were finally implemented are illustrated in Figure 49. These steps start with capturing images in the field and end with classifying available targets. The methodology used at each of these steps is described in detail to show the challenges

that were posed and taken under consideration through the overall process. A MATLAB script was developed for this implementation.

Figure 49. Image Classification Scheme

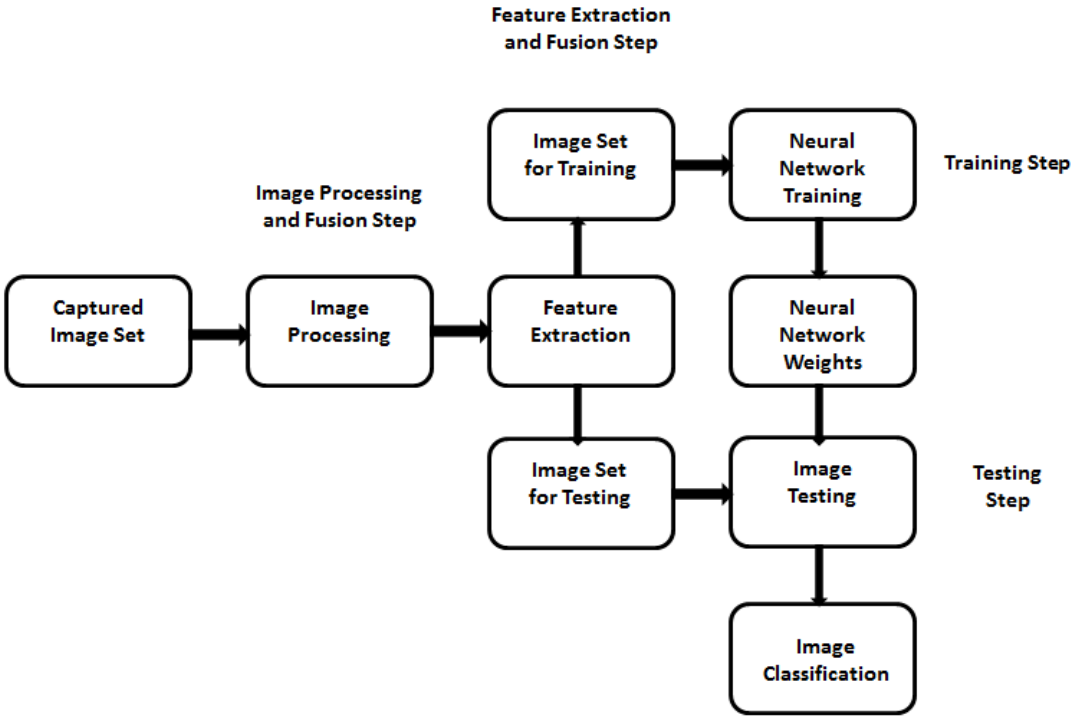

Proposed scheme for the image classification of the targets that includes the necessary steps from image processing to the final step of image classification.

1. Image Capture and Collection

Since the intention of this research was to study all the concepts under the littoral environment, the image set had to reflect this case. Furthermore, we had to investigate the impact of fusion in the classification process. One of the requirements in the proposed scheme, then, was to handle images randomly captured with no control over their aspects, distances, background, or lighting conditions. Thus, the image set had to be acquired from the field since no images were available that included the same scene captured by dissimilar sensors. Both cameras had these capabilities, which were described in Chapter II. The final image set included three different categories of images, as shown in Figure

50. All categories were directly acquired by the cameras, except for the multispectral images from FLIR SC640, which were derived after an image-to-image registration process.

Figure 50. Categories of Captured Images

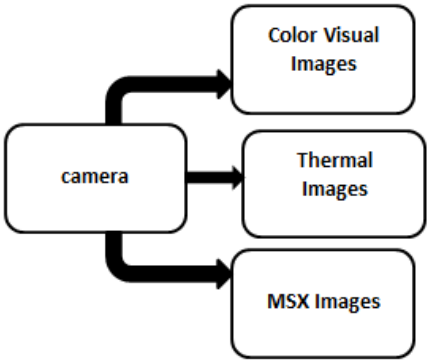

The image set included color-visual and thermal images from both cameras and additional MSX images from FLIR C2. The multispectral version from FLIR SC 640 was derived after registration of the color-visual and thermal images.

The available targets in the area were powerboats and sailing boats. Hence, the images in our experiment were captured to include these targets with various backgrounds. The background was selected to be either the sea or combined sea and land to simulate the background of images expected in littoral waters (see Figure 51). Background extraction of the images, then, became a very complex task, which was not accomplished—as different algorithms and methods used were able to extract the background from only part of the image set.

Figure 51. Sample Images with Different Background

Images were purposely captured with different backgrounds to pose the challenge of classifying boats in such a complex background.

The total number of the dataset was also a key factor for performance during the whole process. The total number of images included in the experiment was 85. A large number of images were rejected because of the poor resolution, especially in IR for longer distances or when too many targets were in the image. The cameras did not have advanced capabilities or zoom features usually met in cameras used for ISR purposes. Instead, the acquired images were preprocessed in such a way that zoom was simulated, so only one boat, or at least boats only from the same category, would be included in the image (see Figure 52).

Figure 52. Original and Zoomed Images

Original (a) versus zoomed (b) images in order for the object to cover the majority of the image.

2. Low Level Image Fusion Implementation

Data fusion from the two sensors was a process that investigated whether images coming from different sensors, either similar or dissimilar, could be handled by one system in our proposed scheme for ATR. Additionally, we examined whether fused images would result in better classification performance outcomes. Therefore, the fusion process was implemented in several stages. Initially, after the images were captured, low-level fusion had to be applied to the FLIR DSC 640 thermal and visual images to produce multispectral ones. For this implementation, ENVI's image-to-image registration was finally used—after many unsuccessful trials using feature-based registration in MATLAB. The best result in MATLAB and the final registered image for one pair of images are shown in Figure 53. The steps for the final implementation are described in the appendix.

Figure 53. Fusion Result Comparison from MATLAB and ENVI

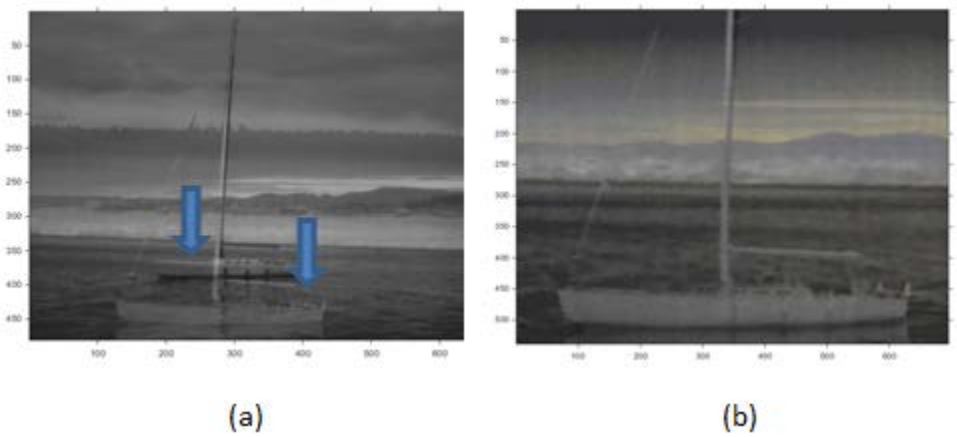

In (a): the best derived result after feature-based registration in MATLAB. In (b): the final registered image in ENVI.

Moreover, images from different sources and sensors were fused in sets of images falling under the same category, in our case, either color-visual or multispectral (MSX). The thermal images from FLIR C2 demonstrated very poor results due to the poor resolution, so they were not fused with the other images. The category of MSX images involved images already fused in the FLIR C2 and the multispectral products of image

registration from the FLIR SC640's pairs of images. The third case in which fusion was implemented was the medium-level fusion after the feature extraction step, which is discussed later this chapter. Finally, all the images—MSX, thermal, and visual—were fused to investigate whether the classification performance was improving.

3. Image Processing

In the image processing step, all images were converted to grayscale, and subsequently, histogram equalization was applied as shown in Figure 54. Initially, the images were .jpg files, which means they were represented in MATLAB as three-dimensional matrices with the number of elements equal to the pixels of the images, as discussed in Chapter II. This step was mandatory since the feature-extraction method works only with grayscale images, which were represented by individual matrices of the same size as the original three color channels. The values of the elements of these matrices were the intensities on which pixel operations were performed.

Figure 54. Image Processing

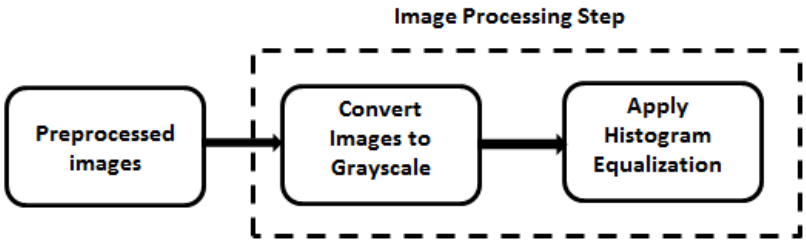

Preprocessed images were converted to grayscale, and histogram equalization was subsequently applied.

Applying histogram equalization in the images was also necessary after the results were derived without taking this step. Because of the limited capabilities to adjust brightness and contrast before capturing each image, the extracted SURF features were very poor, especially in the lower analysis images. Since histogram equalization is a gray-level mapping process and there is no gain when applying it to separate color channels, it was applied after the step for changing images to grayscale. This process calculated the probability density function (PDF) of the normalized intensities of the

images' pixels, ranging from 0 to 1. Then, cumulative distribution function (CDF) was used as a transformation function [50]. The result of the histogram equalization was enhancement and uncovering of details that had been lost due to poor contrast ratios [46], [71]; an example is given in Figure 55.

Figure 55. Image before and after Histogram Equalization

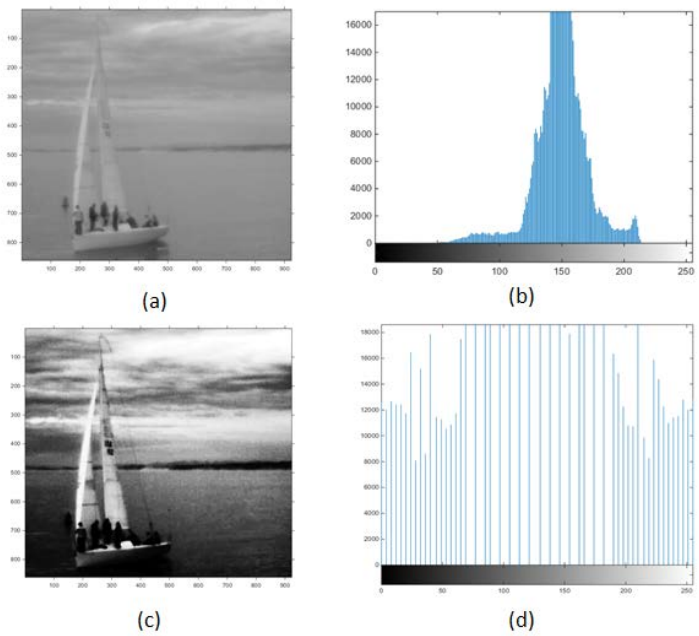

In (a) and (b), the original image and its histogram are presented while in (c) and (d), the corresponding results after histogram equalization was applied.

4. SURF Features: Detection and Description

The next step was the extraction of the features to be used as inputs in the artificial neural network (ANN). Speeded-up robust features (SURF) were finally selected and used for this step as they produce scale and rotation invariant features. These characteristics are particularly important in the maritime environment since platforms are constantly moving at unpredictable directions. Additionally, the detection of the interest points and the extraction of the corresponding descriptors were fast enough to support real or near real-time recognition based on these features. The steps that were carried out to finalize the features fed into the ANN are presented in Figure 56.

Figure 56. Steps for SURF Features Extraction

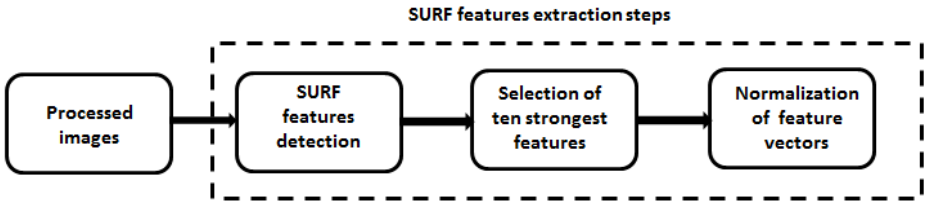

After image processing, SURF features were extracted, and the final features to be fed in the ANN were extracted after normalization of the ten strongest, as shown in the step-by-step process.

When SURF features were extracted for the image set, we noticed that a large number of images were formed around interest points from the background, thus creating multiple potential outliers that would eventually degrade the classification process. This problem could have been avoided if background extraction had been possible in the previous steps, and a larger number of the strongest features selected could have been possible early in the process. After experimentation with the number of the strongest features in each image, we identified the ten strongest. This selection provided enough features from various characteristic points of the boats to significantly reduce the outliers in the majority of the images. The results of detecting SURF features in one of the images are presented in Figures 57 and 58. As shown in these two images, the SURF features before and after histogram-equalization was applied differed but, still, no outliers were detected.

Figure 57. Total and Ten Strongest SURF Features in an Image

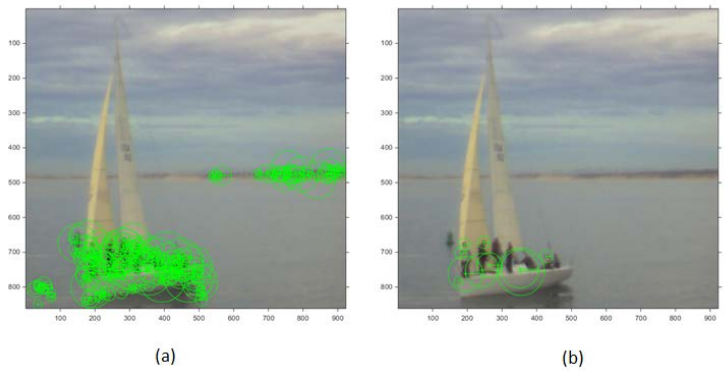

In (a), all the detected SURF features are displayed while in (b), only the ten strongest. All outliers were removed in this image by this reduction of selecting only the ten strongest.

Figure 58. SURF Features after Histogram Equalization

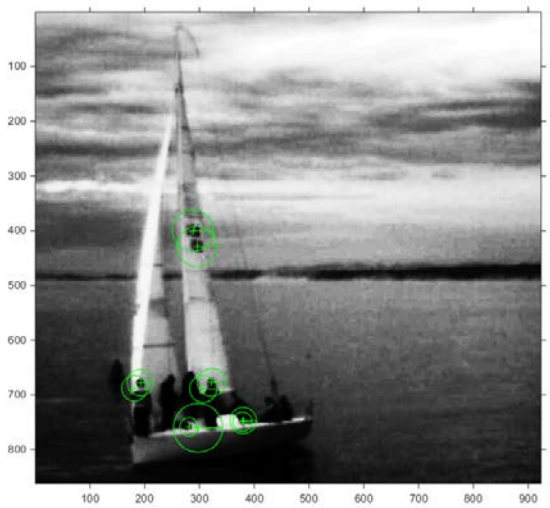

The ten strongest features detected in an image after histogram equalization. Notice that these features are different from the ones detected in Figure 57 (b).

The final step taken before the final features were formed was the normalization step. The maximum value of each feature vector was detected and used to normalize the 64 values of which each vector was composed. With this step, potential matching and scaled patterns of feature vectors could become easier for the ANN to associate.

5. Medium Level Image Fusion Implementation

During this step, feature vectors derived from the pairs of the visual and the thermal images were combined to investigate whether better classification performance occurred. The way the fusion of the features was applied is depicted in Figure 59,.

Figure 59. Medium Level Fusion of SURF Features

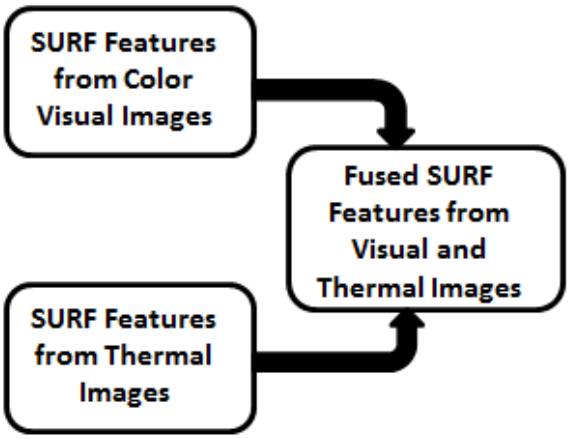

The extracted SURF features from the thermal and visual images were fused to create another feed for the ANN.

6. Image Classification Using an Artificial Neural Network

The classification process involves training an ANN, extracting the net with its weights, and finally, using it to classify the samples of the testing data, which were separated to ensure that they were not involved in the previous steps. In the following subsections, the procedure that was followed in these steps is further explained. Figure 60 presents the processes during the classification step.

Figure 60. Steps for Image Classification with ANNs

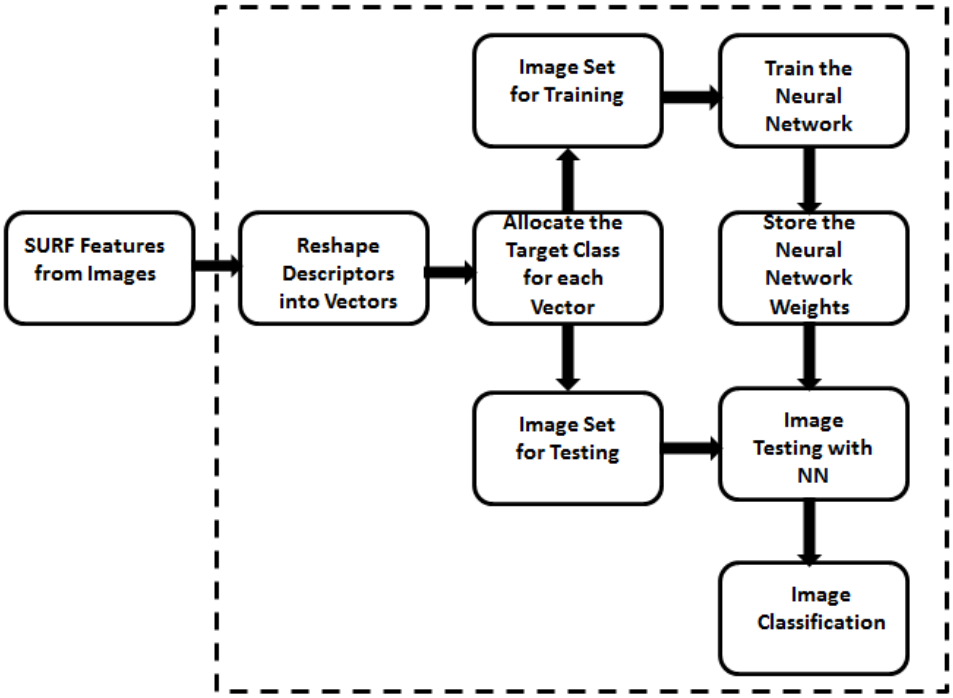

a. Training the Artificial Neural Network

Initially, the topology of the ANN had to be defined. As we had to deal with a binary classification process, as previously discussed, the number of outputs at the output layer had to be two. The number of neurons in the input layer was always equal to the number of the input features in all the different cases we tested; these sets are presented in Table 8. In order to determine the final number of neurons in the hidden layer, several tests were conducted that ranged from 20 to 400 neurons. It was important to have enough neurons to deal with the complexity of the problem. However, too many neurons could result in overfitting [72]. In the latter case, even if results during training appeared to be ideal, the results after testing would not be at an acceptable level. As a result, the final number of neurons at the hidden layer was set to 100, for which the conducted tests presented the best performance for the classification process. Hence, the topology finally selected was X-100-2, as shown in Figure 61, in which X was the number of inputs for each of the tests.

Table 8. Description of Tests and Number of Inputs

Trial No	Description	No of inputs	No of images
1	Visual images from DSC640	640	62
2	Thermal images from DSC640	640	62
3	MSX images from DSC640	640	62
4	Fused features from visual and thermal images from DSC640	1280	62
5	Mixed visual images from both cameras	640	85
6	Mixed MSX images from both cameras	640	85
7	MSX, thermal, and visual images from both cameras	640	232

The different sets coming from the corresponding sets of images or their fusion and the fusion of features that are tested are presented in this table. The results will be compared to drive our conclusions.

Figure 61. ANN Topology during Trials

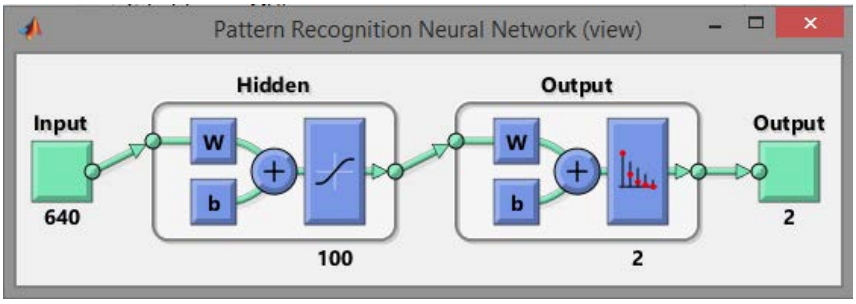

This ANN topology was 640–100-2. There were 640 inputs for the input layer, 100 neurons for the hidden layer, and two outputs.

After the images were separated in training and testing, a target class was assigned to each one of them as is required for the supervised learning problem of classification [49]. In our case, we had a binary classification problem, so the binary classes of 01 and 10 were assigned as target labels. The goal for the ANN in the training process was to learn to map the inputs to the predefined outputs or targets.

Additionally, and because of the small number of samples, early stopping was applied during the training process to further reduce the possibility of overfitting [72],

[73]. In order to implement this step, during each ANN training, the training set was further split into training and validation sets. When the performance of the validation set during training began to increase for a number of epochs without the same behavior detected in the training set, the training stopped. The updated weights of the epoch in which the overfitting initiated were stored for the ANN, as shown in Figure 62. Whenever early stopping was not selected for the trials, the classification rate during training always reached 100 percent, but the testing results obtained were poor and rarely exceeded 40 percent, which was a clear indication of overfitting.

Figure 62. Early Stopping

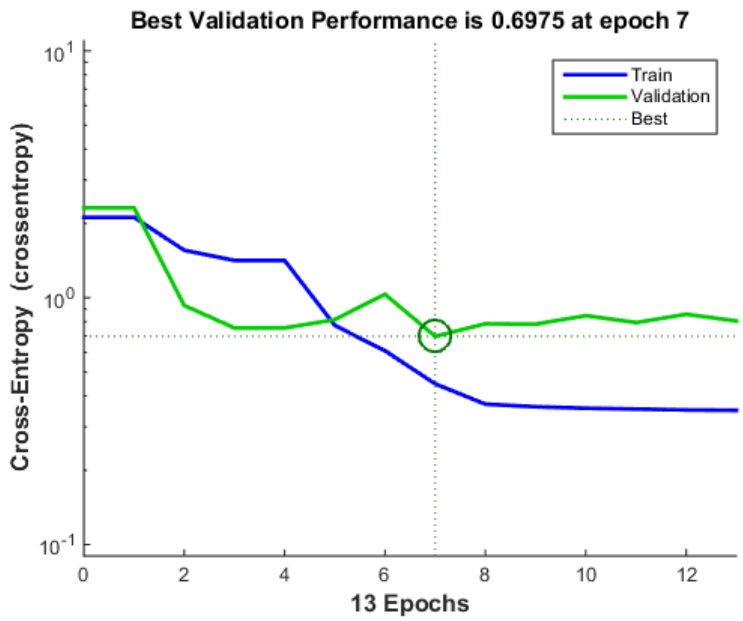

During the training process, the validation performance started increasing at epoch 7 while the same did not happen for training performance. Training stopped at epoch 13, but the weights that were stored were from epoch 7.

b. Classification

The final step was to obtain the classification output after the test data was used to evaluate the network. The techniques implemented in this case to compensate for the small number of samples were to retrain multiple times and to retrain multiple networks since training sessions started with different initial weights and biases [72]. In the first

case, a network was trained 1000 times, and in the second, ten different networks were trained 100 times each. The only change in the ten NNs occurred in the different training sets, and as a result, testing sets as bootstrap methods were used. The basic concept of bootstrapping was to randomly select training datasets with replacements from the total set of images that were formed in each case [69]. In both cases, 1,000 values of the mean-squared-error (MSE), cross-entropy, and classification performance as well as their averages were recorded and plotted. These averages were used as a metric to evaluate the performance of the network. The ANN that yielded the lowest MSE or cross-entropy or the highest classification rate would be the one that best generalized to the test set. Finally, the derived results for each of the cases of Table 8 were compared to help us evaluate whether any fusion process yielded better results than the cases in which only one type of image or feature was used.

C. CENETIX EXPERIMENTATION MODELING

CENETIX field experimentation was used in this thesis to test the hypotheses as well as support and enhance the conceptual idea of the proposed modeling. Several experiments were carried out during the recent constellation experiments that took place in San Francisco Bay during the last week of October. The results of the experiments this thesis could make use of were the ones involving imagery data dissemination from unmanned or manned systems as well as the decision support tools that were tested after the appropriate parameters were implemented to support Wave Relay radio monitoring [74]. Innovative solutions have always been the aim for CENETIX experimentation. Of particular interest for this thesis were the following three aspects of the CENETIX experiments: exchanging imagery data between divers and an unmanned underwater vehicle (UUV) via two-way communications; streaming video from an unmanned ground vehicle (UGV) performing a land search; and integrating CodeMettle network monitoring and management tools.

1. Mesh Networking Implementations for Imagery Data Dissemination

Mesh networking scenarios were planned during the recent CENETIX experimentation and collaboration session in San Francisco Bay that included

disseminating imagery data and streaming video. Manned systems, unmanned systems, and divers were planned as nodes that would extend the TNT-MIO backbone. Depending on the network's availability Wave Relay, satellite link, and 4G would be used. Previous experiments had resulted in successful networking of unmanned systems and swimmers, as shown in Figure 63. A step forward was attempted to include divers among the networked assets.

Figure 63. Networked Swimmers

Swimmers were successfully incorporated in the network in previous experiments.

2. CodeMettle's Network Monitoring and Management Tool

CodeMettle, as it is open source software, was configured to monitor Wave Relay mesh-network traffic and performance [75]. This was feasible since Wave Relay could be configured and monitored through the supporting application programming interface (API). This interface could run over the Wave Relay hypertext transfer protocol over SSL or secure (HTTPS) interface, thus allowing communication with programs that submitted requests conforming to the hypertext transfer protocol (HTTP) [6], [37]. The data and metrics enabled in management interface could be monitored through the Code Mettle network management support tool when configured according to the API. As a result, signal-to-noise ratio (SNR), traffic load, node status, GPS information, channel usage, and other parameters were monitored and graphically analyzed to enhance SA concerning

network nodes and enable end-to-end network management. An instance of CodeMettle management tool graphics is shown in Figure 64.

Figure 64. CodeMettle Management Tool Graphics

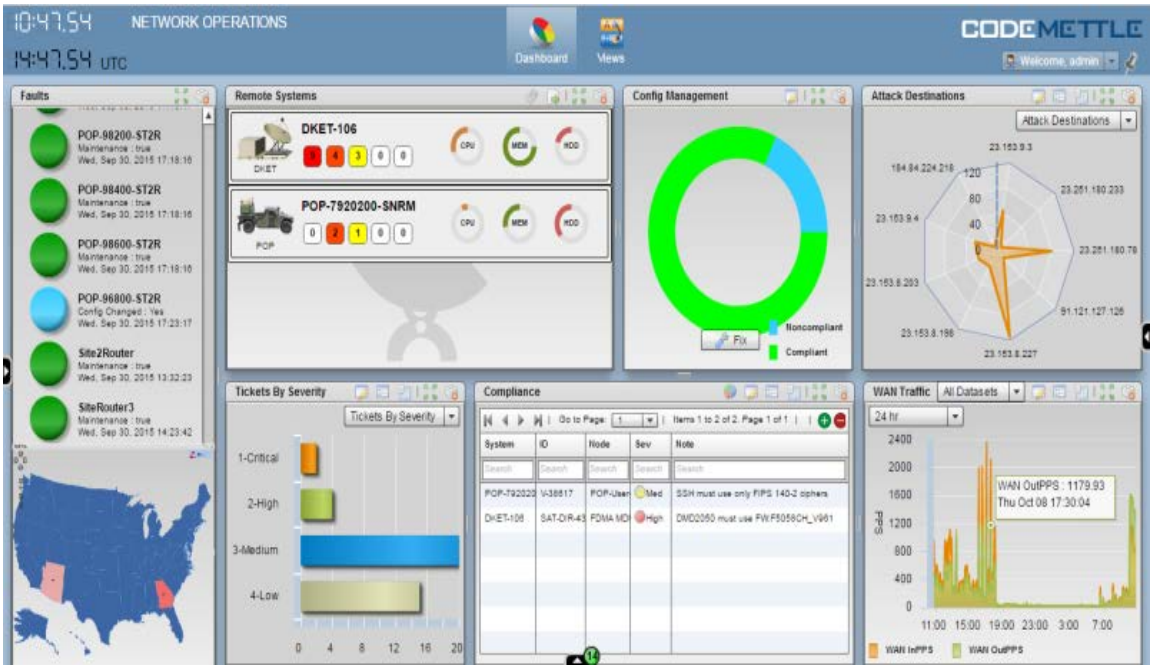

IV. SIMULATION AND EXPERIMENTATION RESULTS

The steps and methods applied for the simulation modeling of automatic target recognition (ATR) through a mesh network of imaging sensors described in the previous chapters gave us a variety of results that are presented in the following sections. The results are separated in three categories. The first category includes the results obtained from the mesh network simulation in Systems Tool Kit (STK) and QualNet. Next, the relevant Center for Network, Innovation and Experimentation (CENETIX) results from field experiments are presented. The third and final category involves the results concerning the image fusion and classification process.

A. STK AND QUALNET SIMULATION

Several problems were detected and delayed the STK and QualNet simulation of the mesh network of multiple heterogeneous nodes through Wave Relay radios. The first step of integrating the QualNet interface was successfully resolved after following already proposed solutions from previous theses, as already discussed. The problems that came up during the replay phase, though, were not solved within the time available for this thesis. The results obtained from the overall STK simulation are presented in the following subsections.

1. STK

The STK simulation was intended to give us an insight into what ranges we should expect to establish communications between the several nodes that were imported in the scenario. The scenario involved two surface units, an unmanned aerial vehicle (UAV), one ground vehicle, and three ground stations. In Figure 65, an instance of the simulation is shown. The white lines represent the routes followed by the platforms, and the brown lines represent the communication links between the nodes. In this instance, the range between the two surface units was the maximum observed in the scenario. The height of the antennas was set to 10 meters, and the measured distance was 14.6 km. The rest of the ranges that were measured cannot be considered as a basis since they were dynamically formed. The altitude and route of the UAV, the height of the ground

stations, and the geography were the parameters that affected the various ranges that links were closing between the nodes.

Figure 65. Wireless Mesh Links of the Participating Nodes

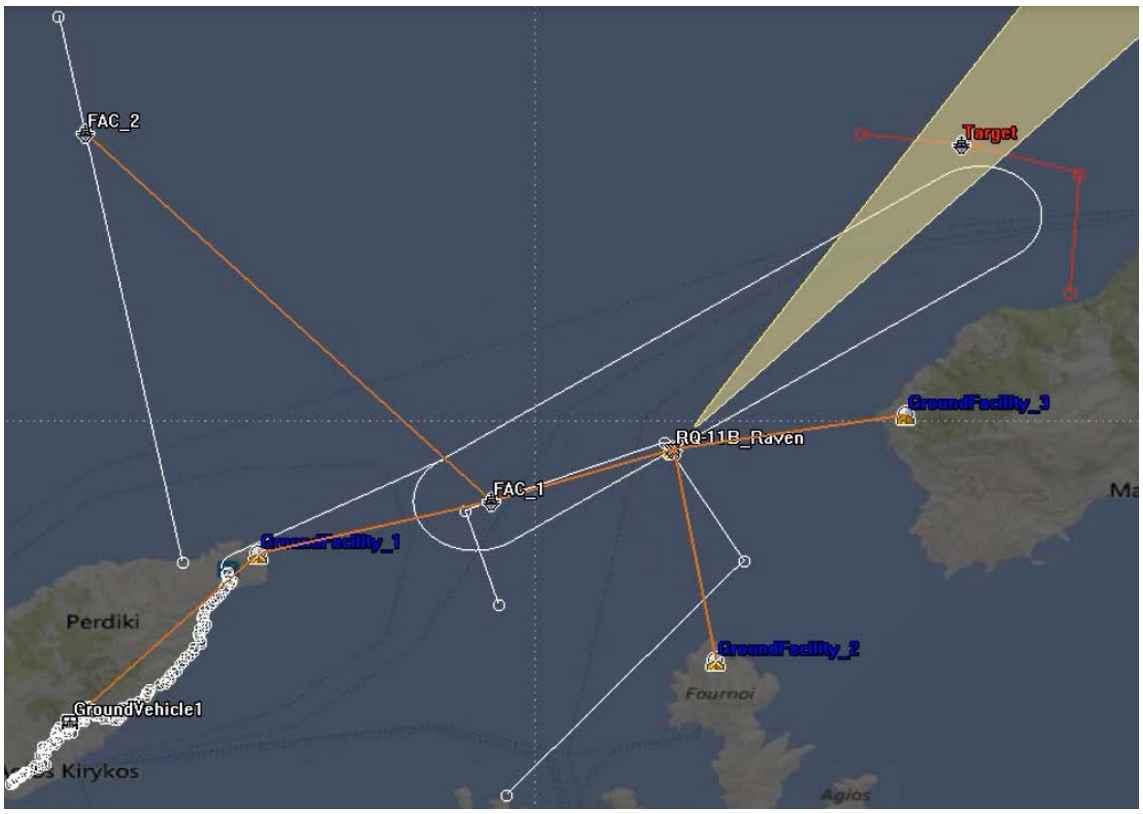

An instance of the wireless mesh network simulation is depicted in this image, as extracted from the STK scenario. The various platform-nodes are moving along the routes shown in white. The dynamic forming of communication links is represented by the brown lines.

Additionally, results were also derived concerning the availability of the imaging satellites. A theoretical field-of-regard (FOR) within which the look angle could be tasked is depicted by the brown sector in Figure 66. The time window that the field of view (FOV), depicted with a red sector, could be tasked inside the FOR and the area of interest (AOI) was calculated to nine minutes over a 24-hour period from the STK tools. Small intervals in which imaging sensors were not available were reported as expected and can be easily assumed from Figure 66. The scenario, though, did not have as a goal to demonstrate continuous access but rather to demonstrate the availability of imaging

capabilities for low earth orbit (LEO) cube-satellites. The orbits could be redesigned accordingly to give the desired availability of the sensors.

Figure 66. Image of Cube-Satellites in STK Scenario

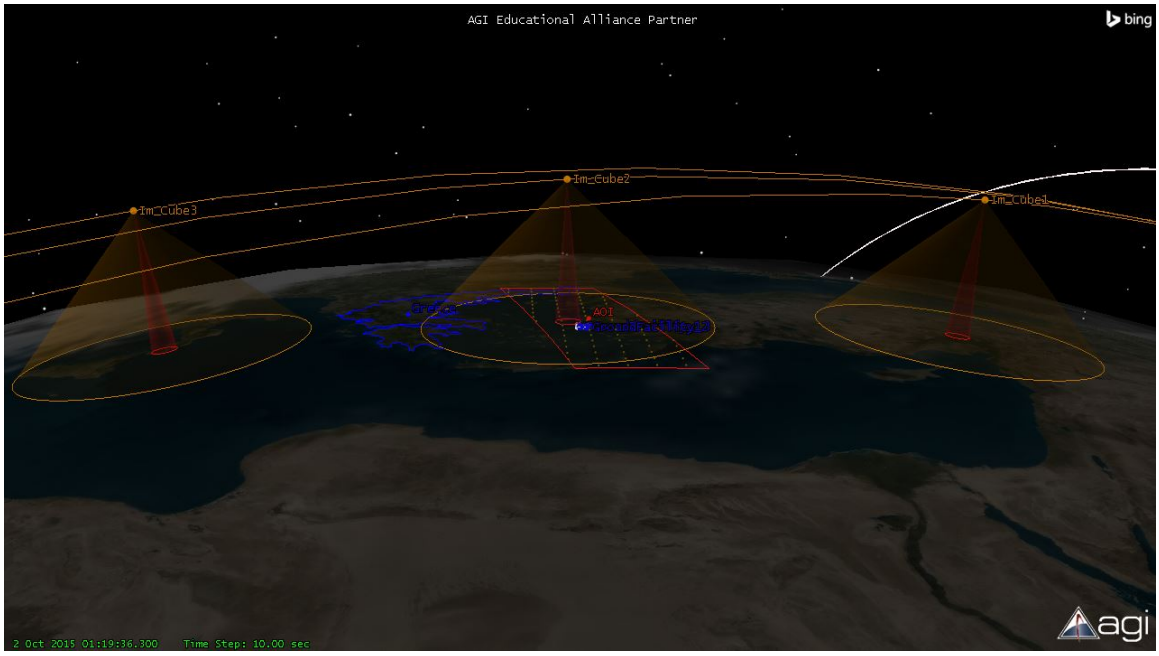

FOR and FOV of the imaging satellites are depicted in this figure as extracted from the 3D graphics window of the STK simulation.

The total time that communication links could be established between the imaging satellites and the ground stations was calculated to 22 minutes from STK tools. In Figure 67, an instance from 2D graphics of STK simulation is presented. The brown lines in the figure represent the closed links between the ground stations and an imaging satellite. Part of the crosslink between the satellites is also shown. The crosslinks make it possible for the time window of communications within each orbital period to be continuous. While these communication links are available, they contribute to communications between the nodes, especially when links between ground stations are broken due to range and geographical restrictions.

Figure 67. Image of Cub-Satellite Links

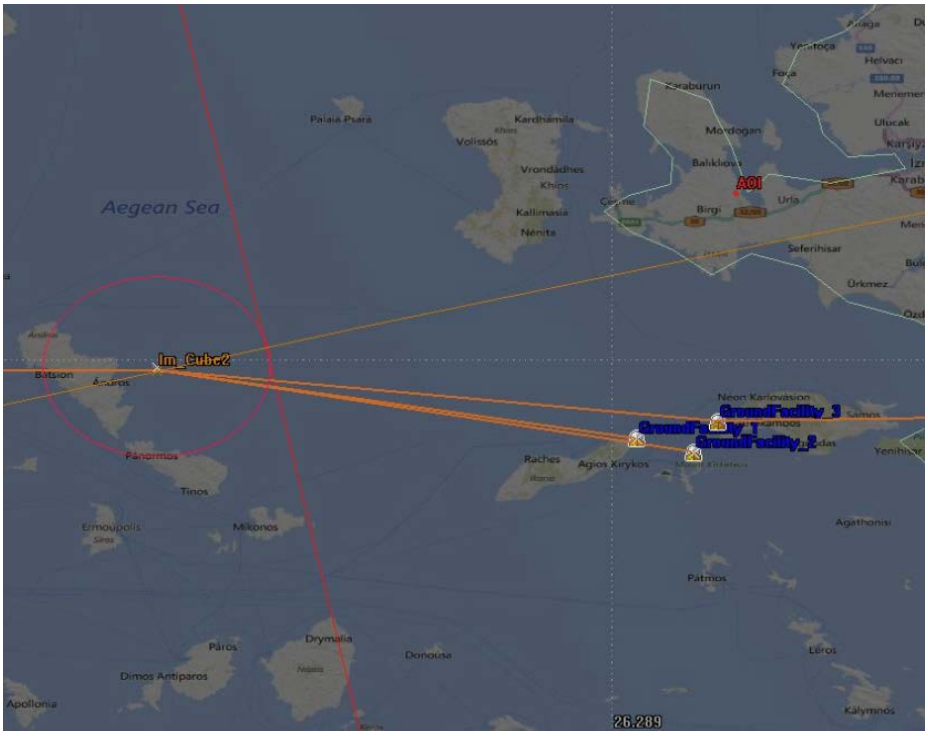

In this instance of 2D graphics extracted from the STK scenario, communication links between ground stations and satellites as well as crosslinks are depicted in brown.

After adding a constellation of communication relay satellites, crosslinks were multiplied. The time window that communications with the imaging satellites and thus tasking them was possible was then increased to three hours over the 24-hour period of the simulation run. In this case, communication intervals were evident and the tasking, even if possible at the same time, was not restricted in the specified AOI but instead, in the random locations of the imaging satellites. In Figure 68, the communication relay satellites and their orbits are depicted in white while the imaging satellites are depicted in brown. The purpose for this implementation was, again, to demonstrate the ability to increase the available time for communicating with the imaging satellites. Certain limitations continue to exist since the availability cannot be continuous. However, the benefits are obvious for the mesh networks of the sensor since the contribution of the satellite constellation was increased from 22 minutes to 3 hours.

Figure 68. Communications Relay and Imaging Cube Satellite Constellations

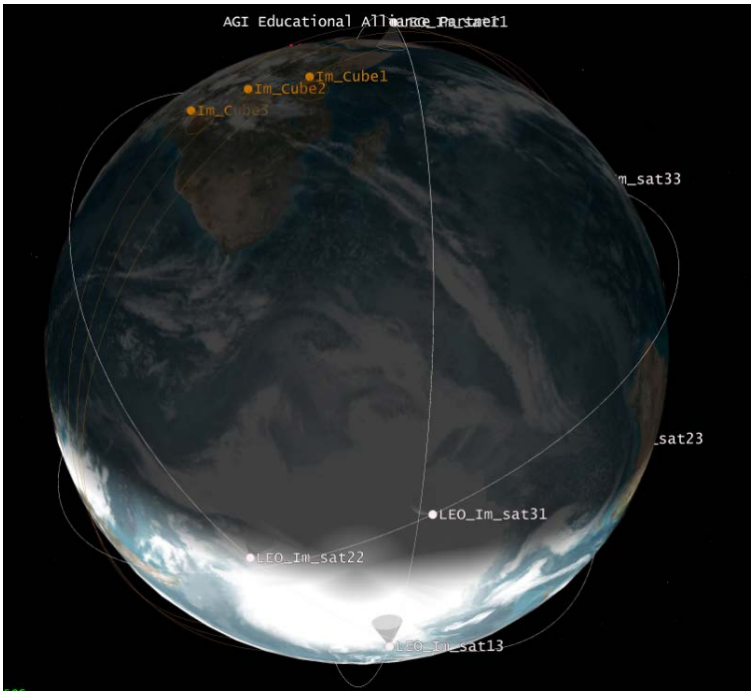

In this instance of 3D graphics extracted from the STK scenario, the two satellite constellations are depicted. The communications relay satellites and their orbits are shown in white and the imaging ones in brown.

2. QualNet

The QualNet add-in, although successfully integrated and configured for the needs of this scenario, always crashed the STK simulation. Several attempts were made to recover it and run the replay of QualNet to evaluate the Wave Relay performance under the constraints of the available applications. Unfortunately, there was no success and, thus, this task is left for future work in this research area. What we expect from this interface is that it can give us a more realistic range than applications over Wave Relay could in the field.

B. CENETIX FIELD EXPERIMENTS

From the several CENETIX experiments that were carried out in San Francisco during the most recent experiments, the extracted results of some of them prove the feasibility of this thesis concept. Previous fourth generation Wave Relay performance, integration of the CodeMettle network-managing and monitoring tool, as well as

incorporation of divers and unmanned ground vehicles (UGVs) into the tactical-network-topology (TNT) reachback, demonstrate the potential of a system with these capabilities. More detailed results for each of these experiments are presented in the following subsections.

1. Wave Relay Performance

Wave Relay was widely used to network marine units of the TNT testbed. The interest of this thesis was to extract a maximum distance at which node to node communications link could be closed. As shown in Figure 69, the maximum detected range during this scenario was 4.02 km. This range matches what was expected based on previous experience and CENETIX field experimentation. The maximum range derived from fourth generation Wave Relay radios is obviously shorter since power is one-third of what the fifth generation of radios offers.

Figure 69. Wave-Relay Node Tracks Replayed in Google Earth

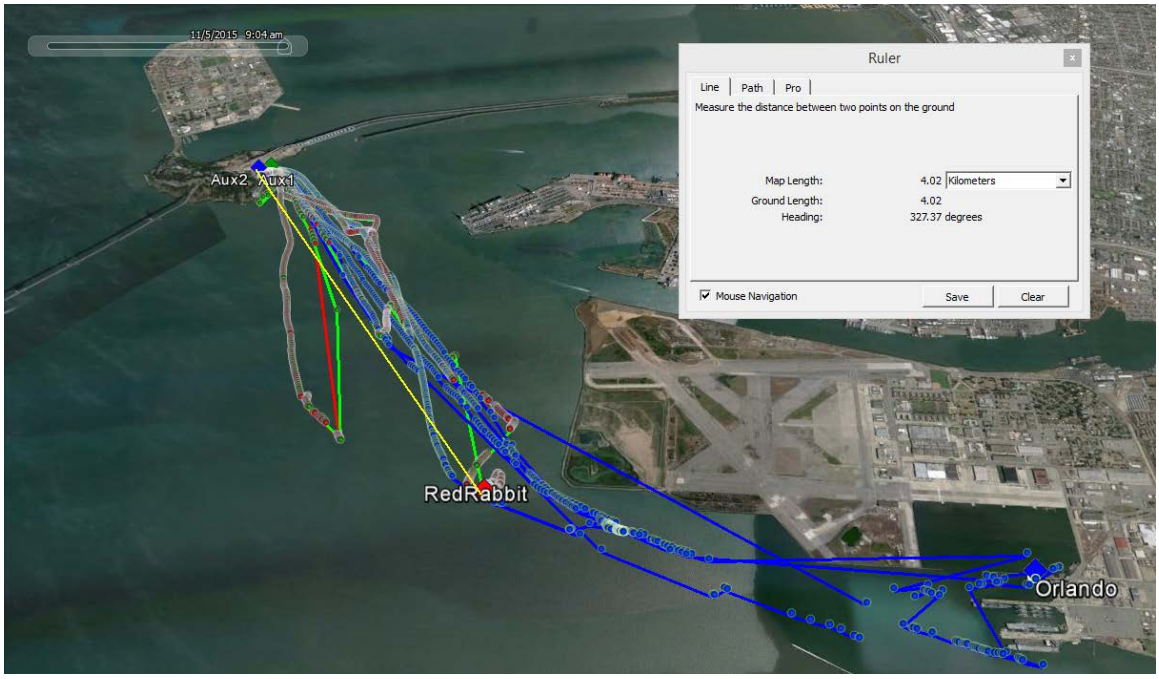

Tracks of marine boats as Wave-Relay nodes as replayed from SA Replay Control page on CENETIX site and displayed in Google Earth. Source: "SA Replay Control," http://cenetix.nps.edu/SA1/SAReplay/#

2. CodeMettle

After the successful integration of the CodeMettle hybrid network orchestration tool for the monitoring and management of the CENETIX backbone and testbed reachback, the visualization of the current status of the nodes and the overall performance metrics of the network were possible. As shown in Figure 70, geographic information of the nodes and the overall network was possible as well as the capturing of their tracking data. Additionally, network traffic and latencies were visualized, which made it possible to estimate the source of any detected network downgrades.

Figure 70. CENETIX Backbone Network Details via CodeMettle Dashboard

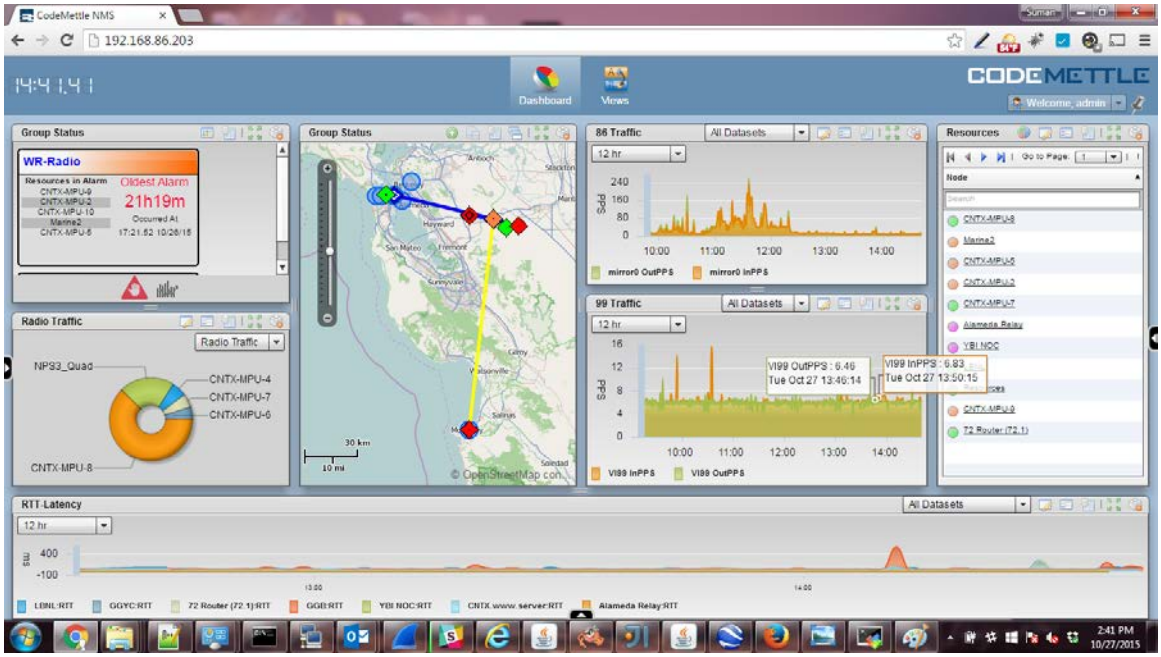

In this extracted instance of the CodeMettle dashboard, several metrics and visualizations of the CENETIX backbone and testbed reachback are presented.

During the monitoring of the wireless mesh network formed by the Wave Relay nodes, CodeMettle made it possible to feed the network operations center (NOC) with live geo-data that was additionally captured for replay and analysis purposes. As it is shown in Figure 71, traffic analysis by node of the mesh network was possible as well as access to further details of the nodes such as IP addresses of the nodes, connectivity strength, and quality between the nodes. The availability of these visualizations and metrics enhanced the situational awareness (SA) of the NOC personnel and assisted in decision making processes in terms of corrective actions for a more efficient use of the network and its nodes' capabilities. In this thesis concept, the available information from CodeMettle could support the efficient use of the available bandwidth based on the operational needs. The capability that CodeMettle demonstrated to perform hybrid-network orchestration—since it is designed to be network agnostic—makes it a necessary tool for future implementation of distributed operations solutions.

Figure 71. CENETIX Wave-Relay Mesh Network Details via CodeMettle Dashboard

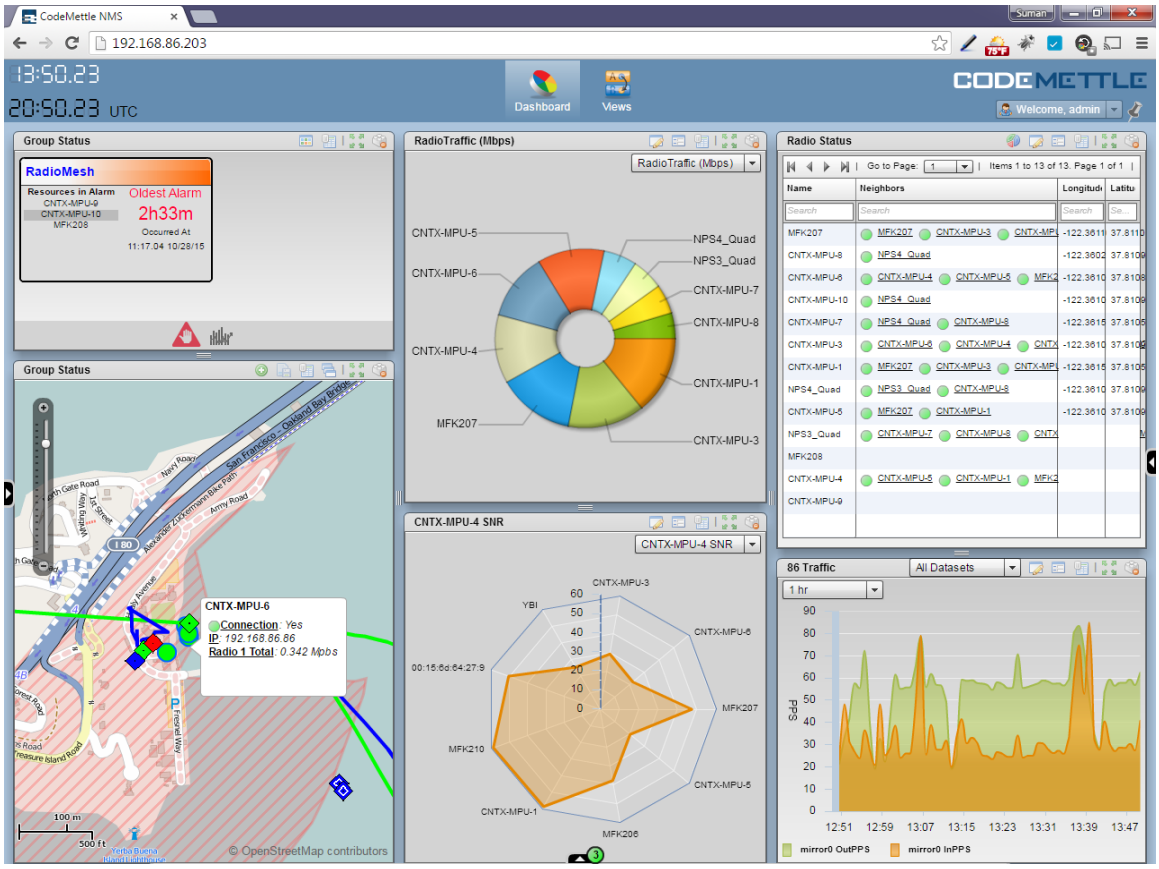

3. Wireless Communication with Divers and UGV

Both UGV and divers were successfully incorporated into the CENETIX reachback. In Figure 72, the components that made possible imagery data dissemination to divers are demonstrated. More analytically, in Figure 72 (a), the diver is shown ready to dive after configuring his android device, which was encapsulated in a waterproof case. Because of the pressure when underwater and, therefore, the inability to activate the camera through the touch screen, the solution of a near-field-communication (NFC) tag was successfully implemented. In Figure 72 (b), a message is shown on the screen that informs the diver that the captured image is ready to be uploaded in the application that enables communication with the NOC. The image is captured by activating the camera through an NFC tag. In Figure 72 (c), an instance of the application is shown, whereby the diver receives in his device an image captured from an unmanned underwater vehicle

(UUV) in Keyport (Seatttle) through the CENETIX testbed. In Figure 72 (d), the equipment to connect the diver to the CENETIX testbed is shown. The buoy was composed of a computer connected to the CENETIX testbed through the 4G network and was connected through ethernet cable to an android device. Bluetooth was used for the communication between the tethered device and the one that was available to the diver. In Figure 72 (e), an instance of the application running in the NOC is presented. Through this application, dissemination of messages and images with the diver was possible.

Figure 72. Enabling Communications with Divers

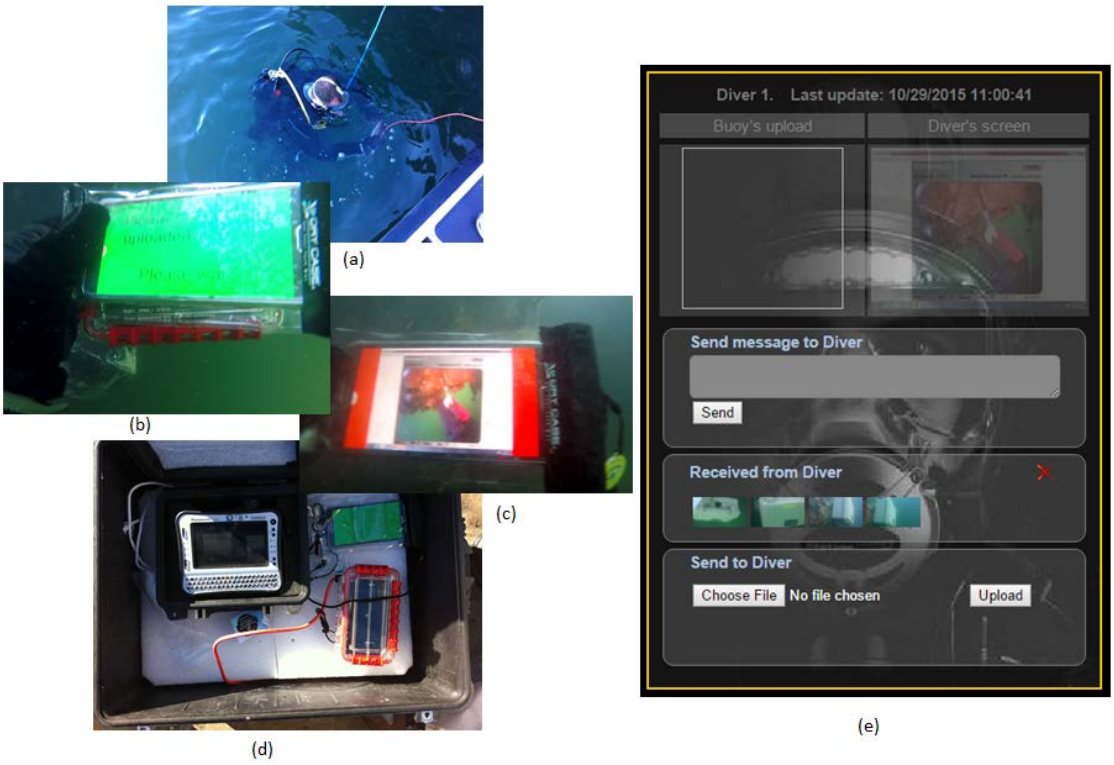

In this figure, components of the implementation of incorporating divers in the CENETIX reachback are presented. In (a), the diver is ready to dive after configuring his android device. In (b), a message is presented that the image the diver captured by activating the camera through a near field communication (NFC) tag, and sent to the NOC, is ready to be uploaded. In (c), the diver receives in his device an image captured from an unmanned underwater vehicle (UUV) in Keyport (Seatttle) through the CENETIX testbed. In (d), the equipment to connect the diver to the CENETIX testbed is shown. The buoy was comprised by a computer connected to the CENETIX testbed through 4G network and was connected through ethernet cable with an android device. Bluetooth was used for the communication between the tethered device and the one that was available to the diver. In (e), an instance of the application running in the NOC is presented. Source: "TNT-MIO Experimentation: Video and snapshots archive" , http://cenetix.nps.edu/cenetix/tnt.asp and author's captured images in the field.

Finally, the UGV was also successfully networked to the CENETIX testbed through Wave Relay. A ground station acting as a gateway interconnected the Wave Relay mesh network with the TNT testbed via satellite communications.

Figure 73. Enabling Communications with a UGV

In (a), the UGV connected through Wave Relay to the TNT testbed is shown. In (b), the Wave Relay radio and the application that the UGV runs for the detection of radioactive materials is presented. Source: "TNT-MIO Experimentation: Video and snapshots archive" , http://cenetix.nps.edu/cenetix/tnt.asp.

C. IMAGE FUSION AND CLASSIFICATION

The methodology that was followed for this part of the experiments was described step-by-step in the previous chapter. The datasets presented in Table 9 were processed twice through the classification procedure using a MATLAB script. The first time, the test set was kept the same for 1000 trials. The second time, 10 ANNs were simultaneously trained with 10 random test sets, respectively. In an effort to yield unbiased results in the first case, the tests comprised the same images for the groups of datasets that had the same number of images as in the test set. The final classification performance results for each dataset is our final aim to evaluate whether multi-sensor image fusion adds value in the classification process.

Table 9. Datasets for Testing

Trial No	Description	No of images	No of test images
1	Visual images from DSC640	62	7
2	Thermal images from DSC640	62	7
3	MSX images from DSC640	62	7
4	Fused features from visual and thermal images from DSC640	62	7
5	Mixed visual images from both cameras	85	9
6	Mixed MSX images from both cameras	85	9
7	MSX, thermal, and visual images from both cameras	232	23

1. Feature Extraction and Training Results

The MATLAB script used to obtain the results is graphically described in Figure 74. After the image processing steps, each image set was scanned, so SURF features could be extracted. Consequently, the ten strongest features were turned into vectors and assigned a binary class of 01 or 10, matching to the classes of powerboats and sailing boats, respectively. The descriptors had 640 elements for each image in all datasets, except for dataset four in Table 9 in which the fused features resulted in descriptors with a doubled size of 1,280 elements. The ANN was then trained, and the extracted weights were stored. The test set was finally gone through the stored ANN weights and the classification performance, as well as the cross-entropy and the MSE were stored for each trial to be used as metrics for the evaluation of the overall results.

Figure 74. Image Classification Steps

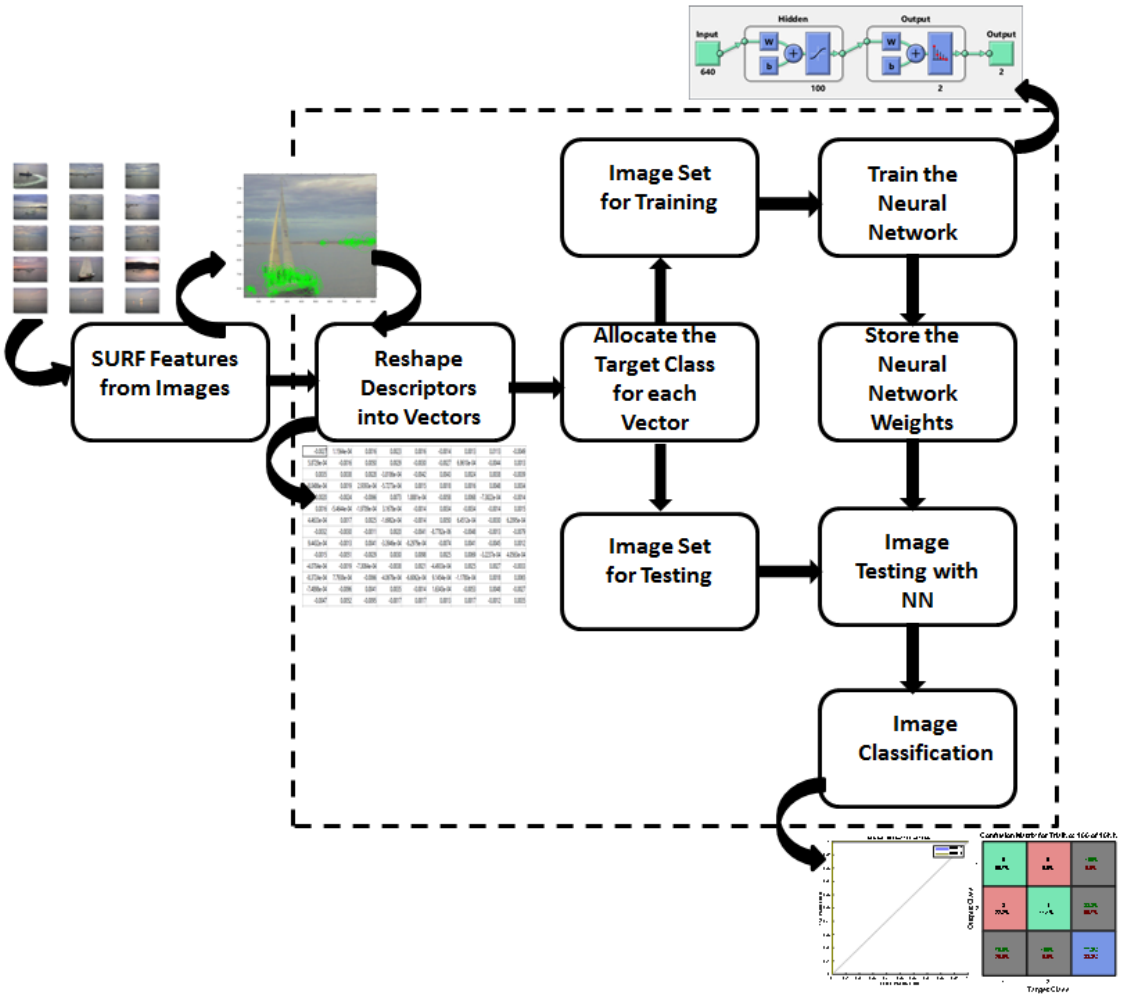

After comparing the extracted features for each dataset, it was observed that SURF features were indeed repeatable but different for the distinct datasets of the images. The depiction of this result is presented in Figure 75.

Figure 75. Ten Strongest SURF Features for the Different Image Sets

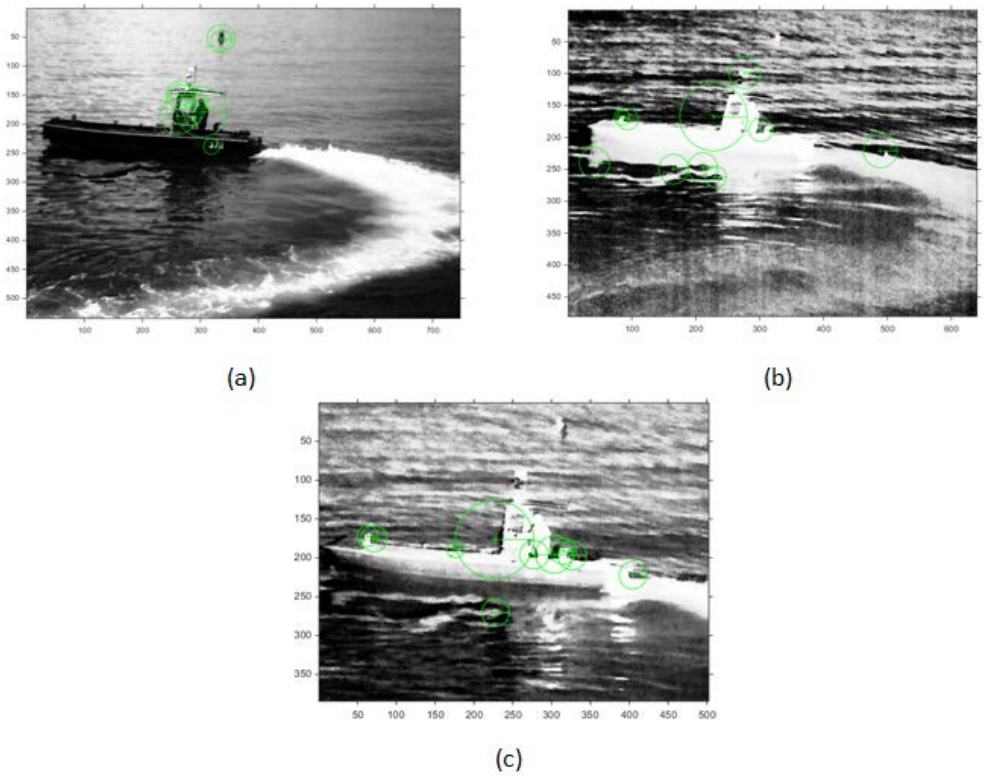

The ten strongest SURF features were always repeatable but different for visual in (a), thermal in (b), and multi-spectral in (c). All the images were in grayscale.

As discussed in Chapter III, early stopping was applied during all the training sessions as the results were better than the ones obtained when it was not applied, even though cross-entropy was smaller in the latter cases. This fact was evidence that the implementation of early stopping succeeded in avoiding overfitting.

Furthermore, classification performance during training was constantly monitored and, in the case of the multispectral dataset, demonstrated very good results. The confusion matrix and the ROC curves from one training session are presented in Figure 76. From the monitoring of the training processes, it was concluded that the classification of the sailing boats class demonstrated constantly higher percentages. The factors that possibly contributed to that result were the larger number of sailing boats in the dataset compared to that of powerboats, as well as the fact that powerboats had a wide variety of shapes and structures.

Figure 76. Confusion Matrix and ROC Curves for Training and Validation

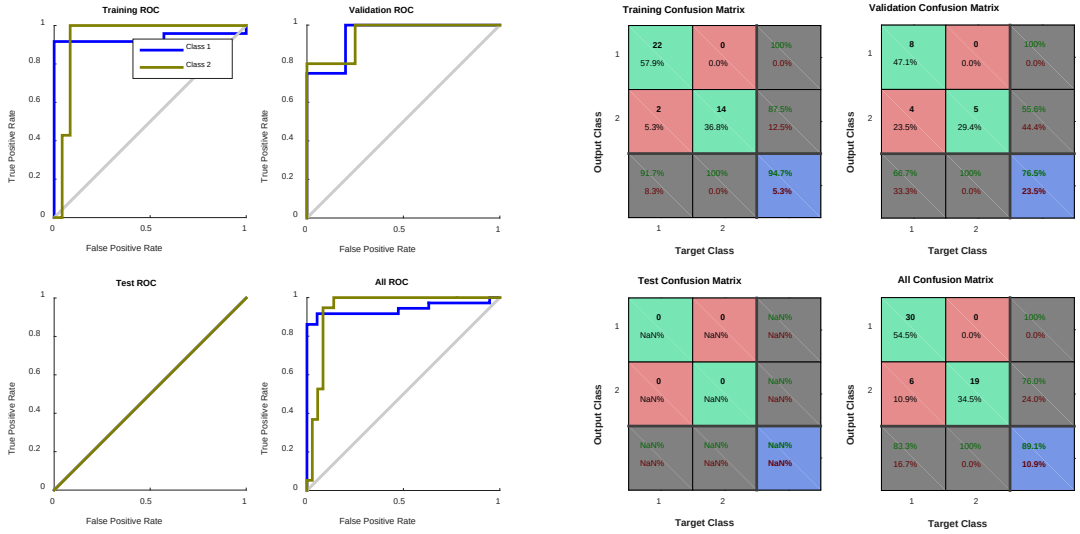

The presented confusion matrices and curves refer to one training session of the 1000 trials over the 10 NNs.

2. Testing Classification Results

After the training process was completed and the parameters and weights of the NN were stored, the test set was fed into the NN. The results were also monitored and stored. Fourteen sets of plots were derived from the MATLAB code implementation concerning the metrics and results relevant to the classification performance of the test sets. The set that represents the best results are presented and described to support the overall analysis. This set was obtained from the MSX images from dataset 3 of Table 9 and for the case of the ten different ANNs. Figure 77 shows the results obtained from an individual trial.

Figure 77. Confusion Matrix and ROC Curve for One Trial

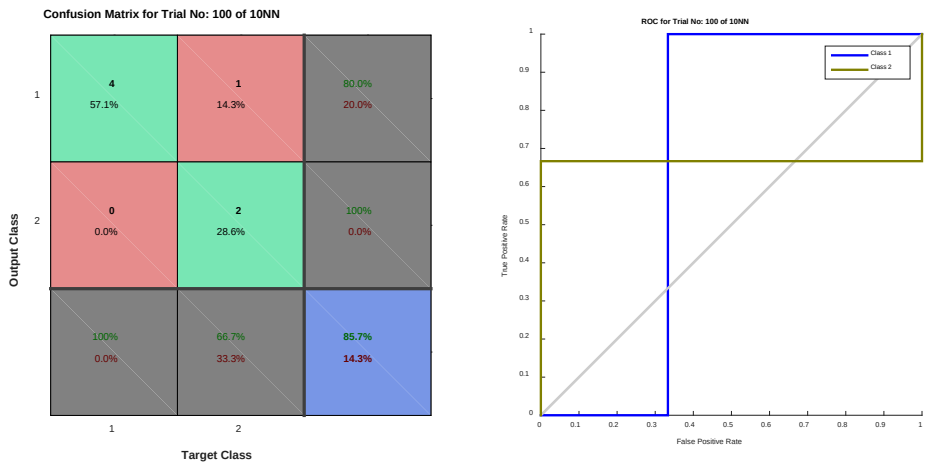

The presented confusion matrix and ROC curves refer to one testing session of the 1000 trials over the 10 NNs.

The stored values of each testing process were plotted to present an overall pattern of the classification performance. In Figures 78 and 79, the average classification over 100 trials for each of the ten NNs and the individual 1,000 trials are presented. The average classification performance of this set was above 62 percent, but the individual results per trial demonstrated a wide spread from 0 to 100 percent. The previous observation denotes that there were some cases in which the NNs did not generalize well on the test set. In the majority of the cases, the powerboat class yielded the worst classification rates. Possible reasons for this result could be the smaller number of sample images compared to the sailing boats as well as their variety in shape and type. Conversely, sailing boats had less varying shapes.

Figure 78. Average Correct Classification Performance for the 10 NNs

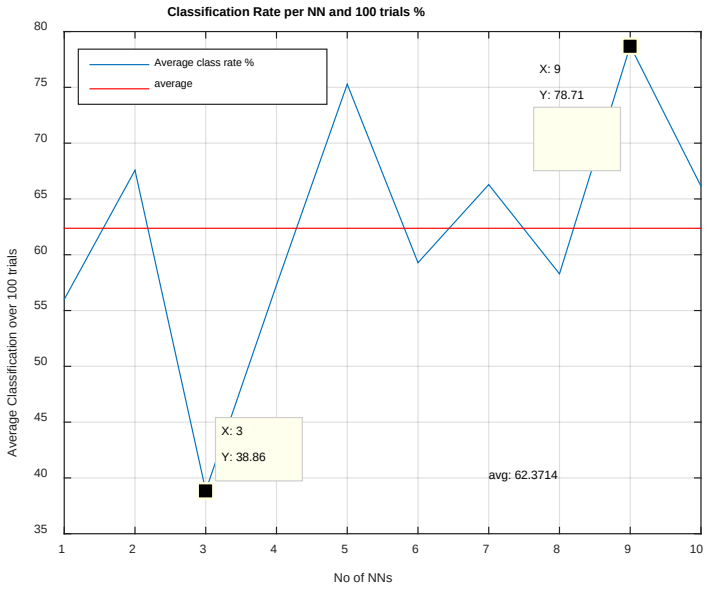

Figure 79. Correct Classification Performance for Each of the 1000 Trials of the 10 NNs

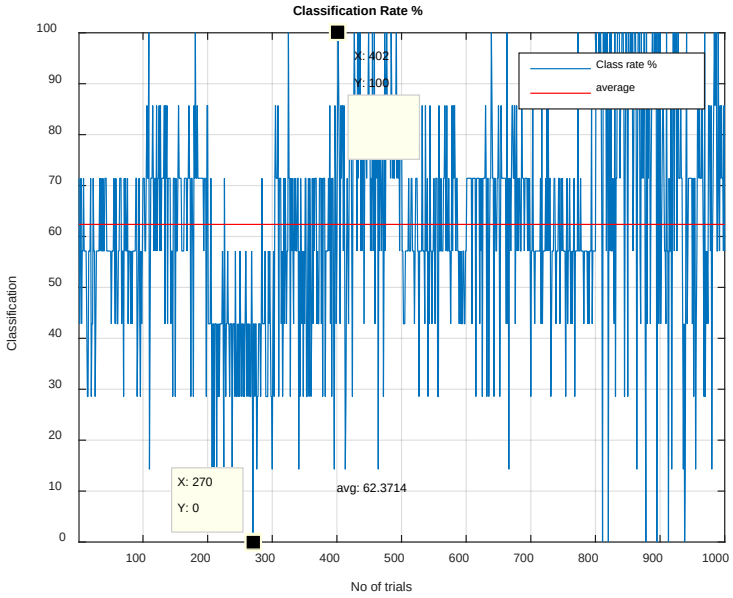

Additionally, cross-entropy and mean-squared-error (MSE) were plotted for each trial and used as a measure of fit. The lower values represent NNs that better generalized to the test dataset. In Figures 80 and 81, the obtained results for these metrics over 1000 trials are shown.

Figure 80. MSE over 1000 trials

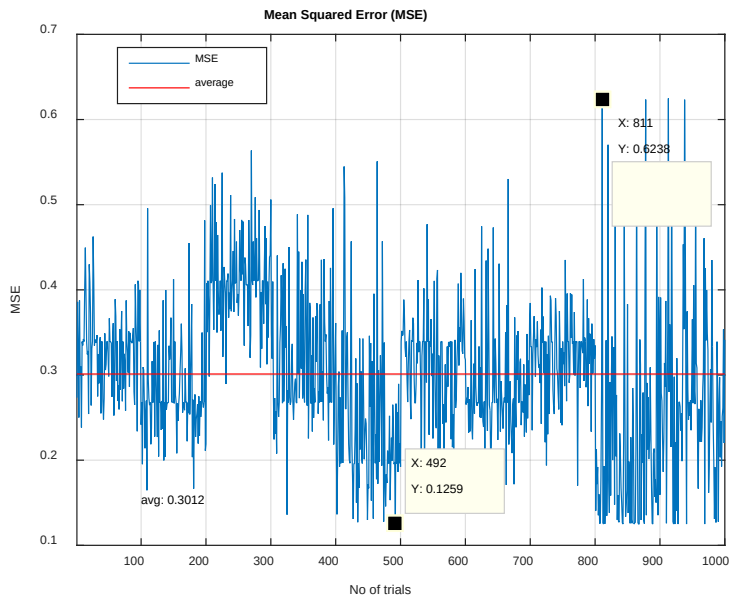

Figure 81. Cross-entropy over 1000 Trials

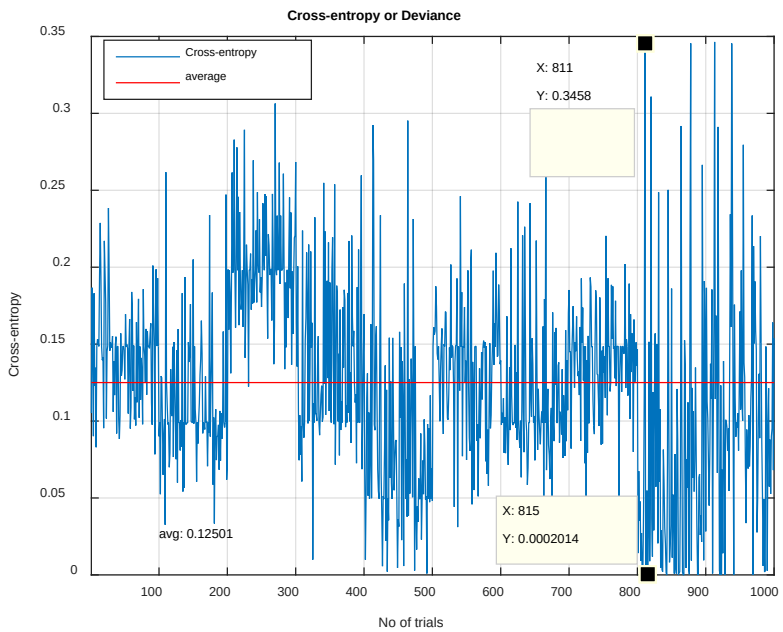

As previously discussed, the smaller the derived values of cross-entropy and MSE, the better the generalization over the test value as well as the classification rates.

3. Summary of Image Classification Results

The classification results for all the datasets and the case of 10 NNs are presented in Table 10. The best rates were obtained for the MSX images closely followed by the thermal-image sets. In general, when images only from the better camera were used, the obtained results were clearly better. Additionally, low-level fusion of the MSX images clearly gave better classification results than medium-level fusion of the SURF features obtained from the visual and thermal images.

Table 10. Overall Classification Results

Trial No	Description	No of images	No of test images	Test set	Average Classification (%)	Average MSE	Average Cross-entropy
1	Visual images from DSC640	62	7	10 random	58.8857	0.3193	0.13748
2	Thermal images from DSC640	62	7	10 random	60.3714	0.31225	0.13277
3	MSX images from DSC640	62	7	10 random	62.3714	0.3012	0.12501
4	Fused features from visual and thermal images from DSC640	62	7	10 random	55.2	0.3424	0.15248
5	Mixed visual images from both cameras	85	9	10 random	50.6	0.35521	0.1632
6	Mixed MSX images from both cameras	85	9	10 random	54.4778	0.33654	0.15019
7	MSX, thermal, and visual images from both cameras	232	23	10 random	54.5522	0.33704	0.15055

Derived results after averaging 100 trials for 10 ANNs trained with 10 random test sets. While the test sets were the same in each one of the 100 trials, training and validation sets were randomly selected with a ratio of 7:3, respectively. The best classification result was obtained from the MSX image set captured with the FLIR DSC 640 camera, which had the best resolution.

THIS PAGE INTENTIONALLY LEFT BLANK

V. CONCLUSIONS

This thesis demonstrated simulation modeling of the concept of automatic target recognition (ATR) via mesh networking of imaging sensors as part of the concept of distributed management of littoral operations. Proof of the feasibility for specific parts of the overall concept was verified with simulations and field experimentation. The parameters for the simulations were based on commercial and already tested solutions either in field experiments by CENETIX field experimentation or in published results.

Initially, different platforms with imaging capabilities were simulated as nodes in an ad-hoc mesh tactical network scheme. The quality of service (QoS) of this network was then studied. The extracted results from STK, field experiments, and Qualnet showed the feasibility of using this type of network for the timely dissemination of critical imagery data. Furthermore, images of boats were captured in the field to simulate images taken from sensors of the networked platforms, which cover the visible and part of the IR spectra. Captured images were selected to have noisy background that is usually met in littoral environments. Low- and medium-level fusion were applied on three types of imagery data—visual, thermal, multi-spectral (MSX)—and speeded-up robust features (SURF) were extracted from them. Results have proven that MSX images from low-level fusion contribute to better classification results in this thesis' binary classification problem. Artificial neural networks (ANNs) were used to derive the classification results and demonstrated the ability to obtain these results in a timely manner that can accommodate near real-time classification of COIs at the tactical level.

Finally, CENETIX's latest experimentation results were used to demonstrate not only the operational advantages of mesh networks but also the capabilities of managing them. Hence, this thesis suggests that major units should have the capability to deploy mesh tactical networks augmented by sensor management, operational databases, geographic information, and an appropriate level of automation for target recognition, especially when assuming the role of mother ships for other platforms. More specific conclusions from the research in mesh tactical networking and image fusion and

classification, as well as future work recommendations are discussed in the following sections of this chapter.

A. MESH TACTICAL NETWORKING

The scenario implemented in Systems Tool Kit (STK) demonstrated great potential to evaluate equipment capabilities and test them in operational scenarios with simulated platforms. The simulated mesh tactical radios demonstrated increased ranges from already tested, in-the-field, fourth-generation Wave Relay radios. This result seems reasonable since power was three times more than the previous version and technologies, such as multiple-input multiple-output (MIMO), had embedded.

The QualNet add-in was successfully installed, but during the attempts to run its replay and test the performance of the network with a simulated application, the STK scenario crashed. What would be expected had the scenario run successfully, would be that the ranges the actual applications would demonstrate acceptable performance would be less than the ones that the communications link were closing. Furthermore, the various ranges that the fifth generation of Wave Relay gave as results for establishing communication between the assets used in the simulation showed that these ranges are highly dependent on the geography and the routes of the assets.

Additionally, field experimentation demonstrated very promising results both for communications with divers and the UGV that could become part of the mesh network. Gateways connecting mesh network with 4G and satellite links were used to establish communication between the remote platforms and the network operations center (NOC) through the CENETIX TNT-MIO testbed. In all the cases, imagery data dissemination was successful. Especially in the case of the diver, obtained results revealed new ways that could be developed to allow for continuous communication with special forces even when underwater.

Finally, CodeMettle was successfully implemented for management and monitoring of the wireless mesh tactical network. Results showed that real time monitoring of the performance of the network and the nodes through the dashboard supported decision-making. The reasons that the network demonstrated downgrades and

reduced performance could be easily recognized. Corrective actions could then be determined. An overall implementation would eventually enhance situational awareness (SA) by taking into consideration the network parameters for a more effective deployment of the available assets.

B. IMAGE FUSION AND CLASSIFICATION

Operational experience and previous experiments have proven that operators of imaging sensors find beneficial the use and projection of multi-spectral imagery data from low-level fusion as they reveal richer combined information. The fusion of thermal and visual images in our experiment obviously enhanced the perception of the operator by revealing details that allowed for faster identification of specific spots or objects in the images. Therefore, current capability of imaging sensors to shift from a visual to IR mode is not as efficient as adding a multispectral mode. This thesis has proven that the same conclusion holds for the case in which computer-vision methods are implemented in automatic target recognition (ATR). Multispectral images gave higher classification results than all the other sets of images that were tested, even when classification rates were not sufficiently high. However, since several limitations were known from the beginning of this research concerning the equipment used as well as the challenges the noisy background poses, the low classification rates were expected, and the results seem to be promising.

In contrast, when all the types of images were fused in several ways or medium-level fusion of extracted features from them was applied, the classification performance did not yield better results. The same result occurred even when multi-spectral images of the two cameras were tested as one set, as shown in Table 10. Therefore, we can drive the conclusion that adding low resolution images results in worse classification performance, even for some sets in which the number of images was four times larger than the set that yielded the best classification performance.

Another conclusion derived from the suggested scheme for ATR is the capability to exploit the received imagery data in a timely manner. The combination of SURF features with NNs proved to be extremely fast and robust. Every time SURF features

were extracted from the image sets, results concerning the interest points were always the same, proving their repeatability. The subsequent use of NNs did not give the same results as initial weights were not the same at each training session. For the testing phase, though, and after the weights from training the NN were stored, the use of the same test set yielded exactly the same results in all the trials.

Finally, we can conclude that the combination of descriptors based mainly on SURF features and NNs could set the frame for a development of an algorithm that yields high classification rates in ATR. Sailing boats demonstrated almost perfect classification rates in the majority of the trials, and the main reason behind the fairly low classification rates is considered to be the smaller number and variety of types of the powerboats. Additionally, the reduction of the number of SURF features to ten, even though it removed most of the outliers generated from the background, did not work as well in all the images.

C. RECOMMENDATIONS FOR FUTURE WORK

The broad topic of this thesis reveals many challenges for future work and further research in the overall concept but also in the specific topics that were more thoroughly examined. Specific recommendations for mesh tactical networking and multi-sensor data fusion and classification are discussed in the following subsections.

1. Multi-Sensor Data Fusion and Classification

The use of only one type of feature in our binary problem yielded acceptable classification rates, especially for the sailing boat class. The use of more sophisticated imaging sensors and the association with metadata from environmental, motion, and relevant-position conditions would filter out not well-matching images for the training process and would provide more features. Feeding the NN additional features—such as size or shape characteristics extracted from the available metadata—could further improve the classification rates.

Further research could also be carried out to determine the types of imagery or other data coming from multiple dissimilar sensors that could be fused to provide richer

and more robust features under specific conditions such as rain or darkness. Synthetic aperture radars (SARs) or IR sensors in MWIR and LWIR could be some to consider.

Additionally, since SURF features are very robust, the reverse problem could be implemented in potential ATR solutions. Filtering out images of a specific or only a small group of COIs, subsequently training an ANN, and performing only a binary classification could yield better classification results. This process could even be completed at the platform detecting the COIs, so the feedback to the network could provide matching data. This type of solution could potentially help intelligence, surveillance, and reconnaissance (ISR) operations through the use of swarms of platforms with imaging sensors. Monitoring of multiple screens would then be impossible, and feedback that would only highlight targets of interest could enhance SA and reduce an operator's work load.

The training and testing processes could also be improved by researching and testing different techniques that could enhance NN performance. Applying deep NN techniques or adding more layers in the ANN could result in better generalization and, consequently, better classification performance. Finally, background extraction or segmentation of the image and application of high-level fusion could potentially improve extracted results.

2. Mesh Tactical Networking

Even if STK gave results that could be used in simulating scenarios with mesh tactical networks through Wave Relay radios, further analysis should be attempted. QualNet analysis would eventually give reduced and different ranges for video streaming, data, and voice applications. CodeMettle could then be used for the evaluation of the results in the field. Finalizing the simulation parameters in STK would then be feasible, and extended simulation scenarios could be tested. This process would be highly beneficial for the evaluation of future field experiments and operational scenarios in different geographic regions. Difficulties and potential problems could then be detected, and the final plan could be executed after the appropriate corrections.

Finally, the implementation of the proposed concept of distributed management of littoral operations in the tactical level could be further tested in the field. Considering the overall results of this research it seems that the use of mesh tactical networks would make possible the availability of ISR capabilities—UAVs and Cubesats—at the tactical level and, thus, the exploitation of available information in a timely manner. One of the benefits could be to enhance the capabilities of units without the need of modernizing them by adding an appropriate kit and networking appropriate platforms according to the missions. This kit could be easily removed and attached to other platforms when necessary. Solutions could then be found in communications and ISR limitations in littoral operations to enhance SA and timely and independent exploitation of information.

APPENDIX. IMAGE TO IMAGE REGISTRATION WITH ENVI

1. Open ENVI Classic

Figure 82. ENVI Classic Menu Bar

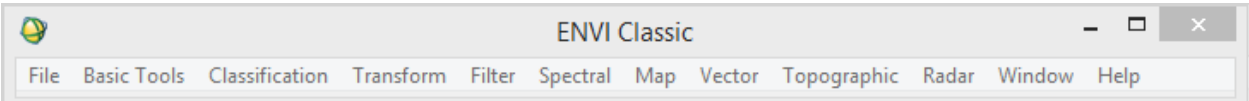

2. Open the images to be registered by selecting File →Open Image File from the ENVI Classic menu bar.

3. Load the RGB images in different displays

Figure 83. Images Shown in Different Displays

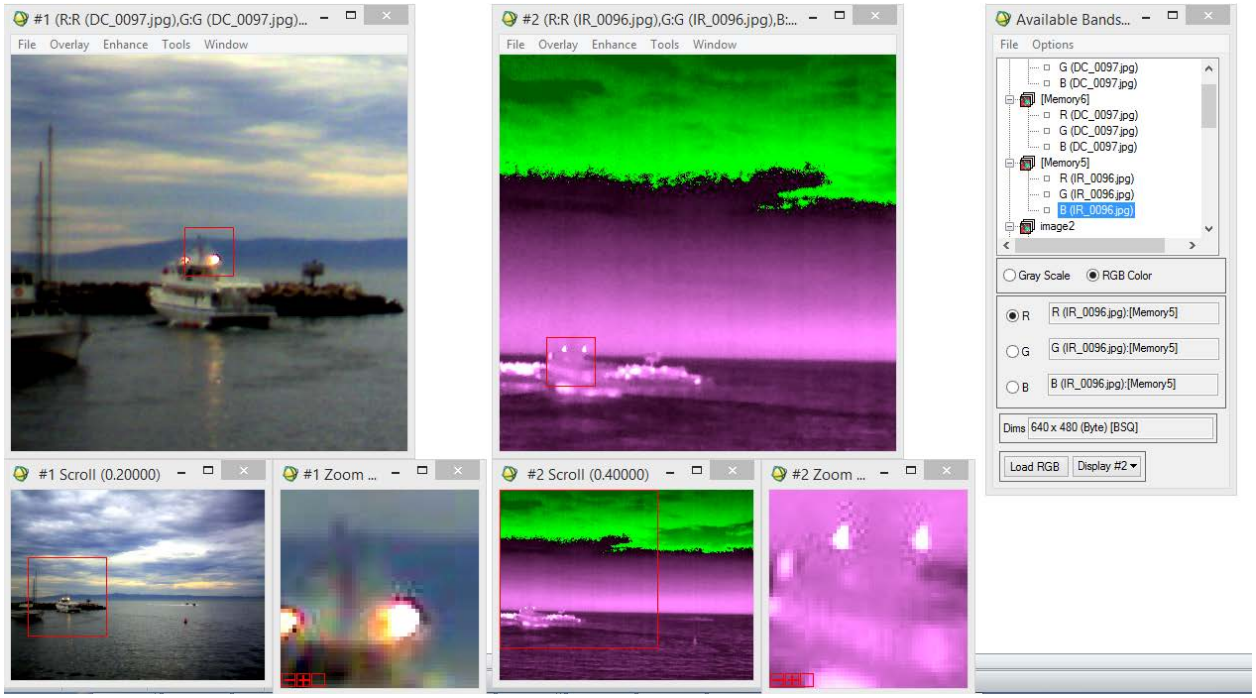

4. Select Map → Registration → Select GCPs: Image to Image from the ENVI Classic menu bar and define the displays for the Base and the Warp image that pops up.

Figure 84. Define Displays

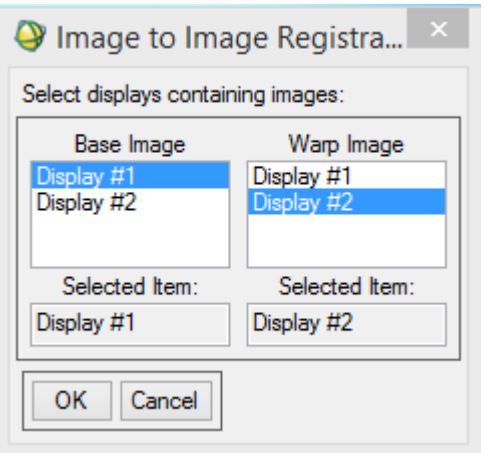

5. The Ground Control Point (GCP) selection pops up. After the selection of the corresponding points in both images, on the GCP selection window select File → Save GCPs to ASCII from the same window.

Figure 85. Ground Control Point Selection Window

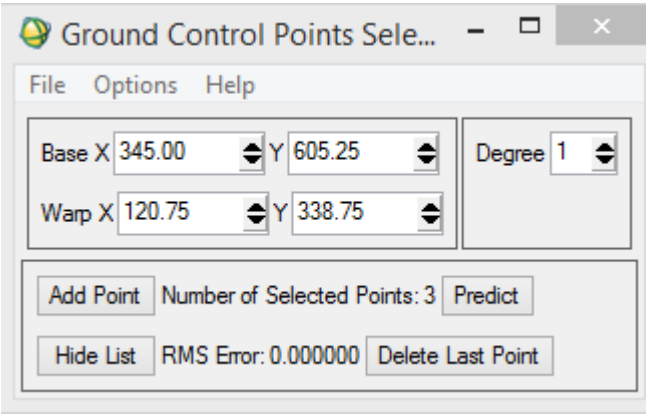

Figure 86. Corresponding Points Selection

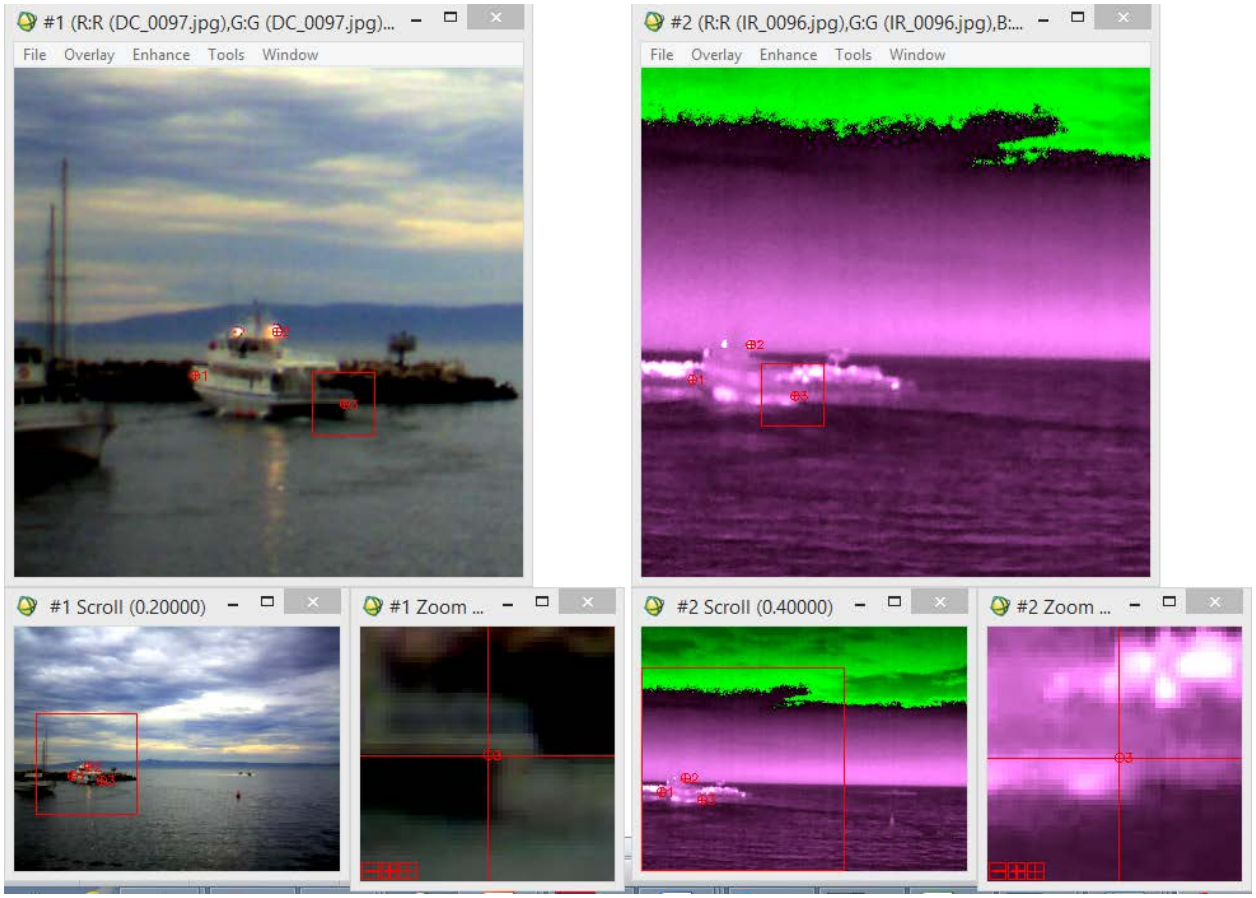

Figure 87. Saving GCPs

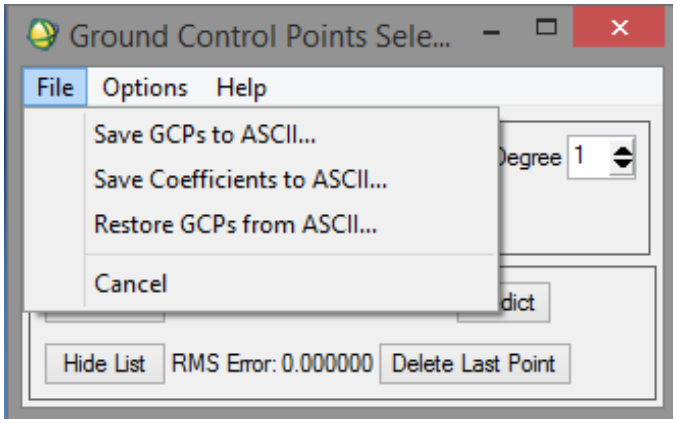

6. Then select Map → Registration → Warp from GCPs: Image to Image from the ENVI Classic menu bar and save the output from the pop up window after selecting the Warp and the Base image

Figure 88. Select Warp and Base Image

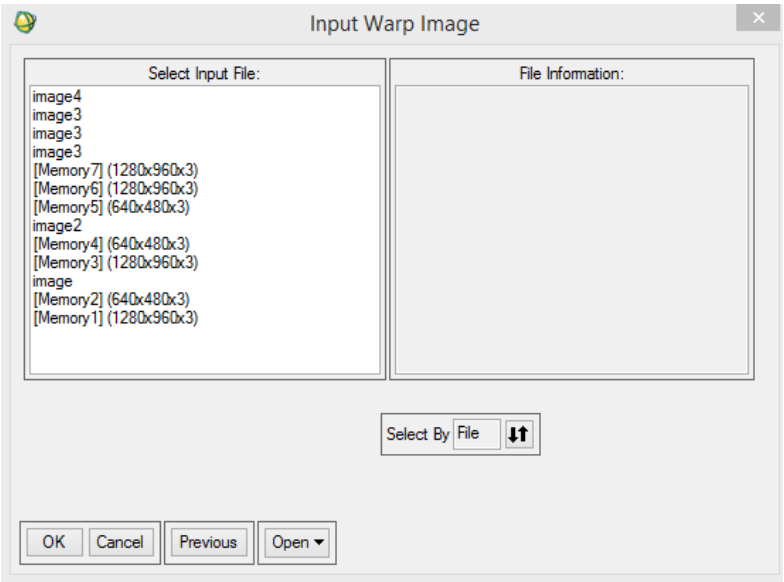

Figure 89. Save the File

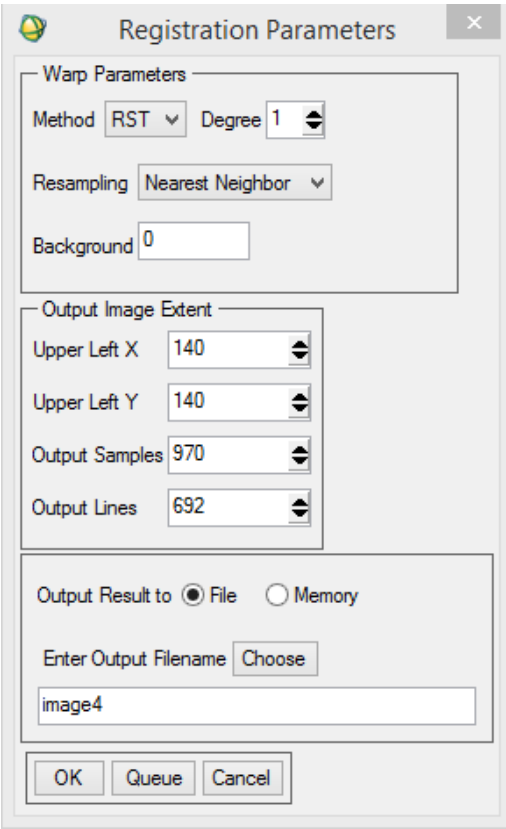

7. Load the Base original image and the output image on ENVI and try moving the indicator in the transparency tool on the menu bar until you get the result.

Figure 90. Registration in ENVI

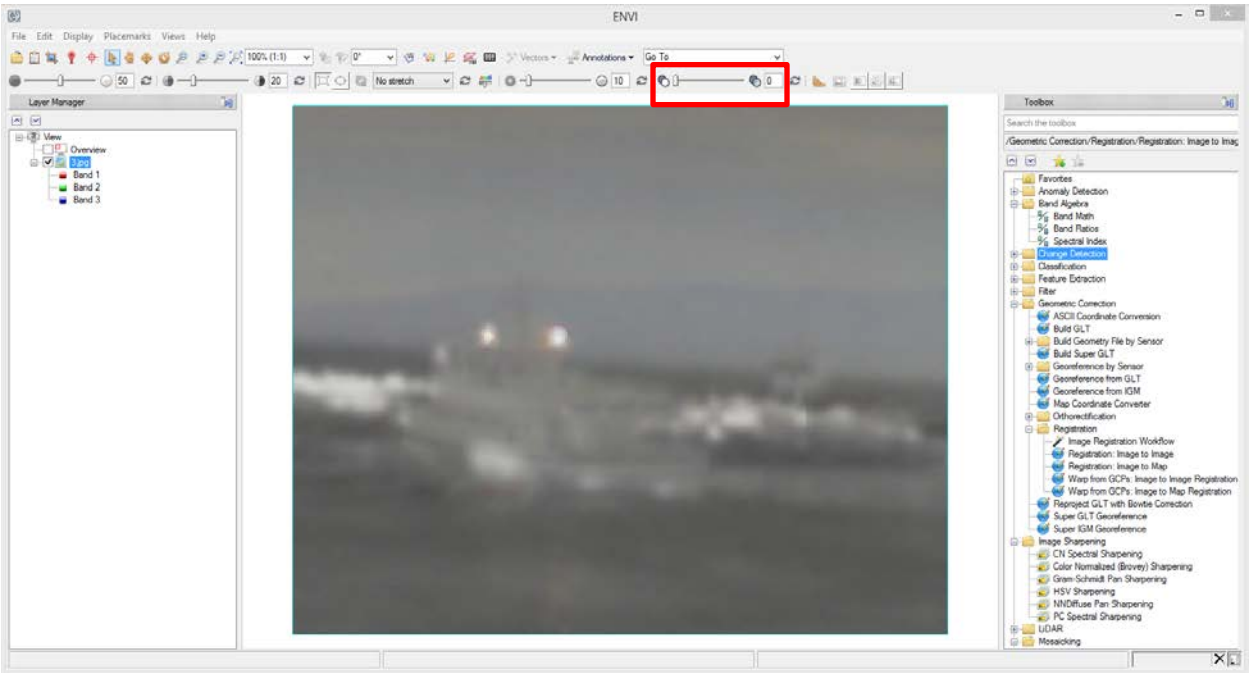

THIS PAGE INTENTIONALLY LEFT BLANK

LIST OF REFERENCES

[1] M. Bohanec, "What is decision support?," *Proceedings of the 4th International Multi-conference Information Society 2001*, vol. A, pp. 86–89, Ljubljana, 2001.

[2] M. Pothitos, "Potential Operational Use of Decision Support Systems," Hellenic Naval Staff and Command College, 2012.

[3] F. Feineigle, Patricia; Morris, Daniel; Snyder, "Ship recognition using optical imagery for harbor surveillance," *Proceedings of Association for Unmanned Vehicle Systems International (AUVSI)*, pp. 1–15, Washington DC, June 2007.

[4] P. W. Singer, *Wired for War - The Robotics revolution and Conflict in the 21st Century*. New York: The Penguin Press, 2009.

[5] G. Iapichino, C. Bonnet, O. Del Rio Herrero, C. Baudoin, and I. Buret, "A mobile ad-hoc satellite and wireless mesh networking approach for public safety communications," *10th Int. Work. Signal Process. Sp. Commun. SPSC 2008*, pp. 1–6, 2008.

[6] D. E. Comer, *Computer Networks and Internets*, 6th ed. New York: Pearson, 2015.

[7] S. Heimlicher, B. Plattner, S. Chandra Misra, S. Misra, and I. Woungang, *Guide to Wireless Mesh Networks*. London: Springer, 2009.

[8] J. Henry and M. Burton, "802.11s Mesh Networking," CWNP Enterprise Wi-Fi Whitepaper, November 2011.

[9] A. Bordetsky and D. Dolk, "A Conceptual Model for Network Decision Support Systems," *Syst. Sci. (HICSS), 2013 46th Hawaii Int. Conf.*, pp. 1212–1221, 2013.

[10] S. Y. Oh, D. Lau, and M. Gerla, "Content Centric Networking in tactical and emergency MANETs," *2010 IFIP Wirel. Days*, pp. 1–5, 2010.

[11] W. P. Alex Bordetsky and B. Hughes, "Mesh Networks In Littoral Operations." *Naval War College Review*, 2015.

[12] "Hybrid Network Orchestration." [Whitepaper.] CodeMettle, Atlanta, GA, 2012.

[13] *The CodeMettle Ecosystem for Network Management in Support of the DOD'sNMS Convergence Efforts*, CodeMettle, Atlanta, GA, 2015.

[14] C. Richards, *Boyd's OODA Loop*, J. Addams & Partners, Atlanta, GA, March 2012.

[15] B. Brehmer, “The Dynamic OODA Loop: Amalgamating Boyd’s OODA Loop and the Cybernetic Approach to Command and Control,” *10th Int. Command Control Res. Technol. Symp. Futur. C2*, 2005.

[16] M. Spitzer, E. Kappes, and D. Böker, “Enhanced intelligence through optimized TCPED concepts for airborne ISR,” vol. 8360, p. 83600A, 2012.

[17] T. Rowden, P. Gumataotao, and P. Fanta, “Distributed Lethality,” *Proceedings*, vol. 141, 2015.

[18] D. Boger, “Agile EMCON - Network-Centric and Network Optional Warfare.” [Slideshow]. Naval Postgraduate School, Monterey, California, 2015.

[19] M. M. Menon, E. R. Boudreau, and P. J. Kolodzy, “An Automatic Ship Classification System for ISAR Imagery,” *The MIT Lincoln Laboratory Journal*, vol. 6, pp. 289–308, 1993.

[20] J. Alves, J. Herman, and N. C. Rowe, “Robust Recognition of Ship Types from an Infrared Silhouette,” Command and Control Research and Technology Symposium, San Diego, CA, 2004.

[21] C. J. S. deSilva, G. Lee, and R. Johnson, “All-aspect ship recognition in infrared images,” *Proc. Electron. Technol. Dir. to Year 2000*, pp. 194–198, 1995.

[22] P. J. Withagen, K. Schutte, A. Vossepoel, and M. Breuers, “Automatic classification of ships from infrared (FLIR) images,” *Proc. SPIE*, vol. 3720, pp. 180–187, 1999.

[23] H. Bay, T. Tuytelaars, and L. Van Gool, “Surf: Speeded up robust features,” *Lect. notes Comput. Sci.*, vol. 3951, p. 14, 2006.

[24] C. W. Therrien, J. W. Scrofani, and W. K. Kreb, “An adaptive technique for the enhanced fusion of low-light visible with uncooled thermal infrared imagery,” *Proc. Int. Conf. Image Process.*, vol. 1, pp. 405–408, 1997.

[25] AGI, “STK 10 Help,” 2015. [Online]. Available: http://www.agi.com/resources/help/online/stk/10.1/. [Accessed: 20 Oct 2015].

[26] AGI, “STK Communications,” 2015. [Online]. Available: http://www.agi.com/products/stk/modules/default.aspx/id/stk-communications. [Accessed: 20 Oct 2015].

[27] S. N. Technologies, “Qualnet,” 2015. [Online]. Available: http://web.scalable-networks.com/content/qualnet. [Accessed: 20 Oct 2015].

[28] D. Schlatow and K. H. Lefherz, “Design , Characterization and Analysis of IT-Based Decision Support within CENETIX,” 2015.

[29] *Mobile WiMAX–Part 1: A Technical Overview and Performance Evaluation*, WiMAX Forum, Clackamas, OR, August 2006.

[30] N. I. of S. and T. (NIST), "Mobile Ad Hoc Networks (MANETs)." [Online]. Available: http://www.antd.nist.gov/wahn_mahn.shtml. [Accessed: 25 Oct 2015].

[31] David Munoz, Frantz Bouchereau Lara, and Cesar Vargas, "Ad hoc and Sensor Network Scenarios," 2011. [Online]. Available: http://www.eetimes.com/document.asp?doc_id=1279149&. [Accessed: 26 Oct 2015].

[32] J. D. C. Perkins, S. Ratliff, "Dynamic MANET On-demand (AODVv2) Routing," 2013. [Online]. Available: http://tools.ietf.org/html/draft-ietf-manet-dymo-26. [Accessed: 25 Oct 2015].

[33] D. M. Johnson, D., Y. Hu, "The Dynamic Source Routing Protocol (DSR) for Mobile Ad Hoc Networks for IPv4." [Online]. Available: http://tools.ietf.org/html/rfc4728. [Accessed: 25 Oct 2015].

[34] K. Gorantala, "Routing Protocols in Mobile Ad-hoc Networks," Master's thesis in Computer Science, Dept.of Comp.Sci., Umea Univ., Sweden, June 2006.

[35] I. S. Ibrahim, P. J. . King, and R. Pooley, "Performance Evaluation of Routing Protocols for MANET," *2009 Fourth Int. Conf. Syst. Networks Commun.*, pp. 105–112, 2009.

[36] D. BORGHINO, "Samsung's giant satellite network could enable high-speed Internet access across the globe," 2015. [Online]. Available: http://www.gizmag.com/samsung-satellite-network-Internet-access/38971/. [Accessed: 25 Oct 2015].

[37] Persistent Systems, *Wave relay User Manual*, Version 3. New York, NY, 2014.

[38] J. Sellers, W. Astore, R. Giffen, and W. Larson, *Understanding Space: An Introduction to Astronautics*, 3rd ed. The Mc Graw - Hill Companies, Inc, 2007.

[39] M. Subramanian, *Network Management: Principles and Practices*, 2nd ed. New Jersey: Prentice Hall, 2012.

[40] "Rods and Cones." [Online]. Available: http://hyperphysics.phy-astr.gsu.edu/hbase/vision/rodcone.html. [Accessed: 03 Nov 2015].

[41] H. Budzier and G. Gerlach, *Thermal Infrared Sensors – Theory, Optimisation and Practice*. New York: Wiley, 2011.

[42] R. Olsen C., *Remote sensing from air and space*. Bellingham, WA: SPIE Press, 2007.

[43] "Wien's Displacement Law." [Online]. Available: http://hyperphysics.phy-astr.gsu.edu/hbase/wien.html. [Accessed: 15 Nov 2015].

[44] S. O. Kasap, *Optoelectronics and Photonics - Principles and Practices*, 2nd ed. London: Pearson, 2013.

[45] S. O. Kasap, *Principles of Electronic Materials and Devices*, 3rd ed. New York: McGraw Hill, 2006.

[46] R. Szeliski, *Computer Vision : Algorithms and Applications*, vol. 5. London: Springer, 2010.

[47] Hyperphysics, "The C.I.E. Color Space." [Online]. Available: http://hyperphysics.phy-astr.gsu.edu/hbase/vision/cie.html.

[48] Mathworks, "How MATLAB Represents Pixel Colors." [Online]. Available: http://www.mathworks.com/company/newsletters/articles/how-matlab-represents-pixel-colors.html. [Accessed: 08 Nov 2015].

[49] E. Alpaydin, *Introduction to Machine Learning*, 3rd ed. Cambridge, Massachusetts: MIT Press, 2014.

[50] S. L. E. Rafael C. Gonzalez, Richard E. Woods, *Digital Image Processing using MATLAB*, 2nd ed. Gatesmark, LLC, 2009.

[51] H. Huang and S. Tai, "Facial Expression Recognition Using New Feature Extraction Algorithm," *Electron. Lett. Comput. Vis. Image …*, vol. 11, no. 1, pp. 41–54, 2012.

[52] D. Schmitt and N. McCoy, "Object Classification and Localization Using SURF Descriptors," CS 229 Final Projects, pp. 1–5, 2011.

[53] V. Muhammed Anees, G. Santhosh Kumar, and M. Sreeraj, "Automatic image annotation using SURF descriptors," *India Conf. (INDICON), 2012 Annu. IEEE*, vol. 68, no. 4, pp. 920–924, 2012.

[54] H. M. Sergieh, E. Egyed-Zsigmond, M. Doller, D. Coquil, J.-M. Pinon, and H. Kosch, "Improving SURF Image Matching Using Supervised Learning," *2012 Eighth Int. Conf. Signal Image Technol. Internet Based Syst.*, pp. 230–237, 2012.

[55] Badgerati, "Computer Vision – The Integral Image." [Online]. Available: https://computersciencesource.wordpress.com/2010/09/03/computer-vision-the-integral-image/. [Accessed: 01 Nov 2015].

[56] H. Bay, A. Ess, T. Tuytelaars, and L. Van Gool, "Speeded-Up Robust Features (SURF)," *Computer Vision and Image Understanding*, vol. 110, no. 3, pp. 346–359, September, 2008.

[57] J. T. Pedersen, “Study group SURF: Feature detection & description,” Department of Computer Science, Aarhus University, 2011.

[58] F. Castanedo, “A Review of Data Fusion Techniques,” *The Scientific World Journal*, vol. 2013, 2013.

[59] J. L. Martin E. Liggins, David L. Hall, *Handbook of Multisensor Data Fusion - Theory and Practice*, 2nd ed. Boca Raton, Florida: CRC Press, 2009.

[60] “Machine Learning,” Stanford University, 2015. [Online]. Available: https://www.coursera.org/learn/machine-learning. [Accessed: 08 Nov 2015].

[61] W. S. Sarle, “FAQs on Artificial Neural Networks,” 2002. [Online]. Available: ftp://ftp.sas.com/pub/neural/FAQ.html. [Accessed: 08 Oct 2015].

[62] Mathworks, “Multilayer Neural Network Architecture,” *MATLAB R2015b*, 2015. [Online]. Available: http://www.mathworks.com/help/nnet/ug/multilayer-neural-network-architecture.html. [Accessed: 09 Nov 2015].

[63] Mathworks, “Choose a Multilayer Neural Network Training Function,” *MATLAB R2015b*, 2015. [Online]. Available: http://www.mathworks.com/help/nnet/ug/choose-a-multilayer-neural-network-training-function.html. [Accessed: 09 Nov 2015].

[64] Mathworks, “Trainscg,” *MATLAB R2015b*, 2015. [Online]. Available: http://www.mathworks.com/help/nnet/ref/trainscg.html?searchHighlight=trainscg. [Accessed: 09 Nov 2015].

[65] Mathworks, “Multilayer Neural Networks and Backpropagation Training,” *MATLAB R2015*, 2015. [Online]. Available: http://www.mathworks.com/help/nnet/ug/multilayer-neural-networks-and-backpropagation-training.html. [Accessed: 09 Nov 2015].

[66] F.-F. Li and A. Karpathy, “Convolutional Neural Networks for Visual Recognition.” [Online]. Available: http://cs231n.stanford.edu/. [Accessed: 05 Nov 2015].

[67] Mathworks, “mse,” *MATLAB R2015b2*, 15AD. [Online]. Available: http://www.mathworks.com/help/nnet/ref/mse.html. [Accessed: 02 Nov 2015].

[68] Mathworks, “Crossentropy,” *MATLAB R2015*, 2015. [Online]. Available: http://www.mathworks.com/help/nnet/ref/crossentropy.html. [Accessed: 22 Nov 2015].

[69] T. Hastie, R. Tibshirani, and J. Friedman, *Teh Elements of Statistical Learning - Data Mining, Inference and Prediction*, 2nd ed. London: Springer, 2013.

[70] NPS, “Center for Network Innovation and Experimentation (CENETIX),” 2015. [Online]. Available: http://cenetix.nps.edu/cenetix/cenetix.asp. [Accessed: 10 Nov 2015].

[71] MathWorks, “Histeq,” *MATLAB R2015b*, 2015. [Online]. Available: http://www.mathworks.com/help/images/ref/histeq.html?s_tid=srchtitle. [Accessed: 29 Oct 2015].

[72] “Improve Neural Network Generalization and Avoid Overfitting,” *2MATLAB R2015b*, 2015. [Online]. Available: http://www.mathworks.com/help/nnet/ug/improve-neural-network-generalization-and-avoid-overfitting.html. [Accessed: 02 Nov 2015].

[73] Mathworks, “Improve Neural Network Generalization and Avoid Overfitting,” *MATLAB R2015*, 2015. [Online]. Available: http://www.mathworks.com/help/nnet/ug/improve-neural-network-generalization-and-avoid-overfitting.html. [Accessed: 05 Nov 2015].

[74] A. Bordetsky, “Constellation Experimentation Planning Oct 2015.” NPS CENETIX Lab, Monterey, CA, 2015.

[75] M. Maupin, “Hybrid Mesh Networking for Distributed Operations.” [Slideshow]. NPS, Monterey, California, 2015.

INITIAL DISTRIBUTION LIST

1. Defense Technical Information Center
   Ft. Belvoir, Virginia

2. Dudley Knox Library
   Naval Postgraduate School
   Monterey, California